2019

TARGETED THERAPIES FOR EWSR1-FLI1 TRANSLOCATED EWING FAMILY OF TUMORS

Daniel A.R. Heisey
Virginia Commonwealth University

TARGETED THERAPIES FOR *EWSR1-FLI1* TRANSLOCATED EWING FAMILY OF TUMORS

A dissertation submitted in partial fulfillment of the requirements for the degree of Doctor of Philosophy at Virginia Commonwealth University.

by

DANIEL ANDREW RUSSELL HEISEY
B.S, Christopher Newport University, 2011

Director: ANTHONY FABER
ASSISTANT PROFESSOR, PHILIPS INSTITUTE, SCHOOL OF DENTISTRY

Virginia Commonwealth University
Richmond, Virginia
June, 2019

Dedication

This work is dedicated to family, my wife Kayla who has been a source of unending support and held my sanity in check throughout graduate school.

To my Mother Susan, Father Andrew, and my siblings Justin and Kara who have both nurtured my love of science from a young age and served as my source of inspiration.

I could not have done it without your love and support, thank you for all you do.

.

Table of Contents

Page

List of Tables

Page

List of Figures

Page

List of Abbreviations

%	Percentage
°C	Celsius
µg	Microgram
µl	Microliter
µM	Micromolar
ANOVA	Analysis of Variance
BCL2L1	BCL-X_L (BCL2 Like 1)
BIM	BCL-2 Interacting Mediator of Cell Death
BRCA1	Breast Cancer Type 1 Susceptibility Protein
CCND1	Cyclin D1
ChIP	Chromatin Immunoprecipitation
COG	Children's Oncology Group
CV	Crystal Violet
DMEM	Dulbecco's Modified Eagle's Medium
DNA	Deoxyribonucleic acid
DTT	Dithiothreitol
EDTA	Ethylene diamine tetraacetic acid
EFS	Event Free Survival

ERG	ETS1-Related Gene
ES	Ewing Sarcoma
ETS	E26 transformation specific
ETV4	ETS Variant 4
ETV1	ETS Variant 1
EWFT	Ewing Family of Tumors
EWSR1	EWS RNA binding protein 1
EZH2	Enhancer of Zeste Homolog 2
FBS	Fetal Bovine Serum
FET	FUS/EWSR1/TAF15
FEV	Fifth Ewing Variant
FLI1	Friend Leukemia Integration 1 transcription factor
FUS	Fused in Sarcoma
g	Gram
H3	Histone 3
H3K27ac	Histone 3 Lysine 27 Acetylation
H3K27me3	Histone 3 Lysine 27 tri-methylation
HAT	Histone Acetyl Transferase
HDAC	Histone Deacetylase
hMSC	human Mesenchymal Stem Cell

HR	Homologous Recombination
hr	Hour
IC50	Inhibitory Concentration 50%
IgG	Immunoglobulin G
JMJD3	Jumonji D3
KDM6A	UTX
KDM6B	JMJD3
kg	Kilogram
LSD1	Lysine-Specific Histone Demethylase 1
M	Molar
mg	Milligram
min	Minute
ml	Milliliter
mm^3	Cubic millimeters
NKX2.2	NK2 Homeobox 2
nM	Nanomolar
NPY1R	Neuropeptide Y Receptor Y1
NR0B1	Nuclear Receptor Subfamily 0 Group B Member 1
PARP	Poly(ADP-ribose) polymerase
PBS	Phosphate Buffered Saline

PMSF	Phenylmethylsuflonyl Fluoride
PNET	Primitive Neuroectodermal Tumor
pRNAP II	phosphorylated RNAP II
PVDF	Polyvinylidene difluoride
RT-qPCR	Real Time quantitative Polymerase Chain Reaction
RNAP II	RNA Polymerase II
RPMI	Roswell Park Memorial Institute medium
RT	Room Temperature
SDS	Sodium Dodecyl Sulfate
SDS-PAGE	SDS-Polyacrylamide Gel Electrophoresis
ser	Serine
shRNA	Short Hairpin RNA
STEAP1	Six Transmembrane Epithelial Antigen of the Prostate
TAF15	TATA-BOX Binding Protein Associated Factor 15
TCGA	The Cancer Genome Atlas
TSS	Transcription Start Site
UTX	ubiquitously transcribed tetratricopeptide repeat, X chromosome

Abstract

TARGETED THERAPIES FOR *EWSR1-FLI1* TRANSLOCATED EWING FAMILY OF TUMORS

By Daniel Andrew Russell Heisey, B.S.

A dissertation submitted in partial fulfillment of the requirements for the degree of Doctor of Philosophy at Virginia Commonwealth University.

Christopher Newport University, 2011

Director: Anthony Faber, Ph.D.
Assistant Professor, Philips Institute, School of Dentistry

The *EWSR1-FLI1 t(11;22)(q24;q12)* translocation is the pathognomonic genomic alteration in 85% of the Ewing Family of Tumors (EWFT) a malignancy of the bone and the surrounding tissue, predominantly affecting children and adolescents. This translocation results in the formation of a chimeric oncoprotein which acts as an aberrant transcription factor that is currently not pharmaceutically druggable, driving the need for more effective targeted therapies. The *EWSR1-FLI1* translocation induces a variety of changes including dysregulation of the epigenome and altered gene expression to drive tumorigenesis, and consequently contributes to the hypersensitivity of EWFT to several

classes of chemotherapeutics. We sought to exploit these intrinsic sensitivities by employing a matched pair of cell lines derived from the same patient with Ewing sarcoma prior to and following chemotherapy, a panel of Ewing sarcoma cell lines, and several patient-derived xenografts (PDX) collected at the time of relapse or autopsy, which led us to the development of two novel combination targeted therapies for EWFT.

In our matched pair of EWFT cell lines, we found sensitivity to the Poly(ADP-ribose Polymerase (PARP) inhibitor olaparib was diminished following chemotherapy, despite a predicted sensitivity. In addition, we discovered increased expression of the antiapoptotic protein BCL-2 in the chemotherapy-resistant cells, conferring apoptotic resistance to olaparib. We found that EWS-FLI1 increases BCL-2 expression; however, inhibition of BCL-2 alone is insufficient to sensitize EWFT cells to olaparib, revealing a dual necessity for BCL-2 and BCL-X_L (*BCL2L1*) in EWFT survival. These data reveal BCL-2 and BCL-X_L act together to drive olaparib mediated apoptotic resistance in Ewing sarcoma and identify a novel, rational combination therapy using olaparib and the BCL-2/BCL-X_L inhibitor navitoclax.

In addition, using high throughput drug screening we have identified a novel epigenetic susceptibility in EWFT to GSK-J4 (GlaxoSmithKline), an inhibitor of lysine 27 of histone 3 (H3K27) demethylases: ubiquitously transcribed tetratricopeptide repeat, X chromosome (UTX) and Jumonji D3 (JMJD3). Treatment with GSK-J4 leads to a decrease in H3K27 acetylation (H3K27ac) and ultimately, the silencing of EWS-FLI1 gene targets.

We sought to sensitize GSK-J4-mediated inhibition of EWS-FLI1 targets by blocking RNA polymerase II activity using the Cyclin Dependent Kinase 7 (CDK7) inhibitor THZ1. By targeting CDK7-mediated transcription we were able to sensitize EWFTs to H3K27 demethylase inhibition. We therefore propose co-targeting of H3K27 demethylases and CDK7 acts as a surrogate EWS-FLI1 inhibitor. Given the difficulties targeting EWS-FLI1, these strategies may present viable clinical therapies.

CHAPTER 1 - Introduction

Targeted Cancer Therapies

For many decades, systemic chemotherapy has been the cornerstone of cancer treatment despite toxicity, low therapeutic indexes, and challenges in drug discovery (1-3). Recent advances in molecular profiling and genomics have led to a greater understanding of cancer biology (4-6), allowing for the optimization of treatment using targeted therapies (7-9). This technological revolution has led to the emergence of new studies aimed at the systemic mapping of cancer genomics and the characterization of pharmacological vulnerabilities (10, 11). These include programs such as the Cancer Genome Atlas (TCGA) , the Cancer Cell Line Encyclopedia (CCLE), and the Genomics of Drug Sensitivity in Cancer (GDSC) (12, 13), which have helped to identify many of the genes responsible for disrupting the cellular processes which lead to cancer. Despite the complexities found in cancers, they are often driven by specific genetic aberrations known as oncogenes, whose direct inhibition can have a dramatic effect on cancer growth and survival (14, 15). This “oncogene addiction” serves as the rationale behind the development of targeted therapies, aimed at the pharmaceutical impairment of cancer specific oncogenes. Targeted therapies are effective due to their low toxicity and highly specific anti-tumor activity in a cytotoxic or cytostatic manner. This is accomplished by designing drugs that target oncogenes specific to each cancer type, which by definition are more heavily relied on by cancer cells for survival compared to normal healthy cells (1).

One of the first and most significant of these targeted therapies is imatinib mesylate (Novartis) (16). Imatinib is a small molecule kinase inhibitor with specificity for BCR-ABL, the fusion protein resulting from a chromosomal translocation which drives oncogenesis in chronic myeloid leukemia (CML) (17). Imatinib has been employed to successfully treat CML while having little effect on normal cells, demonstrating its specificity and effectiveness as a targeted therapy (18). Unfortunately, a common occurrence in cancer is acquired resistance which becomes problematic for single agent targeted therapies, driving the need to develop and implement new generations of inhibitors with higher efficacy and the employment of combination targeted therapies (3, 7).

The Ewing Family of Tumors

The Ewing Family of Tumors (EWFT) are the second most common form of pediatric bone cancer, with ~250 new cases diagnosed in the United States each year (19) and accounts for roughly one-third of all pediatric bone tumors (20). The malignancy was first described in 1921 by its namesake James Ewing, where it was distinguished as a separate disease from osteosarcoma and identified as being highly sensitive to radiation therapy (21). The Ewing Family of Tumors consists of Ewing Sarcoma of the bone (ES), Extraosseous Ewing Tumors (22), and Peripheral Primitive Neuroectodermal Tumors (PNET), all of which share a common family of translocations. These translocations consist of the amino terminus of one the *FUS/TLS*, *EWSRI* and *TAF15* (FET) family of RNA-binding proteins fused to the carboxy terminus of one of the E26 transformation-

specific (ETS) family of transcription factors. This fusion results in the formation of proto-oncogenes which display neomorphic functions which deregulate the transcriptome and epigenome of cells and have been identified as the driving force behind EWFT tumorigenesis. (23). This is accomplished through FET/ETS oncoproteins binding to ETS gene targets at GGAA binding motifs located within enhancer or promoter regions, which results in chromatin remodeling that alters gene expression (24-26) and to a lesser known extent results in the downregulation of tumor suppressors (27, 28).

Occurrence rates are higher in the male population compared to female (sex ratio of 1.5:1) and is predominantly higher among Caucasians, with a much lower incidence in people of Asian and African descent. Of note, there is a difference in the size and grouping of the GGAA ETS binding motifs found between Caucasian and African/Asian populations which may help explain the observed differences in disease frequency. However, within all population's a high number of GGAA microsatellites occur at ETS target genes, with 20-26 repeats found in European samples and 30 or more in African samples. These greater numbers of GGAA consecutive repeats may be attributed to a more aggressive phenotype and help explain the lower survival rates found in African populations despite their decreased rate of occurrence. Despite these findings, a possible genetic distinction between the 10 fold greater rate of occurrence in people of European ancestry still remains unclear (24, 25, 29, 30).

Recent advances have been made in the treatment of primary EWFT tumors using systemic chemotherapy to increase the 5-year survival rate to 70%. Unfortunately, 25% of patients are asymptomatic for micrometastasis at the time of diagnosis and these patients,

or those who relapse following chemotherapy have a 5-year survival rate of less than 30% (19, 31). The current standard of care (VDC-IE: Vincristine, Doxorubicin, Cyclophosphomide – Ifosfamide and Etoposide) for EWFT in North America relies heavily on adjuvant and neoadjuvant systemic chemotherapy followed by surgical resection of the primary tumor and continued chemotherapy or radiation therapy (32-34). In a study by the Children's Oncology Group (COG), the event free survival (EFS) was significantly increased in patients treated with a more intense regimen of VDC-IE chemotherapy at 2-week intervals compared to patients treated at 3-week intervals (COG-AEWS0031 [NCT00006734]), which suggests more aggressive treatment regimens are necessary for improved patient outcomes. Due to the aggressive nature of the disease, a high prevalence of metastasis/relapse and the intense chemotherapy treatments required, there exists a dire need to develop more potent and effective targeted therapies.

FET/ETS Fusion	Chromosomal Translocation	Frequency
EWSR1-FLI1	t(11;22)(q24;q12)	~85%
EWSR1-ERG	t(21;22)(q22;q12)	~10%
EWSR1-ETV1	t(7;22)(p22;q12)	<1%
EWSR1-ETV4	t(17;22)(q12;q12)	<1%
EWSR1-FEV	t(2;22)(q35;q12)	<1%
FUS-FEV	t(2;16)(q35;p11)	<1%
FUS-ERG	t(16;21)(p11;q24)	<1%

Table 1.1 Fusions which result in EWFT.

EWS

EWS is a nuclear protein encoded by EWS RNA binding protein 1 (*EWSR1*) and is a member of the FET family of RNA binding proteins. Within this family are Fused in Sarcoma (*FUS*), *EWSR1*, TATA-Box binding protein Associated Factor 15 (*TAF15*), and translocations of these FET family of genes has been associated with a number of diseases (31, 35, 36). The carboxy-terminus of EWS consists of its RNA binding domain and is responsible for its ability to interact with RNA splicing factors while the amino-terminus

of EWS contains a transcription activation domain which is maintained in translocations that result in EWFT. EWS is considered an intrinsically disordered protein (IDP) due to its repetitive (SYGQQS) low complexity amino acid sequence Prion-like domain, located within the transcriptional activation region of the N-terminus, and is hypothesized to allow for its transcriptional activation through the process of multimerization (37, 38). This subsequent multimerization allows for the aggregation of EWSR1 and imbues phase transition properties which are essential for the stabilization required to recruit co-activators and the chromatin remodeling complex BRG1/BRM-associated factor (BAF) to induce the gene activation profiles associated with EWFT when translocated (39-41).

ETS

The ETS (E26 Transformation-Specific) family of transcription factors was first discovered and initially named while researching the avian erythroblastosis virus, E26 in 1983 (42). This group contains 28 transcription factors in humans that all share a highly conserved DNA binding domain (ETS domain), consisting of a winged helix-turn-helix which binds the major groove, making it critical for a vast majority of cellular processes as they occupy 15% of all human promoters and regulate pathways responsible for cell cycle regulation, differentiation, proliferation, and apoptosis (30, 43-45). In addition, knocking out the ETS family member: Friend Leukemia Integration 1 transcription factor (*FLI1*) has proven to be embryonic lethal demonstrating its importance in development (46, 47). For these reasons the ETS family members are often implicated in the tumorigenesis of multiple cancer types (43-45, 48, 49). This often occurs through their direct amplification

or as a result of gene fusions such as *TMPRSS2/NDRG1-ERG* (transmembrane protease serin2/N-Myc downstream regulated 1 - ETS-related gene) in prostate cancer (50) and *EWSR1-ETS* in Ewing Sarcoma. In addition to the DNA binding domain, many ETS family members possess an additional pointed (PNT) domain, which plays a role in protein-protein interaction, however the PNT domain in FLI1 is lost in the EWS-FLI1 translocation (43, 48, 49, 51).

The *EWSR1-FLI1* translocation is present in 85% of all EWFT cases, while the remaining 15% harbor *EWSR1-ERG* t(21;22)(p22;q12), *EWSR1-ETV1* t(7;22)(p22;q12), *EWSR1-ETV4* t(17;22)(q12;q12), or *EWSR1-FEV* t(2;22)(q33;q12) translocations (44, 52, 53). Both FLI1 and ERG expression is relatively low in adult tissues, however they are highly expressed in both the spleen and bone marrow due to their role in hematopoiesis (47, 54). In addition, the FLI1 and ERG transcription factors involved in EWFT have been shown to induce very similar clinical phenotypes and gene expression changes, likely due to only minor differences in their N terminus, suggesting they share gene targets and serve similar functions that contribute to disease when translocated to EWSR1 (27, 55).

EWS-FLI1

Within the Ewing Family of Tumors the majority are driven by the specific *EWSR1-FLI1 t(11;22)(q24;q12)* translocation event, which results in the DNA binding domain of *FLI1* fused to and regulated by the strong transcriptional activation domain of *EWSR1* (27, 56-60). *FLI1* was first identified over 20 years ago, where it was quickly found to represent the dominant translocation event which causes Ewing Sarcoma (Fig.

1.1). The resulting EWS-FLI1 fusion retains a more potent level of transcriptional activity compared to the wild type FLI1 which has a relatively weak transcriptional activation domain (61). The remaining 15% of EWFTs harbor alternative EWS-ETS fusions whose functions mimic that of EWS-FLI1 (45, 49). Both *EWSR1* and *FLI1* are required for transformation, as deleting portions of either gene results in a loss of the transformation phenotype (25).

In addition to the gene specific chimeric fusion, there are subtypes of each translocation determined by the breakpoint regions of EWSR1 and FLI1. The most common EWS-FLI1 transcript variant is that of EWSR1 exon 7 fused to FLI1 exon 6 (7/6 fusion), and is known as type 1 (62). These specific EWS-FLI1 oncoprotein subtypes were previously reported to influence factors such as the tumorigenicity and propensity to form metastasis (63, 64). However, more current studies have refuted this claim, suggesting that the fusion subtype has no effect on clinical phenotypes (52, 65). Recent studies have shown that the EWS-FLI1 translocation is not only required for EWFT tumorigenesis, but its expression is able to transform mesenchymal stem cells (MSCs), the proposed cell of origin of EWFT. When the EWS-FLI1 translocation is expressed in pediatric MSCs, a gene expression profile is induced which emulates that of EWFT (26, 66, 67).

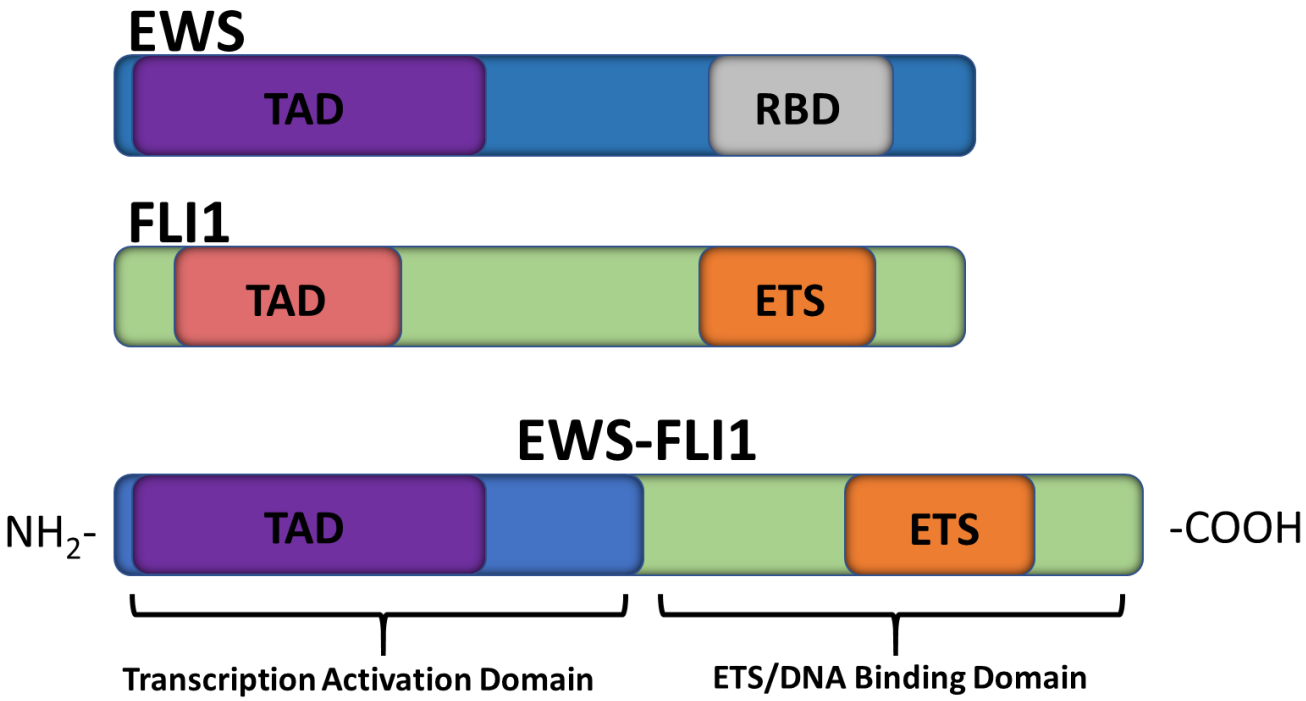

Figure 1.1 EWS-FLI1

Chromosomal translocation which creates the EWS-FLI1 oncoprotein, binding the TAD of EWS to the ETS domain of FLI1.

Cell of Origin

Within the EWFT there is a lack of knowledge concerning the most likely cell lineage of origin, whose identification would serve to elucidate more reliable markers of disease and therapeutic agents. Early studies have demonstrated that a subset of EWFT display neural markers, and expression of the EWS-FLI1 translocation in neuroblastoma cells is sufficient to induce a gene expression profile associated with EWFT. The expression of EWS-FLI1 in pediatric mesenchymal stem cells induces the expression of genes responsible for neuroectodermal differentiation (57, 68). However, more recent

data suggests EWFT is of mesenchymal origin, and that it may exude a partial neural phenotype as a consequence of the EWS-FLI1 reprogramming.

Riggi and colleagues (69) demonstrated that expression of the EWS-FLI1 translocation in bone-derived human mesenchymal stem cells (hMSC) alone is enough to transform the cells and generate tumors which mimic that of the Ewing Family of Tumors. This translocation induces a cellular phenotype analogous to the small round blue cells that are the hallmark of EWFT, and a gene expression profile comparable to FLI1 target gene expression. In addition, the knockdown of EWS-FLI1 in EWFT cell lines results in the cellular expression of cell surface markers and gene expression profiles closely resembling mesenchymal stem cells (26, 66, 67, 70, 71). Of the various progenitor cell types that have been proposed, only mesenchymal stem cells are able to stably express the EWS-FLI1 fusion. In addition, the CD99 antigen, which is normally expressed on the surface of hMSC is the most widely used histological marker for EWFT detection (72). Taken together, this data would strongly suggest that these tumors arise from a mesenchymal stem cell of origin.

EWFT Transcriptional Regulation

EWS-FLI1 preferentially binds to specific microsatellite motifs consisting of repetitive GGAA sequences. Interestingly, the GGAA core consensus sequence is a direct binding target of wild type FLI1, and only the translocated EWS-FLI1 results in the activation of de novo enhancer elements. Gene activation is achieved when GGAA motifs contain 4 or more repeats, and optimal binding is attained at 12-14 repeats (25, 30). EWS-

FLI1 has a higher binding affinity to these repeats than wild type FLI1 resulting in FLI1 displacement and consequential alterations of gene expression (24, 39, 73). More importantly, the presence of multiple GGAA microsatellite repeats has been detected in 75% of the genes activated by EWS-FLI1, while 85% of genes repressed by this chimeric protein displayed non-repetitive GGAA sequences (26). In addition, the clinical phenotypes of other EWS-ETS fusions such as EWS-ERG mimic that of EWS-FLI1 suggesting a similar global deregulation of gene expression within EWFT (55).

Although the exact functions of EWS is not currently understood, the EWS amino-terminus is shown to exhibit direct interactions with transcriptional machinery such as RNA polymerase II and the co-activator p300/CBP (26, 39, 58, 74, 75). Both wild type EWSR1 and the EWS-FLI1 fusion are able to interact with the BRG1/BRM-associated factor (BAF) chromatin remodeling complex which contributes to gene activation. This leads to the recruitment of the BAF complex to tumor-specific enhancers at FLI1 binding targets, resulting in their activation (39). However, the method of EWS-FLI1 gene repression is poorly understood. It is hypothesized to be an indirect mechanism, through miRNA and epigenetic mechanisms which alter post-transcriptional gene regulation, as EWS-FLI1 does not bind directly to the enhancers of repressed genes (76, 77). Another possibility is through the Enhancer of Zeste homolog 2 (EZH2), a bona fide EWS-FLI1 gene target, which is directly upregulated by EWS-FLI1, and is the enzymatic subunit of the polycomb repressive complex 2 (PRC2) responsible for methylation of histone 3 Lysine 27 (78-81). Increases in methylation at lysine 27 are marks of repressed chromatin, and the upregulation of EZH2 suggests a method of EWS-FLI1 mediated

indirect gene silencing through the remodeling of chromatin. It has also been demonstrated that wild-type FLI1 binds to single GGAA repeat motifs and once bound is capable of recruiting the p300 co-activator. However, the EWS-FLI1 oncoprotein has a higher binding affinity for these GGAA motifs but requires multimerization for p300 and BAF recruitment, effectively silencing many EWS target genes with less than 4 GGAA motifs (26).

Research Goals

The Ewing Family of Tumors serves as an excellent model to study the paradigm that chromosomal translocation-driven cancers represent. Due to the low mutational burden found in EWFT and the specific FET-ETS driver events, we are presented with a unique transcription factor driven deviation from normal cell regulatory processes (82). Unlike many specific oncogene addictions which we are able to pharmaceutically inhibit, EWS-FLI1 is not a viable target, however the changes in gene expression that it causes represent potential therapeutic targets (20, 58). The principle goal of our research is to investigate and address a means of pharmaceutically targeting the driving force behind EWFT pathogenesis: the EWS-FLI1 translocation, through indirect targeting of its downstream effects. Taken together, these studies hope to expand upon the mechanisms by which the EWS-FLI1 translocation evades traditional therapies, and to develop novel targeted therapies which can be utilized in a clinical setting.

The work herein evaluates and achieves the following aims:

1. **Elucidate the mechanism by which EWFT become resistant to Poly(ADP-ribose) polymerase inhibition (PARPi) and develop a means of countering this resistance.** EWFT are extremely sensitive to PARPi *in vitro* due to their lack of efficient homologous recombination repair. However, the PARP1/2 inhibitor olaparib had little efficacy in a clinical trial comprised of patients with chemo-refractory disease (83). Understanding the disconnect between the observed deficiency of PARP inhibitor activity, and the altered gene expression profile induced by EWS-FLI1 (which likely contributes to chemotherapy resistance), is critical to better understand and develop new targeted therapies effective in patients who relapse or acquire drug resistance.
2. **Identify a means of pharmaceutically targeting the vast genomic remodeling that occurs as a result of EWS-FLI1.** This work focuses on targeting the epigenetic mechanisms that EWS-FLI1 utilizes to dysregulate the epigenome. This refers to DNA modifications which can result in the alteration of gene expression without changing the sequence of DNA. These modifications are caused by the methylation of DNA at cytosine residues, the remodeling of chromatin, and through modifications to histone tails which result in their methylation or acetylation (84, 85). EWS-FLI1 is capable of altering the expression of histone marks at enhancer and super-enhancer regions, these resulting changes to the epigenome alter the transcriptional activity of genes. Two of the histone modifications most highly regulated by

EWS-FLI1 are H3K27ac and H3K4me1, both ubiquitous markers of active enhancers, and are found to be enriched at known EWS-FLI1 gene targets (26, 76). By combining histone demethylase and RNAP II inhibitors we sought to disrupt the EWS-FLI1 transcriptional machinery and H3K27ac modifications which promote EWFT oncogenesis.

CHAPTER 2 – Materials and Methods

Cell Lines

A673 (ATCC® CRL-1598™) and HEK293T cells were cultured in DMEM (Gibco) with 10% FBS (Seradigm) and 1μg/ml penicillin and streptomycin. CHLA9 and CHLA10 cells were grown in DMEM with 20% FBS, 1ug/ml penicillin and streptomycin, and 1% Insulin-Transferrin-Selenium 100x (Gibco). SK-ES-1(ATCC® HTB-86™) was grown in DMEM/F12 (Corning) with 15% FBS and 1ug/ml of penicillin -and streptomycin. ES4 and EW16 cells were grown in RPMI1640 (Lonza Group) with 10% FBS and 1μg/ml of penicillin and streptomycin. Routine mycoplasma testing was performed on all cell lines. CHLA9, CHLA10 and the PDX models TX-E-270x and TX-E-351x were obtained from the Children's Oncology Group (COG) Cell Culture and Xenograft Repository, special thanks to Dr. C. Pat Reynolds, Texas Tech University Health Sciences center. PDX models SA10233 and SA13542 were obtained from Crown Bioscience. *Ex vivo* PDX lines were derived using selective trypsinization (86) over consecutive passages and cultured in RPMI 1640 with 10% FBS. ES4, EW16, HEK293T, A673 (ATCC® CRL-1598™), and SK-ES-1 (ATCC® HTB-86™), were obtained from either the Molecular Center Therapeutics laboratory at Massachusetts General Hospital

which performs routine testing of cell lines using STR and SNP analysis, or from the American Type Culture Collection (ATCC).

Antibodies and Reagents

Primary antibodies used for Western blotting were GAPDH (Santa Cruz sc-3233) , RNAP II (Santa Cruz sc-56767), FLI1 (Santa Cruz sc-365294) Santa Cruz Biotechnology (Dallas, TX); Cleaved PARP1 (Cell Signaling 5625), BCL-2 (Cell Signaling 4223), BCL-X_L (Cell Signaling 2764), MCL-1 (Cell signaling 5453), p-Ser2 RNAPII (Cell Signaling 13499), p-Ser5 RNAPII (Cell Signaling 13523), CCND1 (Cell Signaling 2922), EZH2 (Cell Signaling 5246), Tri-Methyl-Histone H3 (Lys27) (Cell Signaling 9733), Histone H3 (Cell Signaling 3638), PARP1 (Cell Signaling 9532), pH2A.X (Cell Signaling 9781), and BIM (Cell Signaling 2933) from Cell Signaling Technology (Beverly, MA); FLI1 (Abcam ab15289), NPY1R (Abcam ab91262), from Abcam (Cambridge, UK); Acetyl-Histone H3 (Lys27) (Active Motif 39133), from Active Motif (Carlsbad, CA). Secondary antibodies used were mouse IgG (GE Healthcare Life Sciences NXA931) and rabbit IgG (GE Healthcare Life Sciences NA934) GE Healthcare (Little Chalfont, United Kingdom). IgG (Santa Cruz sc-2027) for immunoprecipitation was from Santa Cruz Biotechnology (Dallas, TX). Olaparib (AZD-2281) was from Abmole (Houston, TX), A-1331852, navitoclax (ABT-263) and venetoclax (ABT-199) were kindly provided by AbbVie Inc. (North Chicago, IL), GSK-J4 and THZ1 were from Abmole (Houston, TX).

Western Blotting

Cell lines and tumor lysates were prepared using standard procedures (87) and lysis buffer (50mM Tris, 15mM NaCl, 1%NP-40, 1% SDS, 0.5% NaDOC, 1mM EDTA, 1mM EGTA, 10% glycerol, protease and phosphatase inhibitors), incubated on ice for 15 minutes and centrifuged at 10,000 rpm for 10 minutes. Tumor lysates were homogenized using the Tissuemiser (Fisher Scientific) in RIPA lysis buffer (15mM NaCl, 50mM Tris, 1%NP-40, 1%SDS, 0.5% NaDOC, glycerol, protease and phosphatase inhibitors), followed by a 30 minute incubation on ice and 10 cycles of sonication - 30 seconds on 30 seconds off (Bioruptor 300, Diagenode). Equal concentrations of lysates were run using the NuPAGE Novex Midi Gel system using 4-12% Bis-Tris Gels (Invitrogen), and transferred onto PVDF membranes (PerkinElmer). Membranes were blocked in 5% non-fat milk in TBST, primary antibodies were incubated overnight. Chemiluminescence was detected after incubation with SuperSignal West Femto (Thermo Fisher) using a Syngene G:Box camera (Synoptics).

Immunoprecipitation

Immunoprecipitation experiments were performed as previously described (87). A673 cells were lysed using the same buffer for western blotting experiments. 25 µl of protein A sepharose beads (GE Healthcare, Bio-Sciences) were added to the lysates followed by 0.5 µg of the indicated antibodies: BCL-2 (Cell Signaling 4223), H3K27ac (Diagenode C15410196), or rabbit IgG (Santa Cruz sc-2027). Samples were incubated with motion at 4°C overnight. Immunoprecipitated complexes were washed three times in the same lysis buffer and for IP's were run using 4-12% Bis-Tris Gels (Invitrogen), and

transferred onto PVDF membranes (PerkinElmer) in parallel with whole cell lysates containing 5% of the immunoprecipitation input. Membranes were blocked in 5% non-fat milk in TBST, primary antibodies were incubated overnight. Chemiluminescence was detected after incubation with SuperSignal West Femto (Thermo Fisher) using a Syngene G:Box camera (Synoptics). For ChIP, immunoprecipitated complexes were fixed using 1% formaldehyde and isolated, DNA was purified and Quantitative RT-qPCR of primers for the 5' region of the FLI1 binding site of putative enhancers was run on the 7500 Fast Real-Time PCR System (Applied Biosystems) measuring fluorescence of SYBR Green (Applied Biosystems). Primers used are listed in table 2.1 as described within each chapter. Results were normalized to the input chromatin using the Delta-Delta Cycle Threshold method.

Immunohistochemistry

BCL2 IHC was performed on a DAKO Omnis autostainer using Clone 124 (DAKO; predilute 10 minutes), with high pH antigen retrieval with standard HRP/DAB detection, using tonsil control. BCL- X_L IHC was performed using a Leica Bond autostainer using clone H-5 (Santa Cruz Biotech; 1:250), per manufacturer instructions and standard HRP/DAB detection, using manufacturer recommended control. Expression of BCL-2 and BCL- X_L: Cytoplasmic immunostaining in non-necrotic/preserved areas of whole sections was evaluated by surgical pathologist (SCS) in accordance with IRB HM20002579 and scored semi-quantitatively as 0 (negative); 1+ (weak positive); 2+ (moderate positive); or 3+ (strong positive). Proportion positive was scored as focal

(<10%); multifocal (10-50%), or diffuse (>50%). Images were taken using an Olympus DP73 using Olympus cellSens imaging, version 1.16.

Immunofluorescence

Cells were grown in 6-well plates on cover slips. Cells were treated for 24 hours with the indicated drug treatment. Following completion cells were fixed in cold methanol followed by a 10 minute incubation in 0.2% Triton X-100. Cells were then blocked in 5% normal goat serum with 0.1% tween in PBS for 1 hour at room temperature. Cells were incubated with pH2A.X (Cell Signaling 9718S) diluted with antibody buffer (1% BSA in 0.1% tween in PBS) and incubated in a humid chamber at 4°C overnight. Following incubation, Alexa Fluor 488 labeled antibody was added for 1 hour at room temperature. Cells were washed, and the nucleus was stained with DAPI. Slides were mounted and sealed with vectashield and imaged on under a zeiss axio observer 7 fluorescent microscope. Quantification of pH2A.X was performed using matching capture parameters in randomly selected regions of interest. Using ImageJ, images were converted to grayscale binary and individual cells were counted and analyzed based on pH2A.X fluorescent intensity as RFU (88).

Apoptosis

Cells were prepared using standard procedures described previously (89) and were seeded in triplicate. Cells were treated for 24 , 48, or 72 hours with the indicated drug treatment. Following treatment cells were stained with propidium iodide and Cy5-Annexin

V and analyzed using the Guava easyCyte FACS machine (Millipore). Cells were considered apoptotic if they stained positive for Annexin V alone or Annexin V and propidium iodide.

Cell Cycle Analysis

Cells were seeded in triplicate in 35mm dishes and treated as indicated. After 24 hours cells were trypsinized and re-suspended in binding buffer with 0.1% Triton in PBS and stained with Propidium Iodide, followed by incubation for 20 minutes at 37 °C and analyzed using the Guava easyCyte FACS Machine.

Cell Viability Assays

For CellTiter-Glo assays, dose response curves, and IC50 curves, cells were seeded at 3,000 cells per well in 96-well flat bottom black plates and treated the next day in quadruplicate with serial dilutions of the indicated drugs. After 72 hours, 25µl of CellTiter-Glo (Promega) was added to each well and read on a Synergy H1 Hybrid Reader (BioTek). For crystal violet staining, cells were seeded at a density of 50,000 cells per well in 35mm dishes. The next day cells were treated with the indicated drugs and allowed to grow for 3-5 days until the control (no rx) well grew to confluency. The cells were then fixed with glutaraldehyde (Sigma-Aldrich) and stained with 0.1% crystal violet (Sigma- Aldrich).

Cleaved Caspase-3 Activity Assays

Cells were seeded in quadruplicate at 5 x10^4 in a 96 well plate. After 24 hours, the medium was changed, and cells were treated for 24 hours with the indicated drug treatment. Cells were assayed for caspase-3 activity as per the manufacturer's protocol (Cell Signaling Technology, 5723S). Plates were read after a 2 hour incubation period.

RNA Isolation and RT-qPCR

Total RNA was isolated from cells grown at sub-confluency using the Quick-RNA MiniPrep Kit (Zymo Research) for olaparib/navitoclax treatments or the Isolate II RNA Mini Kit (Bioline) for GSK-J4/TZH1 treatments, and RNA was reverse-transcribed to cDNA using the iScript Adv cDNA Kit for RT-qPCR (BIO-RAD) on a GeneAmp PCR System 9700 (Applied Biosystems). Quantitative RT-PCR of reported primer sets and β-actin was run on the 7500 Fast Real-Time PCR System (Applied Biosystems) measuring fluorescence of SYBR Green (Applied Biosystems). Primers used as described in each chapter are listed in table 2.1. Results were normalized to *ACTB* using the Delta-Delta Cycle Threshold method. The melting curves of the primers are included in Figure 3.7.

Gene	Forward Primer	Reverse Primer
BCL2	CTGCACCTGACGCCCTTCACC	CACATGACCCCACCGAACTCAA
EZH2	GTTCAAAACTCGGGGGTGGT	CACCACTAGGAGCGGCCAG
ACTB	AGAGCTACGAGCTGCCTGAC	AGCACTGTGTTGGCGTACAG
NPY1R	CCATCGGACTCTCATAGGTTGTC	GACCTGTACTTATTGTCTCTCATC
STEAP1	GGCAATACTGGCTCTGTTGGCT	GCGTGTATTGTGCCCAGTAGAAG
PKRCB1	AAAGAGATCCAGCCCCCTTA	TATCAGTGGGGGTCAGTTCC
LOX	GCGACGACCCTTACAACC	GGACGCCTGGATGTAGTAGG
CCND1	TCGAGAGGCCAAAGGCTGGT	GGGGTTTTACCAGTTTTATTTCTAGAC
NPY1R	CCATCGGACTCTCATAGGTTGTC	GACCTGTACTTATTGTCTCTCATC
NPY1R (ChIP, putative enhancer)	TCATCCTTGGGCTTCTGTACC	AAGGACCCAGCTGCTTTTCAG
EZH2	AACCCGCAAGGGTAACAAA	TGATCACCGTTAACCATCATAACT
EZH2 (ChIP, putative enhancer)	CAGCTTTGCGGAAAAACTCCA	TGTGGTGGATGAACATCACTCTT
NKX2.2	CAGCGACAACCCGTACAC	GACTTGGAGCTTGAGTCCTGA
NKX2.2 (ChIP, putative enhancer)	GGCCCCTTGAGACAGGTTGA	CCTGAGGCCAAGTTTCCATCC

Table 2.1 List of Primers

Gene Expression and Knockdown Studies

The EWS-FLI1 Type1 fusion plasmid (plenti4-FLI1) and Empty Vector (plenti4-EV) was a gift from Miguel Rivera (26). To knockdown BIM, siRNA transfection was performed with Lipofectamine 2000 Transfection reagent (ThermoFisher, 11668-019) and Bim siRNA Hs_BCL2L11_5 FlexiTube siRNA (Qiagen, SI02655359). The siRNA ON-TARGETplus Non- targeting Pool (Dharmacon, D-001810-10-05) was used as a control and cells were treated 24 hours after transfection. To over express GFP, BCL-2 and BCL-X_L CHLA10 cells were transfected using Lipofectamine 2000 Transfection reagent (ThermoFisher, 11668-019) and GFP in a pCDNA3.1 vector (GenScript), BCL-2 in a pcDNA3.1, BCL-X_L in a pcDNA3.1 vector. 24 hours after transfection lysates were collected to confirm expression and cells were treated with olaparib for 24 hours before

measuring viability using CellTiter Glo. For EWS-FLI1 knockdown experiments, short hairpin RNA (shRNA) in a pLKO.1 vector was used (26) in parallel with a shRNA control scramble sequence (MISSION pLKO.1-shRNA control plasmid DNA), both shRNA have pLKO.1 puromycin-resistant backbones. shRNA transduction methodology has been previously described (87). For siRNA knockdown studies with TP53, siGENOME SMARTpool Human TP53 (ThermoFisher, M-003329-03) and siGENOME Control Pool Non-Targeting #2 (Dharmacon, D-001206-14-05) were used together with Lipofectamine 2000 and cells were treated with olaparib 24 hours after transfection.

Animal Experiments

For xenograft models, $5x10^6$ cells were injected subcutaneously into the flank of 6-8-week-old Nod/SCID gamma (NSG) mice. The Patient Derived Xenograft Models SA10233 and SA13542 were obtained from Crown Bioscience, TXE-270x and TXE-351x were obtained from the Childhood Cancer Repository (TXCCR.org), and $5x10^5$ cells were injected into the flank of NSG mice subcutaneously. Treatment began when tumors reached ~100-200mm^3 and mice were randomized into treatment cohorts. Tumor size and mouse weight was measured 3 days per week with a digital scale and calipers, where tumor volume was calculated as length x $width^2$ x 0.52. Navitoclax and olaparib were administered by oral gavage. Navitoclax was dissolved in 60% Phosal 50 PG, 30% PEG400, and 10% Ethanol, for a final dosage of 80mg/kg of body weight. Olaparib was dissolved in 10% hydroxypropyl-β-cyclodextrin for a final dosage of 100mg/kg of body

weight. GSK-J4 and THZ1 were administered by intraperitoneal injection (IP). GSK-J4 was dissolved into DMSO for a final dosage of 50mg/kg of body weight. THZ1 was dissolved 10% DMSO and D5W for a final dosage of 10mg/kg of body weight. All drugs were administered once per day 5 days/week. For pharmacodynamics studies, tumor bearing mice were treated with drug for 3 days, and tumors were harvested on the 3rd day 2 hours after the final treatment. Tumors were flash frozen in liquid nitrogen. For the blood toxicity study, NSG mice were treated with no drug (No Rx), navitoclax, olaparib, or the combination. At 3 and 7 days mice were exsanguinated, and blood was sent to IdexxBioResearch for testing. The recovery cohort was treated for 7 days and allowed 24 hours of recovery from treatment before exsanguination. All animal experiments were approved by the Virginia Commonwealth University Institutional Animal Care and Use Committee (IACUC protocol#AD10001048).

Dataset Analysis

The online database for publically accessible drug sensitivity data (www.cancerRxgene.org) was used to generate Figure 3.3C. The CCLE (90) was used to analyze expression between FLI1 and BCL-2 Figure 3.13D. The data analyzed for MCL-1 expression among sarcomas (Fig. 3.3D) was obtained from the R2 genomics analysis and visualization platform, r2.amc.nl/.

Statistical Considerations

For gene expression analyses and the complete blood count analysis (CBC), significance was determined using the non-parametric Mann-Whitney *U* test. Differences were considered statistically significant if $P < 0.05$. All other analyses were performed using the Student's *t* Test and considered statistically different if $P<0.05$. Asterisks indicate levels of significance ns($P \geq 0.05$), *($P < 0.05$), **($P < 0.01$), ***($P < 0.001$), ****($P < 0.0001$).

Synergy Assays

Cells were seeded at 3×10^3 cells in a 96-well plate. 24 hours after seeding, cells were treated with varied concentrations of navitoclax (0 to 2 μM) and olaparib (0.1 to 10 μM) for 72 hours, or cells were treated with varied concentrations of GSK-J4 (0 to 2.5 μM) and THZ1 (0.01 to 160 μM) for 48 hours followed, by measurement of cell viability by CellTiter-Glo. Percent viability was constrained to a maximum of 100. Percent over the bliss score was calculated as previously described (91).

Chapter 3 - The Ewing Family of Tumors Relies on BCL-2 and BCL-X_L to Escape PARP Inhibitor Toxicity

Introduction

The driving force behind oncogenesis in EWFT is the EWS-FLI1 translocation, which is currently undruggable, and effective targeted therapies for treatment remain elusive. Recent findings have highlighted the role EWS-FLI1 plays to induce a wide range of changes throughout the epigenome, affecting both histone marks and enhancers (26, 36, 73, 92, 93), leading to the simultaneous enhanced expression of tumor oncogenes and the reduced expression of tumor suppressors (26). However, these studies have yet to reveal specific, druggable targets with associated clinically available therapies. Due to the lack of any single druggable gene target responsible for EWFT oncogenesis, we have explored two different strategies to treat the disease.

The first approach is to directly target the epigenetic remodeling triggered by *EWSR1-ETS* fusions, in hopes of reversing their massive cellular reprogramming. Until recently, the mechanisms and full extent of EWS-FLI1 epigenetic reprogramming was unknown (24, 26, 39, 76). These new discoveries paired with the development of highly effective drugs capable of targeting histone modifications has paved the way for the development of epigenetic targeted therapies in EWFT. Utilizing these recent discoveries which have identified the epigenetic mechanisms of EWS-FLI1 gene activation through histone modifications and chromatin remodeling, we explored a strategy to

pharmaceutically reverse EWS-FLI1 mediated gene activation. This approach utilized the indirect inhibition of EWS-FLI1 and demonstrated robust anti-tumor efficacy and is further discussed in Chapter 4.

Our second approach sought to exploit drug sensitivities acquired during EWS-FLI1 genetic reprogramming. One consequence of the EWS-FLI1 fusion is an increase in DNA-RNA hybrids called R-loops, which are capable of sequestering and inactivating BRCA1. BRAC1 is critical for the repair of double stranded breaks through its interaction with RAD51 to influence the repair of DNA and maintain genome stability (56, 94). The sequestered BRCA1 leads to a deficiency in DNA repair, rendering EWFT acutely sensitive to DNA damaging agents which have been the focal point of current targeted therapy research (95-99). In this chapter, we sought a means of re-sensitizing EWFT to a promising class of DNA damaging agents which, despite the predicated sensitivity, EWFT tumors were inherently resistant to. Although the mechanisms of these two approaches differ greatly, they both explore unique therapeutic opportunities of targeting the aberrant transcription factor which drives EWFT by exploiting flaws in EWS-FLI1 driven reprograming.

Brenner and colleagues (100) and the Genomics of Drug Sensitivity in Cancer (GDSC), a high-throughput drug screening platform (101), first demonstrated in 2012 that *EWSR1-FLI1*- translocated ES display hypersensitivity to Poly(ADP-ribose) polymerase inhibition (PARP1i); this has since been replicated by several other groups (98, 99, 102). These data have provided a promising drug target for EWFTs, with corresponding FDA-approved PARP1 inhibitors (83). However, in the initial clinical study of olaparib in ES,

no objective responses were observed in 12 evaluable patients (83). While there were no objective responses, 4/12 patients achieved stable disease, with 2 of the 4 achieving minor responses (tumor shrinkage of 9% and 12%), indicating a modest level of efficacy via PARP1 inhibition in these patients.

Based on the hypersensitivity of ES to PARP1i *in vitro* and signs of activity in ES patients with olaparib, we sought to identify upfront resistance mechanisms to PARPi therapy as well as a rational drug combination that could overcome these mechanisms. We and others have shown that a low apoptotic response, even in the presence of growth arrest, mitigates response to targeted therapies (87, 103-107). We therefore hypothesized that mitigated responses of PARPi may be due to loss of apoptotic potential of EWFTs, which could prove particularly true in the chemo-refractory population. This hypothesis was further supported by the fact that deficient DNA damage repair is thought to contribute to, if not define, PARPi sensitivity in ES (99), as well as the established role of anti-apoptotic BCL-2 family proteins in protecting cancer cells from DNA damage-induced apoptosis (104, 108) and their inverse correlation of expression to cytotoxic agent sensitivity (8).

Results

A chemotherapy-naive and chemotherapy-resistant cell line pair respond differently to olaparib

Olaparib performed poorly in ES patients (83) whose tumors were heavily pre-treated and chemotherapy-resistant. We therefore utilized a pair of cell lines established from the same patient prior to and following chemotherapy treatment, at tumor relapse:

CHLA9 (Children's Oncology Group), cells were derived from the chemotherapy-naive PNET, positive for the EWS-FLI1 translocation, whereas the CHLA10 (Children's Oncology Group) cell line was established after four cycles of induction chemotherapy which included cisplatin, doxorubicin, cyclophosphamide and etoposide (109). We first assessed whether sensitivity to olaparib was different in the two cell lines. We found that the chemotherapy-naive cells were more sensitive to olaparib, as evidenced by a 5-day crystal violet viability assay (Fig. 3.1A, *left*), 72h dose-response curve (Fig. 3.1A, *right*), and IC50 curve (Fig. 3.8A) compared to the chemotherapy-resistant CHLA10 cells (Fig. 3.1A), despite both cell lines reportedly expressing high levels of *PARP1* (8, 110) and olaparib inducing similar growth arrest in both the CHLA9 and CHLA10 cells (Fig. 3.8B). In addition, similar levels of DNA damage was observed following olaparib treatment in both cell lines as evidenced by pH2A/X immunofluorescence staining (Fig. 3.9A and 3.9B). Furthermore, we confirmed the CHL10 cells were more resistant to chemotherapy compared to the CHLA9 cells. (Fig. 3.10A and 3.10B).

Chemotherapy-resistant CHLA10 ES cells do not undergo cell death in response to olaparib

Since the lack of robust apoptotic responses can underlie resistance to both chemotherapy and targeted therapies, and the apoptotic response following many chemotherapies and targeted therapies is largely governed by the BCL-2 family of proteins (103, 106, 111-113), we first explored the relationship between anti-apoptotic BCL-2 family expression and olaparib response in the CHLA9 and CHLA10 models. Expression

of BCL-2 was upregulated ($P < 0.05$) in the CHLA10 cells compared to the CHLA9 (Fig. 3.1B and Fig. 3.10C) relative to the sensitive CHLA9 cells, whereas expression of other key BCL-2 family members were not altered (Fig. 3.1B).

The increase in BCL-2 prompted us to evaluate BCL-2 expression in pre-treatment and post- chemotherapy biopsy samples from two ES patients treated at our cancer center. Interestingly, we did not detect an increase in BCL-2 expression in these specimens, in contrast to the cell line pair, however BCL-X_L expression was markedly higher in chemotherapy-resistant tumors (Fig. 3.1C) relative to the matched chemotherapy-naive samples. These data indicate that BCL-X_L is overexpressed in patients' ES tumors that have undergone chemotherapy, and our findings in models of EWFTs implicate BCL-2 as a cooperating partner with BCL-X_L in resisting apoptosis.

Together, these data indicated to us that both BCL-2 and BCL-X_L may be imperative in ES survival. We then moved to chemical interrogation of the cells with specific BCL-2 family inhibitors. Surprisingly, despite the increase in BCL-2, we found the BCL-2 specific inhibitor venetoclax (114) was unable to effectively sensitize CHLA10 cells to olaparib (Fig. 3.11A). Since increased expression of BCL-X_L is sufficient to induce resistance to venetoclax (115-117), we next tested the dual BCL-2/BCL-X_L inhibitor navitoclax (118, 119) to determine if this agent sensitizes the CHLA10 cells. While venetoclax showed little potentiation of olaparib (Fig. 3.11A and 3.11B), navitoclax sensitized CHLA10 cells to olaparib treatment compared to venetoclax ($P < 0.05$), leading to a near complete loss of cell viability (Fig. 3.1D), and showing mild synergy (Fig. 3.11C). Impressively, at low doses of olaparib (1 μM) where there was no single-drug

efficacy in the CHLA9 cells, the addition of navitoclax led to substantial loss of cell viability (Fig. 3.11D). Similar to venetoclax, the BCL-X_L selective inhibitor A-1331852 (120) was not effective at sensitizing CHLA10 cells to olaparib (Fig. 3.11E). Consistent with these findings, we found the CHLA9 cells underwent marked cell death in response to olaparib, as measured by cleaved PARP1 (Fig. 3.1E); in contrast, there was a near absence of a cell death response in the olaparib-treated CHLA10 cells (Fig. 3.1E). However, the addition of navitoclax led to marked cleavage of PARP1 in the presence of olaparib in the CHLA10 cells (Fig. 3.1E), despite the lack of modulation of BCL-2, BCL-X_L or the related MCL-1 (121) by olaparib (Fig. 3.1F).

These data indicate that EWFTs can lose their sensitivity to olaparib following chemotherapy treatment and relapse, underscored by their inability to undergo cell death, and can be rescued by the addition of navitoclax. This was further supported by the observation that, at low concentrations of olaparib where sensitive CHLA9 cells do not yet respond to single-agent olaparib, navitoclax also sensitizes to olaparib (Fig. 3.11D). "In addition, the CHLA9 cells have functional p53, while the CHLA10 cells have non-functioning p53 (32). It is well established that functional p53 is capable of binding to and antagonizing the anti-apoptotic functions of BH3 proteins such as BCL-2 and BCL-X_L (6, 122). In order to rule out p53 as the cause of inherent resistance to olaparib induced apoptosis in the CHLA10 cells when compared to the CHLA9 cells, we used siRNA to knockdown TP53 in the CHLA9 and found no difference in olaparib sensitivity (Fig. 3.11F *left*), consistent with a previous report (123). To further support the role of BCL-2 and/or BCL-X_L overexpression in apoptotic resistance to olaparib treatment we overexpressed

BCL-2 or BCL-X_L in the CHLA9 cells. Here, we saw a significant increase in resistance to olaparib treatment in cells overexpressing BCL-2 or BCL- X_L compared to the GFP controls ($P < 0.0001$) (Fig. 3.12A). Together these data reveal a striking interplay between BCL-2/X_L inhibition and PARPi in ES.

Navitoclax and Olaparib cooperate to inhibit tumor growth in a CHLA10 mouse model

We next grew CHLA10 tumors in NSG mice, and evaluated single-agent olaparib, navitoclax, and the combination of olaparib and navitoclax to see if the *in vitro* results would translate *in vivo*. Consistent with the cell culture experiments (Fig. 3.1D and E), we found the CHLA10 tumors were not sensitive to olaparib or navitoclax as a monotherapy compared to their combination (Fig. 3.1G). However, the combination of olaparib and navitoclax demonstrated robust inhibition of tumor growth (Fig. 3.1G). This contrasted with the venetoclax/olaparib combination, which was ineffective (Fig. 3.1H), consistent with the *in vitro* results (Fig. 3.11A). The olaparib and navitoclax combination did not induce substantial weight loss in the mice or any overt signs of toxicity, suggesting the combination is well tolerated (Fig. 3.12B).

To assess possible hematologic toxicity when using olaparib and navitoclax in combination we performed a complete blood count on NSG mice *in vivo*. Red blood cell and reticulocyte counts were not significantly affected by the combination. We did observe a significant decrease in platelet count as well as neutrophil count following navitoclax treatment that has previously been reported with its use (114), however,

importantly, olaparib did not augment platelet loss at either time point. Also of importance, there was no augmentation of neutropenia or other toxicity by the combination compared to any single-agent dosing at either time point (Fig. 3.2). As thrombocytopenia is the major dose limiting effect of navitoclax (124). we also assayed populations of cells following a 24hr recovery period after 7 days of treatment. Impressively, these mice nearly fully recovered pre-treatment platelet levels (Fig. 3.2). These data demonstrate olaparib plus navitoclax may be both effective and tolerated as a novel combination therapy in EWFTs.

Most ES cell lines do not undergo marked apoptosis following olaparib therapy

Following our findings in the CHLA9 and CHLA10 pair, we next expanded to a panel of ES cell lines to determine the ability of olaparib to induce apoptosis. A kin to CHLA10, these cells had poor apoptotic responses to olaparib (Fig. 3.3A), in contrast to the CHLA9 cells. However, all ES cells underwent G_2/M accumulation, as previously reported (Fig. 3.12C) (96). Caspase 3 activity confirmed both the differential apoptosis between the CHLA9 cells and other EWFTs lines, as well as the apoptosis sensitization by navitoclax (3.10A). These data suggest our findings of mitigated apoptotic responses to olaparib uncovered in the CHLA10 cells extend to other EWFT models.

We next determined whether these other resistant EWFT models had higher levels of BCL-2 or BCL- X_L, as our model would predict. Indeed, in comparison to the CHLA9 cells, these models had higher levels of BCL-2 and/or BCL-X_L (Fig. 3.3B), associated with their poor apoptotic responses to olaparib (Fig. 3.3A). We have uncovered an important

role for both BCL-2 and BCL-X_L in olaparib response in EWFT (Fig. 3.1 and 3.3), and it would strengthen the case of the importance of BCL-2 and BCL-X_L in EWFT survival if these cancers were sensitive to pharmaceutical targeting of these two proteins. We therefore examined in the updated GDSC screen (www.cancerRxgene.org) whether ES cells were more sensitive to navitoclax (Fig. 3.3C) compared to all other solid tumor cell lines grouped together. In fact, ES cell lines were substantially more sensitive ($P=8.69*10^{-5}$), with 8/21 cell lines demonstrating IC50s of 700nM and below (Fig. 3.3C). To corroborate the sensitivity to navitoclax, we analyzed *MCL1* expression which is capable of conferring resistance to navitoclax. Examining RNA expression in sarcomas with translocation events using the R2 platform we found EWS-FLI1 translocated sarcomas expressed lower levels of *MCL1* emphasizing their reliance on *BCL2* and *BCL2L1* for survival (Fig. 3.3D).

Interestingly, expression of EWS-FLI1 in HEK293T cells led to higher BCL-2 transcript levels ($P < 0.05$) compared to the empty vector control, with consistent BCL-2 protein changes (Fig. 3.13B and S3.7C); the FLI1 target genes *EZH2* (81), *STEAP1*, and *PRKCB* (22, 125, 126) were all significantly upregulated as well (Fig. 3.13B). To further evaluate the relationship of FLI1 and BCL-2, we probed the cancer cell line encyclopedia (90) and found a positive correlation ($P < 0.0001$) between FLI1 and BCL-2 (Fig. 3.13D); knockdown of EWS-FLI1 confirmed decrease of BCL-2 expression with the expected decrease in *EZH2* expression (Fig. 3.13E), and de-suppression of the EWS-FLI1 target *LOX*, and *STEAP1*, *NPY1R* and *PRKCB* were all downregulated following EWS-FLI1 downregulation, albeit not all significantly (22, 125, 126). Altogether, these data further

demonstrate the importance of BCL-2 and BCL-X_L in EWFTs, which appear to play complimentary roles, constituting a critical survival signal for EWS-FLI1 driven EWFT.

Navitoclax sensitizes a panel of ES cells to olaparib

We moved to validate navitoclax as a sensitizing agent to olaparib in EWFT cells, as was determined in the CHLA9 and CHLA10 pair (Fig. 3.1). In fact, we noted marked sensitization by navitoclax to olaparib-induced apoptosis in a panel of ES cells as evidenced by cleaved PARP1 (Fig. 3.4A) and FACS measurement of Annexin-V positive cells (Fig. 3.4B). Consistent with the CHLA pair, apoptosis sensitization was sufficient for navitoclax to markedly reduce total viable cells as determined by both crystal violet assays (Fig. 3.4C) and 72h cell-viability assays (Figs. 3.4D and 3.4E). These data again indicate that olaparib induced apoptosis can be rescued by the addition of navitoclax in ES.

Navitoclax sensitizes ES cells to olaparib by augmentation of DNA damage and disruption of BIM complexes

We next examined the DNA damaging activity of the olaparib/navitoclax combination using pH2A/X immunofluorescence staining as a marker for DNA damage. Interestingly, the DNA damage observed following olaparib exposure was substantially increased ($P < 0.0001$) with the addition of navitoclax, which by itself did not induce DNA damage (Fig. 3.5A and Fig. 3.14A). These data are consistent with a direct role of BCL-2 and BCL- X_L in the augmentation of DNA damage (127).

Navitoclax disrupts BIM:BCL- X_L and BIM:BCL-2 complexes, to induce apoptosis (106, 128-130), and can sensitize kinase inhibitors in different cancers through modulation of the BCL-2 family (reviewed in ref (36)). We therefore asked whether reduction of BIM protected from the olaparib/navitoclax combination. As demonstrated in Fig. 3.5B, reduction of BIM by siRNA led to a concomitant loss in cleavage of PARP1. Immunoprecipitation of BIM complexes verified navitoclax disrupted BIM:BCL-2 complexes (Fig. 3.5C and Sup. Fig. 3.14B and 3.14C). These data indicate that olaparib/navitoclax induce apoptosis in EWFTs through disruption of BIM complexes, whereas this complex disruption leads to BIM-mediated apoptosis (130, 131). Together, these data demonstrate multiple mechanisms in which navitoclax sensitizes ES to olaparib.

Mouse models of ES are sensitive to Olaparib plus Navitoclax

To robustly test this novel combination of olaparib and navitoclax, we expanded our analyses to three models of ES; the SK-ES-1 xenograft (ATCC® HTB-86™), and two patient-derived xenografts (PDXs). Mice were treated daily with olaparib (100mg/kg), navitoclax (80mg/kg), or the combination of olaparib (100mg/kg) + navitoclax (80mg/kg). In all three models, there was limited activity of either agent when dosed as a monotherapy. However, the combination of olaparib and navitoclax markedly inhibited tumor growth in the SK-ES-1 model and PDX SA10233 and, impressively, almost completely shrank tumors in the other PDX model, SA13542 (Fig. 3.6A and 3.6B). Again, the combination did not markedly affect mouse weights or induce any overt signs of toxicity (Fig. 3.12B). Assessment of the tumor lysates from the PDX confirmed marked

apoptosis induction with the combination, but not single-agents (Fig. 3.6C), and that both PDX models expressed BCL-X_L and with the SA10233 model expressing high levels of BCL-2 (Fig. 3.14D) confirming RNA sequencing data on *BCL2* mRNA expression levels between the two PDX models (SA10233 3.5045, SA13542 0.672) . These data, along with the CHLA10 chemorefractory mouse model (Fig. 3.1G), demonstrate compelling activity of the combination of olaparib and navitoclax *in vivo.*

Discussion

Through an unbiased high-throughput drug screen, olaparib was discovered to have marked *in vitro* activity in ES (101). Despite several reports demonstrating hypersensitivity of ES to PARP1 inhibition (8, 98-100, 102, 132), subsequent clinical evaluation in a heavily pre-treated cohort of ES patients with single-agent olaparib showed only modest efficacy (83). Here, we demonstrated an important role for deficient apoptosis following olaparib therapy in ES, with the anti-apoptoticproteins BCL-2 and BCL-X_L playing key roles. We believe these experimental findings at least in part explain the disappointing clinical data.

PARP inhibitors prevent single-stranded (ss) DNA break repairs. This mechanism underlies PARPi activity in BRCA-deficient cancers, which are inherently deficient in double-stranded (DS) DNA break repair (94). In ES, PARPi sensitivity has been proposed to occur for several reasons: First, PARP1 expression is higher in Ewing sarcoma (133), probably as a direct result of EWS-FLI1 (100, 133), and higher PARP1 expression is a cause of enhanced PARP inhibitor sensitivity (134), most likely through the mechanism of

PARP trapping at ssDNA breaks (135-137). Second, ES, like BRCA- deficient cancers, appear to have a deficient dsDNA repair system (99). Third, FLI1 drives high *SLFN11* expression (138), a gene tightly linked to DNA-damaging agent efficacy (90, 139). Fourth, EWS-FLI1 expression is sufficient to increase dsDNA breaks (100). Fifth, EWS-FLI1 causes R-loop accumulation, increased replication stress and interferes with BRCA1 function (56).

Although there are several factors that may have contributed to olaparib's lack of efficacy in patients with chemotherapy-resistant ES, it is likely that a biological resistance mechanism served to rescue tumor cells from direct PARP inhibition. We propose that there is an inherent deficiency in many ES to undergo apoptosis following olaparib treatment resulting from a protective effect of BCL-2 and BCL-X_L (Fig. 3.1 and Fig. 3.3). Furthermore, exposure and resistance to chemotherapy appears to contribute to this state of apoptotic resistance to olaparib, as evidenced by our results in the CHLA10 cell line (Fig. 3.1E and 3.3A) and observations in patients' tumor specimens (Fig. 3.1C). It is likely that DNA damaging agents used in induction chemotherapy lead to additional pressure on the ES tumor and, as a result, the emergence of cells particularly reliant on BCL-2/BCL-X_L for survival. Overall, further studies will be necessary to elucidate the precise relationship between these pro-survival BCL-2 members and ES tumorigenesis.

The strategy to sensitize ES to PARPi via BCL-2/BCL-X_L co-inhibition is different from other explored strategies to sensitize ES to PARPi; these include the addition of DNA damaging agents that intensifies the amount of active DNA damage in the cell, like irinotecan and temozolomide (102). Temozolomide has also been demonstrated to enhance

PARP1 trapping (137) and, interestingly, the combination of temozolomide and PARPi cooperatively downregulates MCL-1, sensitizing to mitochondrial-mediated death (102). Although temozolomide-PARPi combinations are poorly tolerated in preclinical ES mouse models (99), irinotecan delivered to an orthotopic ES mouse model in dosing schedules consistent with the pediatric population demonstrated marked activity (99). Consistent with these results, the combination of the PARPi veliparib and irinotecan was well tolerated in a recent phase I trial, including reaching a dose sufficient for PARP inhibition in adult cancers (140). Interestingly, BCL-X_L blocks the ability of irinotecan to induce apoptosis and BCL-X_L inhibition results in a switch from irinotecan-induced senescence to apoptosis (141). Therefore, it is possible that PARPi/irinotecan combinations in other ES models will face the same issues we have found PARPi monotherapy to face, namely a refractory apoptosis response. The PARPi/irinotecan combination is currently being evaluated in pediatric patients with solid tumors (NCT02392793).

The BCL-2 family of proteins monitors the integrity of the mitochondria and integrates the signals of many pathways at the mitochondria (142). Importantly, Javaheri and colleagues (59) elegantly demonstrated that EWS-FLI1 overexpression in mesenchymal stem cells, the presumed cell of origin for ES, was sufficient for blocking differentiation but led to high rates of apoptosis; retrovirus containing BCL-2, BCL- X_L or MCL-1 expression plasmids was able to rescue apoptosis, and importantly, led to sarcoma formation, which was not accomplished in the parallel, control transduced cells. These data together with the data in this manuscript present a compelling case where anti-apoptotic

activity of BCL-2 family members, particularly BCL-2 and BCL- X_L, play an intricate role in ES tumorigenesis and impact ES therapy.

It has been well known for several decades that BCL-2 has a protective role against DNA damage-induced apoptosis (127, 143). Additionally, BCL-X_L expression has been reported tocorrelate inversely with the sensitivity of cancer cell lines to multiple anti-tumor agents, including those acting via a DNA-damaging mechanism (8). This becomes particularly relevant in the light that ES have deficient DNA damage responses (99). Adding to the intrigue, Khan and colleagues recently reported 13% of patients with ES have germline loss-of-function mutations in DNA repair genes (95). It is therefore tempting to speculate that, in order for EWS-FLI1- translocated ES to develop and thrive, there must be an acquired reliance on the anti-apoptotic proteins BCL-2 and BCL-X_L to maintain survival. Consistent with this notion, our analyses of HTS data revealed navitoclax has substantial single-agent activity (IC50 less than 700nM) across ~40% of ES cell lines (Fig. 3.3C).

This notion is further supported by our findings in the CHLA cells derived from a patient prior to and following chemotherapy treatment. The post-chemotherapy CHLA10 cells, derived at progressive disease, had higher BCL-2 expression relative to the matched chemotherapy-naive CHLA9 cells (Fig. 3.1B) and, unlike CHLA9 cells, failed to undergo cell death following olaparib therapy (Fig. 3.1E and 3.3A). It is important to note that we did not account for other changes that occurred during the acquisition of chemotherapy resistance in this model, which could contribute to the resistance of these cells to olaparib. For instance, Sorensen and colleagues demonstrated the CHLA10 cells have enhanced flux

compared to the CHLA9 cells through the PI3K pathway, which is a result of increased ErbB4 expression (144) and which may be contributing to olaparib resistance. Notwithstanding, the fact that navitoclax was sufficient to re-sensitize the cells to olaparib reflects the importance of BCL-2 and BCL-X_L. Interestingly, in the chemotherapy-naive CHLA9 cells, where olaparib was very effective (Fig. 3.1A), navitoclax fully sensitized these cells to a low dose of olaparib (Fig. 3.11D), which did not have marked single agent anti-cancer activity. These data reveal an important interplay between PARP inhibition and BCL-2/X_L inhibition, which likely contributes to the impressive activity of dual PARP and BCL-2/X_L inhibition in ES (Figures. 3.1, 3.3 and 3.4), and, again, supports the notion that BCL-2 and BCL-X_L are important to counteract the intrinsic deficiencies in ES DNA damage repair, which are exacerbated by PARP inhibition. Indeed, BCL-2/BCL- X_L inhibition causes accumulation of DNA damage following PARP inhibition (Fig. 3.9A and Fig. 3.13A). Therefore, the robust activity of PARP inhibition and navitoclax is most likely due to both BCL-2 and BCL- X_L inhibition making these cells more vulnerable to DNA damage-induced apoptosis, but also increasing the DNA damage itself. The result is a substantial increase in apoptosis (Fig. 3.4A-B), mediated by BIM (Fig. 3.5B and 3.5C), which translates to impressive *in vivo* activity.

Overall, we demonstrate ES tumors do not undergo a marked apoptotic response following olaparib therapy; however, co-targeting BCL-2 and BCL-X_L dramatically sensitizes these tumors to olaparib in several mouse models of ES, including chemotherapy-resistant ES and two PDX models of ES. As we found neither drug augmented hematological toxicity of the other (Fig. 3.2), and rational navitoclax-based

combinations with other targeted therapies are ongoing in clinical trials (e.g. NCT02520778), evaluation of PARP inhibitors and navitoclax in ES are warranted.

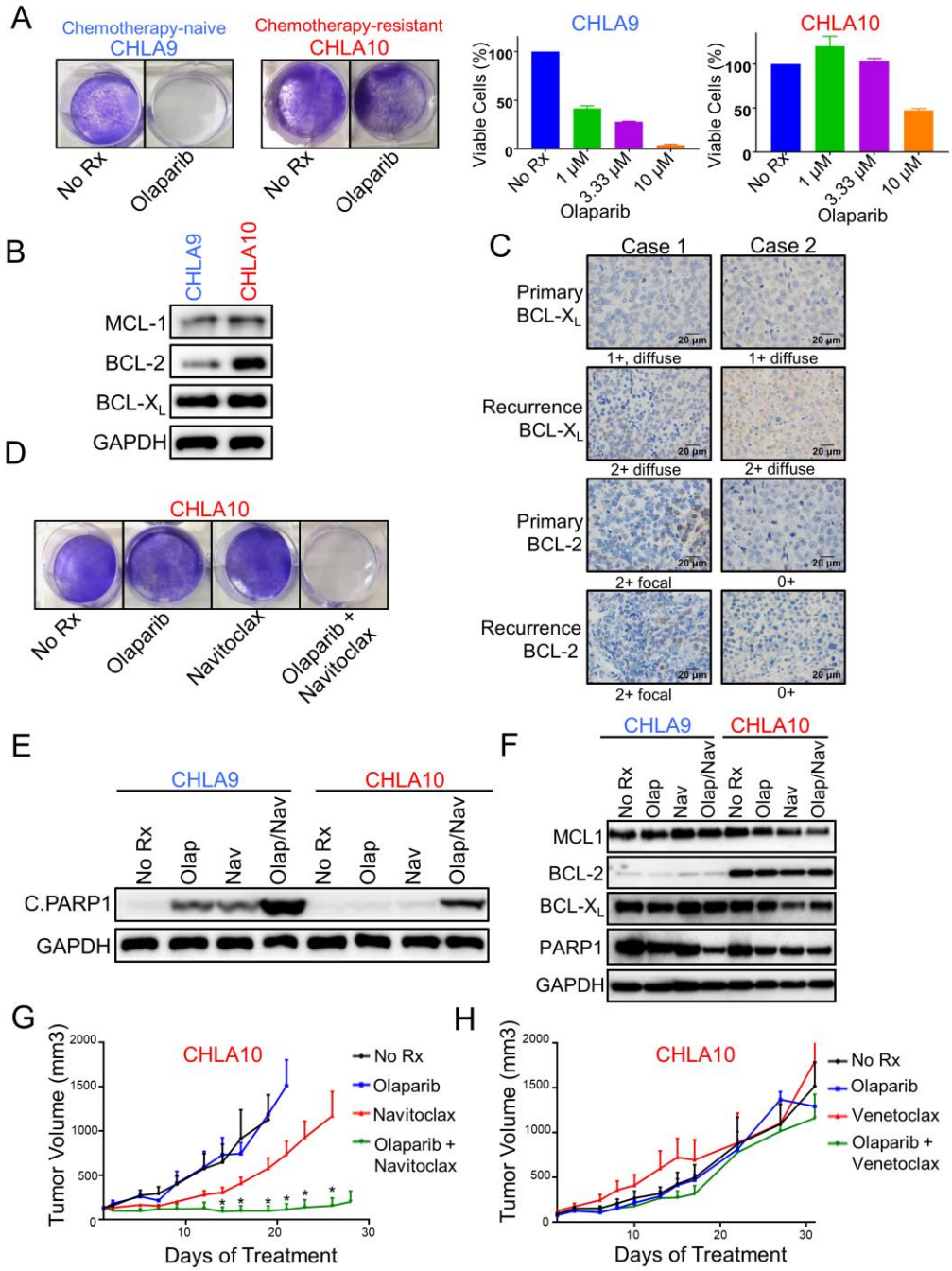

Figure 3.1 Chemotherapy-resistant EWFT are sensitized to olaparib with the Inhibition of BCL-2 and BCL- X_L

(A) (*left)* Crystal violet staining of CHLA9 and CHLA10 after 5-day treatment showing sensitivity to no treatment control (no rx) or 5 μM olaparib. (145) 72 hour CellTiter Glo of CHLA9 and CHLA10 using the indicated concentrations of olaparib. (B) Western blot analysis of the indicated antibodies in chemotherapy-naive and chemotherapy-resistant

Figure 3.1 continued

paired lines. (C) Two cases of Ewing sarcoma with available paired primary and recurrent metastatic tissues were immunostained for BCL-2 and BCL-X_L. In both cases, similar expression of BCL-2 was noted in primary. For BCL-X_L, however, increased expression was noted in both recurrences compared to the primary tumor. Case 1: Primary: Archival sections of the untreated biopsy of the primary tumor (patella), which was localized at presentation. Recurrence: Lung metastasis 5 years subsequent, after systemic chemotherapy (VAC-IE) and localized radiotherapy to the patellar primary site. Case 2: Primary: Archival sections of the biopsy of the untreated primary tumor (thoracic spine), which was metastatic (rib, lung, bone marrow) at presentation. Recurrence: Bone metastasis (right humerus) 8 months subsequent, after systemic chemotherapy (VAC-IE) and localized radiotherapy to the primary and multiple metastatic sites. (D) Crystal violet staining showing olaparib resistant CHLA10 cells after 5-day treatment with no treatment control (no rx), 5 µM olaparib, 1 µM navitoclax or the combination of 5 µM olaparib + 1 µM navitoclax. (E) Western blot analysis of apoptosis indicated by an increase in cleaved PARP1 in CHLA9 and CHLA10 cells after 24 hour treatment with no treatment control (no rx), 5 µM olaparib, 1 µM navitoclax, or 5 µM olaparib + 1 µM navitoclax. (F) Western blot analysis of the indicated antibodies in the CHLA9 and CHLA10 cell lines after 24 hour treatment with no treatment control (no rx), 5 µM olaparib, 1 µM navitoclax, or 5 µM olaparib + 1 µM navitoclax. (G) CHLA10 xenografts treated daily with olaparib (100mg/kg), navitoclax (80mg/kg), or the combination of olaparib (100mg/kg) + navitoclax (80mg/kg) for 28 days. Error bars are +SEM. Asterisks indicate a significant separation between the combination (olap/nav) and all other treatment cohorts using the student's *t* test ($P < 0.05$) (H) CHLA10 xenografts treated daily with olaparib (100mg/kg), venetoclax (100mg/kg), or the combination of olaparib (100mg/kg) + venetoclax (100mg/kg) for 27 days. Error bars are +SEM

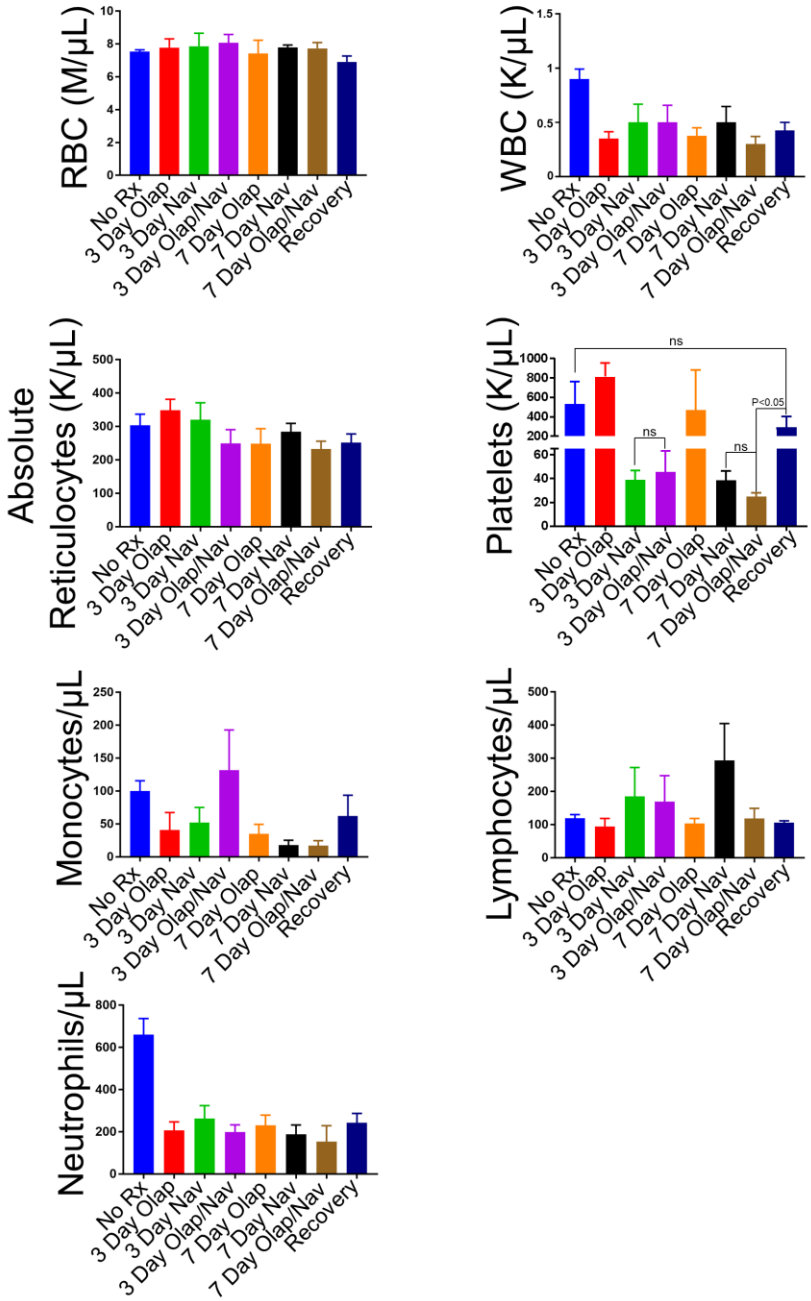

Figure 3.2 Combination of olaparib and navitoclax does not augment toxicity

(A) NSG mice were treated with a no treatment control (no rx), olaparib (100mg/kg), navitoclax (80mg/kg), or the combination of olaparib (100mg/kg) + navitoclax (80mg/kg). After the indicated 3 or 7 day treatment period, blood was collected and sent to IDEXX BioResearch (idexxbioresearch.com) for a complete blood count. The recovery cohort was

Figure 3.2 continued

treated for 7 days with the combination of olaparib (100mg/kg) + navitoclax (80mg/kg) and allowed 24 hours without treatment before blood was collected. Asterisks indicate a significant separation between 7 day treatment with olaparib + navitoclax and 7 day recovery using the Student's *t* Test ($P<0.05$). 3 day treatment with navitoclax not significant compared to 3 day treatment with the combination olaparib + navitoclax, neither was 7 day navitoclax compared to 7 day olaparib + navitoclax.

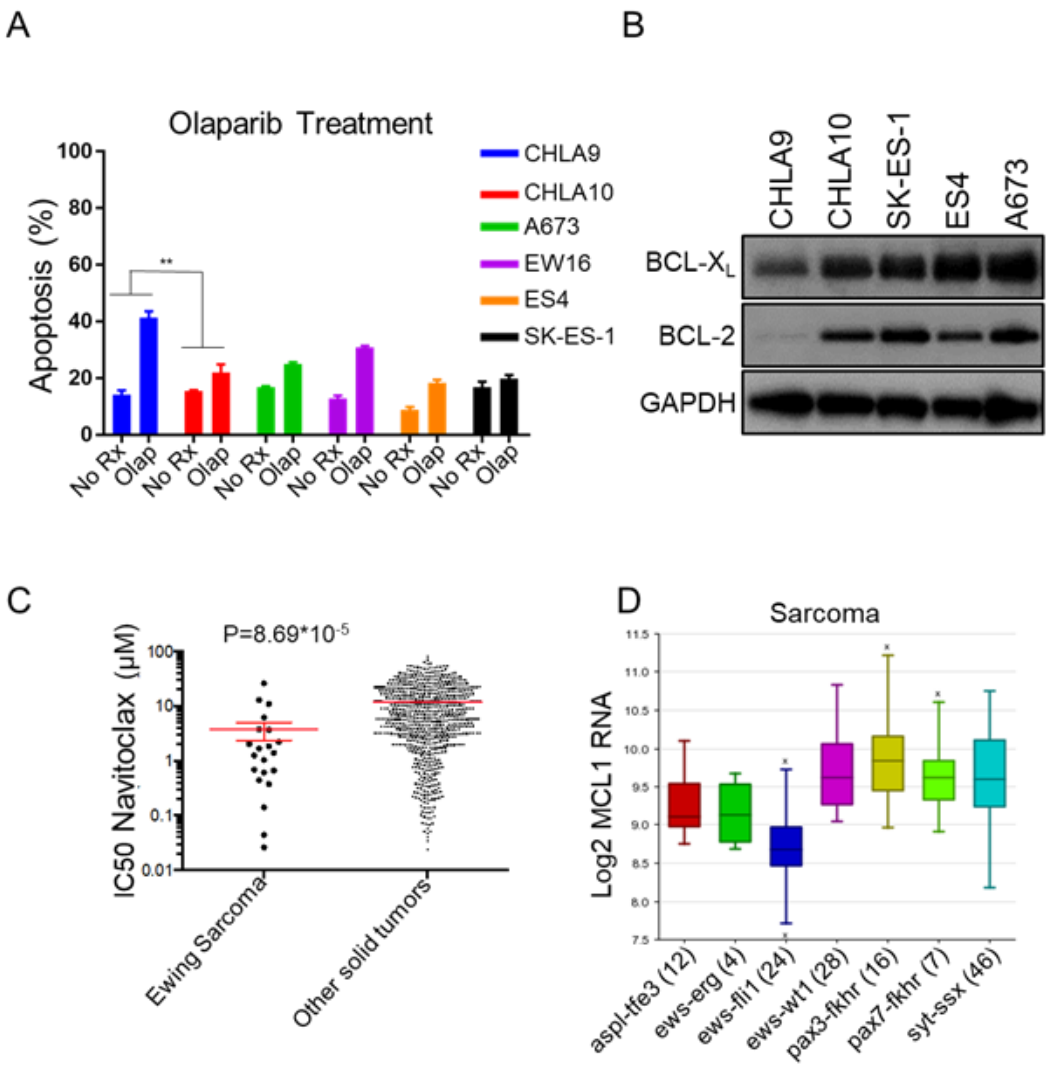

Figure 3.3 EWFT are resistant to olaparib which correlates with increased BCL-2 and navitoclax sensitivity

(A) FACS analysis of apoptosis after 24 hour treatment with 5 μM olaparib. Error bars are +SEM. Asterisks indicate a significant separation between olaparib treatments in the CHLA10 cells compared to CHLA9 cells, using the student's *t* test ($P < 0.05$) (B) Western blot analysis of the indicated antibodies in EWFT cell lines. (C) IC_{50} of navitoclax plotted for solid tumor cell lines and 21 Ewing Sarcoma cell lines from http://www.cancerrxgene.org/. A Mann-Whitney non-parametric test was performed ($P=8.69*10^{-5}$) (D) **)** MCL-1 RNA expression in sarcomas with translocation events (34).
.

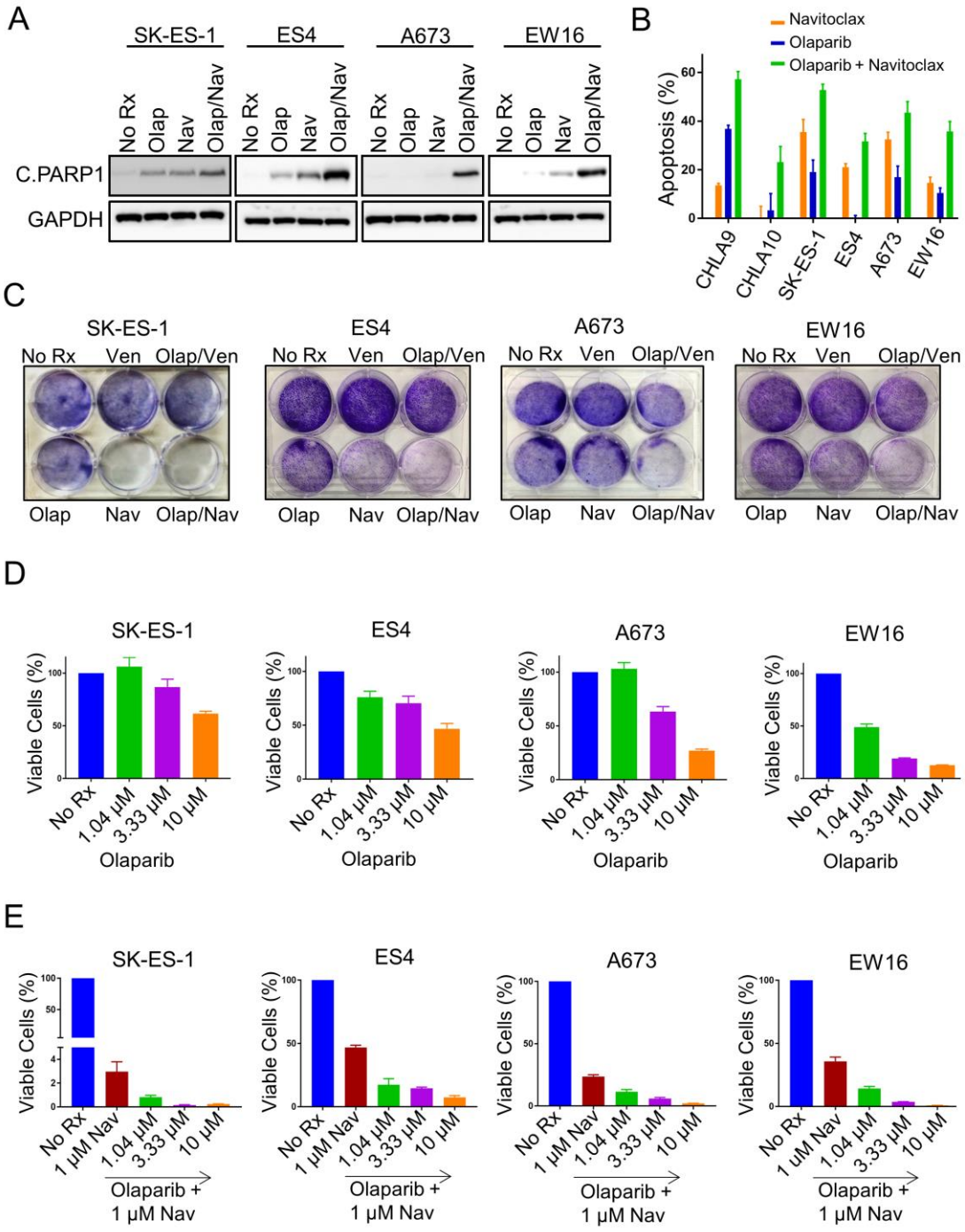

Figure 3.4 Combination of olaparib and navitoclax is effective in multiple EWFT cell lines

Figure 3.4 continued

(A) Western blot analysis of apoptosis indicated by cleaved PARP1 after 24 hour treatment with no treatment control (no rx), 5 µM olaparib, 1 µM navitoclax, or 5 µM olaparib + 1 µM navitoclax. (B) FACS analysis of apoptosis after 24 hour treatment with 5 µM olaparib, 1 µM navitoclax, or 5 µM olaparib + 1 µM navitoclax. Percent of apoptosis induced by drugs is normalized to the no treatment control. Error bars are +SEM. (C) Crystal violet staining after 5-day treatment with 5 µM olaparib, 1 µM navitoclax, or 5 µM olaparib + 1 µM navitoclax. (D) Dose response curves in ES cell lines after 72 hour treatment with increasing concentrations of olaparib. Viability was determined using CellTiter-Glo. Data is graphed as percent viable cells from no treatment control (no rx), performed in quadruplicate. Error bars are +SEM. (E) ES cell lines after 72 hour treatment with 1 µM navitoclax or 1 µM navitoclax in the presence of increasing concentrations of olaparib and viability was determined using CellTiter-Glo. Data is graphed as percent viable cells from no treatment control (no rx), performed in quadruplicate. Error bars are +SEM.

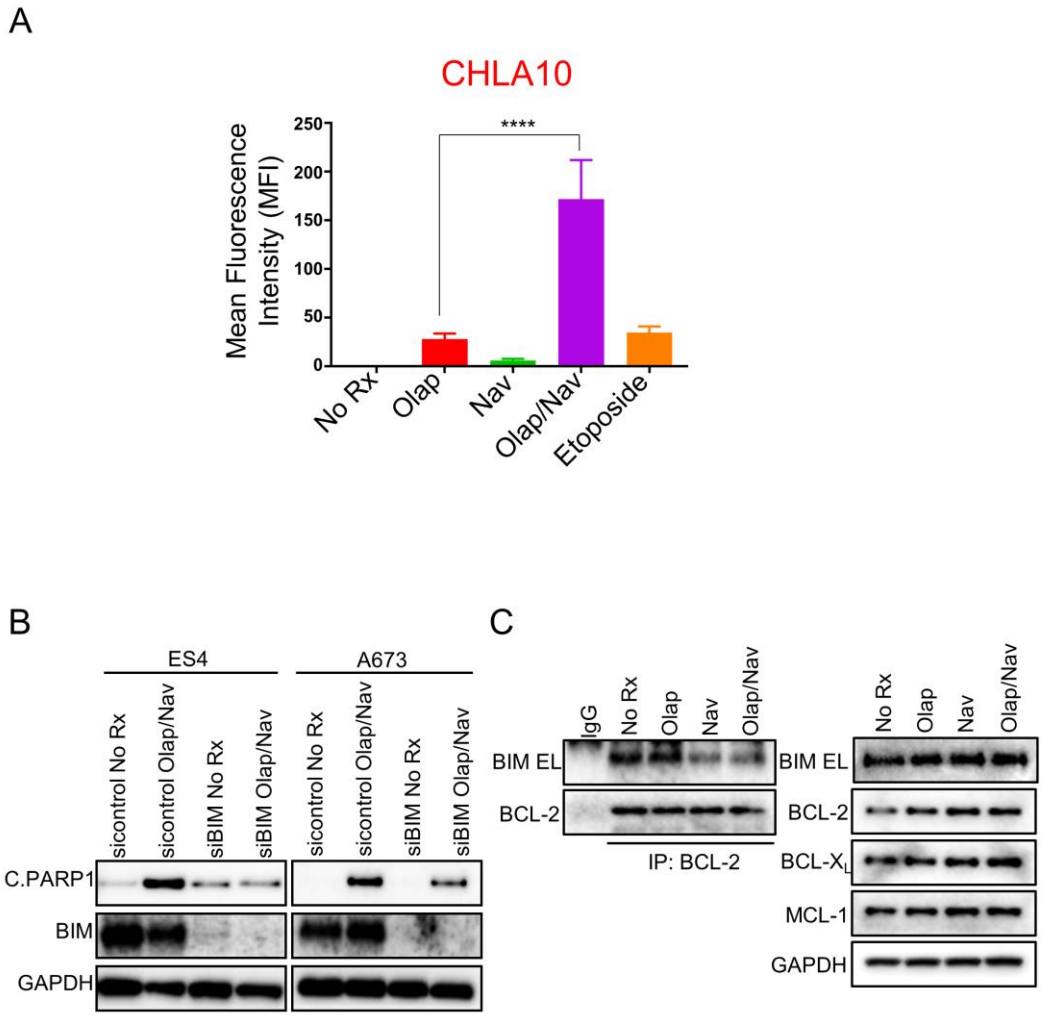

Figure 3.5 DNA damage is increased with the combination of olaparib and navitoclax

(A) Quantification of immunofluorescence images probed for γH2A.X foci intensity following 24 hour treatment using no treatment control (no rx), 5 μM olaparib, 1 μM navitoclax, 5 μM olaparib + 1 μM navitoclax or 1 μM etoposide. Error bars are +SEM. Asterisks indicate a significant separation between olaparib treatment and the combination olaparib + navitoclax. Significance was determined using the Mann-Whitney *U* test. (B) siRNA knockdown of BIM or control (scramble sequence) in ES4 and A673 cell lines followed by 24 hour treatment with either no treatment control (no rx) or 5 μM olaparib + 1 μM navitoclax (Nav/Olap). (C) An immunoprecipitation of lysates from A673 cells using either a BCL-2 antibody or an IgG control antibody (*left*) and the whole cell lysates (5% input) (145), after 4 hour treatment with 5 μM olaparib, 1 μM navitoclax, or 5 μM olaparib + 1 μM navitoclax.

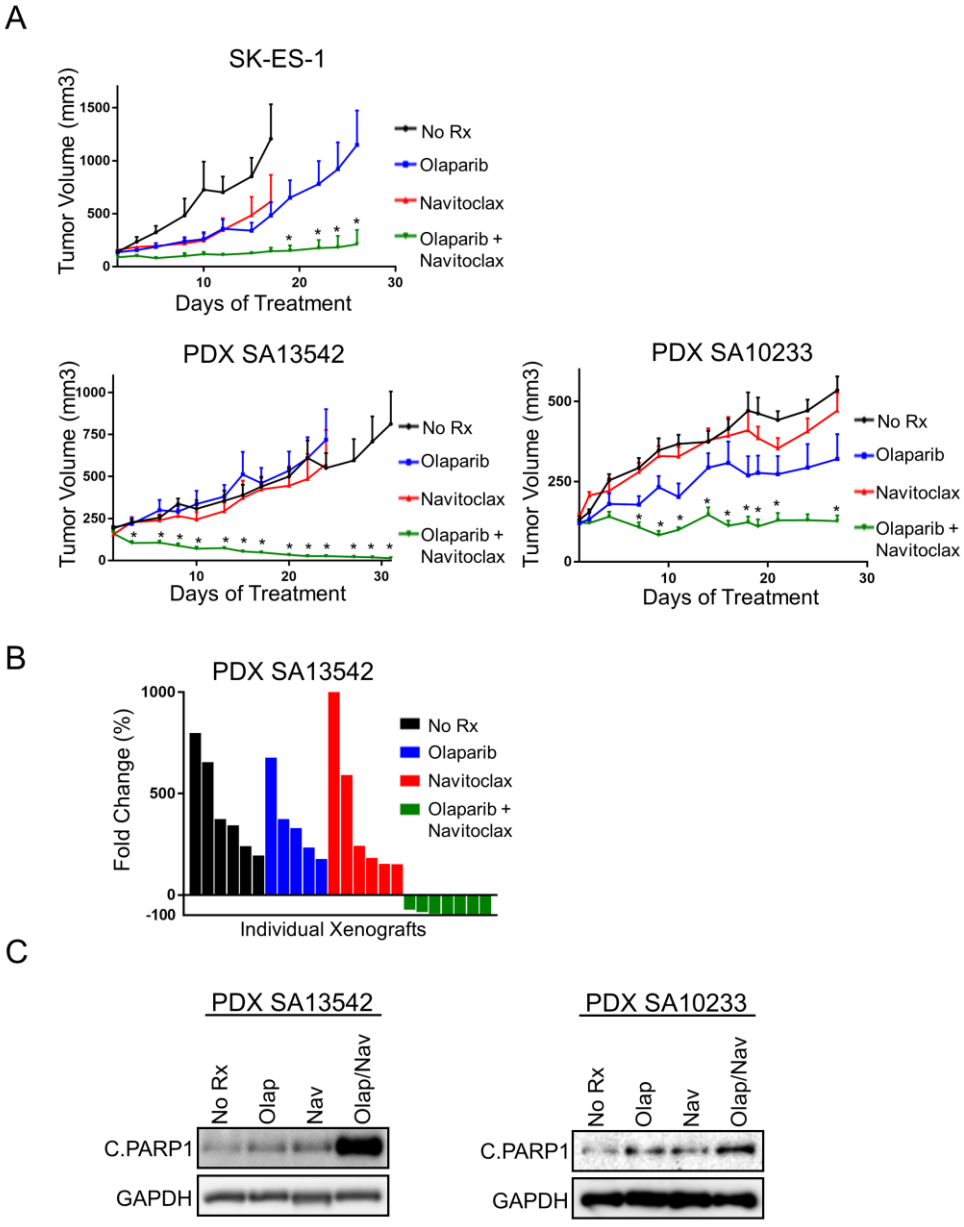

Figure 3.6 Olaparib and navitoclax combination is effective in Mouse Models of EWFT

(A) SK-ES-1 xenografts treated daily for 26 days (*top*) and patient-derived xenografts (*bottom*) treated daily for 31 days (PDX SA13542) or 27 days (PDX SA10233) with olaparib (100mg/kg), navitoclax (80mg/kg), or the combination of olaparib (100mg/kg) + navitoclax (80mg/kg). Error bars are +SEM. Asterisks indicate a significant separation between the combination (olap/nav) and all other treatment cohorts using the student's *t*

Figure 3.6 continued

test ($P < 0.05$) (B) Fold change in tumor volume, please note data is from the experiment shown in Fig. 4A (PDX SA13542) after 31 days of treatment and the x axis denotes individual xenografts. (C) Western blot analysis of cleaved PARP1 from PDX tumor lysates after 3 daily treatments of no treatment control (no rx), olaparib (100mg/kg), navitoclax (80mg/kg) or the combination of olaparib (100mg/kg) + navitoclax (80mg/kg).

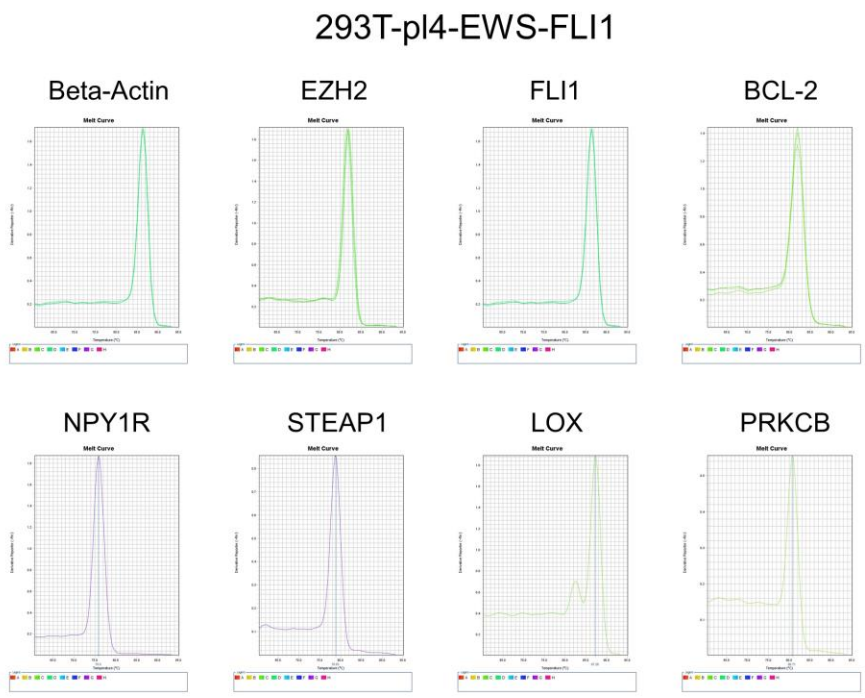

Figure 3.7 Melting Curves

(A) Indicated primer melting curves taken from 293T EWS-FLI1 expressing cells during RT-qPCR

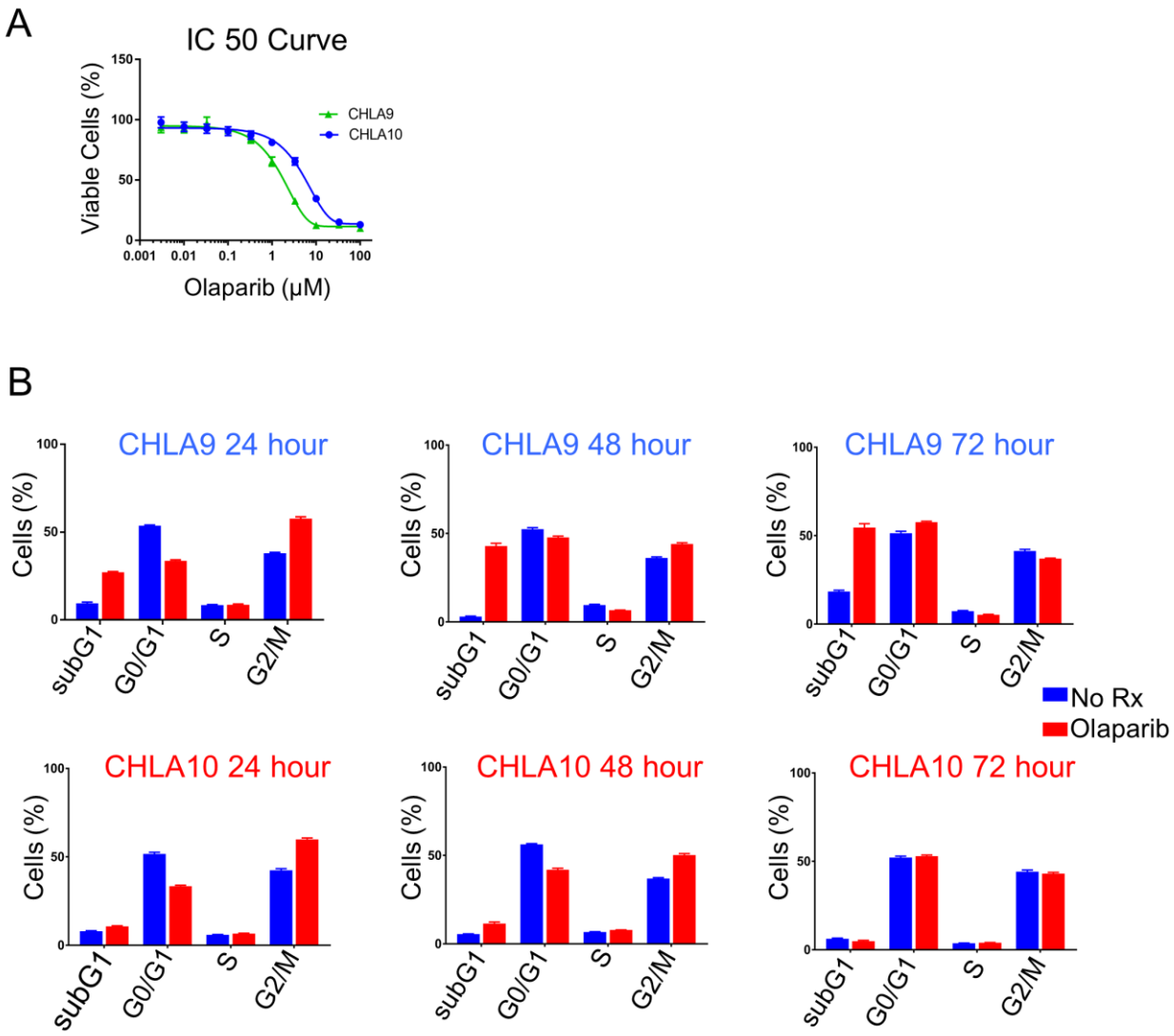

Figure 3.8 A chemotherapy-naive and chemotherapy-resistant cell line pair respond differently to olaparib

(A) IC50 curve of CHLA9 and CHLA10 cells following 72 hour treatment with the indicated concentrations of olaparib. (B) Cell cycle analysis after 24, 48 and 72 hour treatment with 5 μM olaparib, compared to no drug treatment control (No Rx).

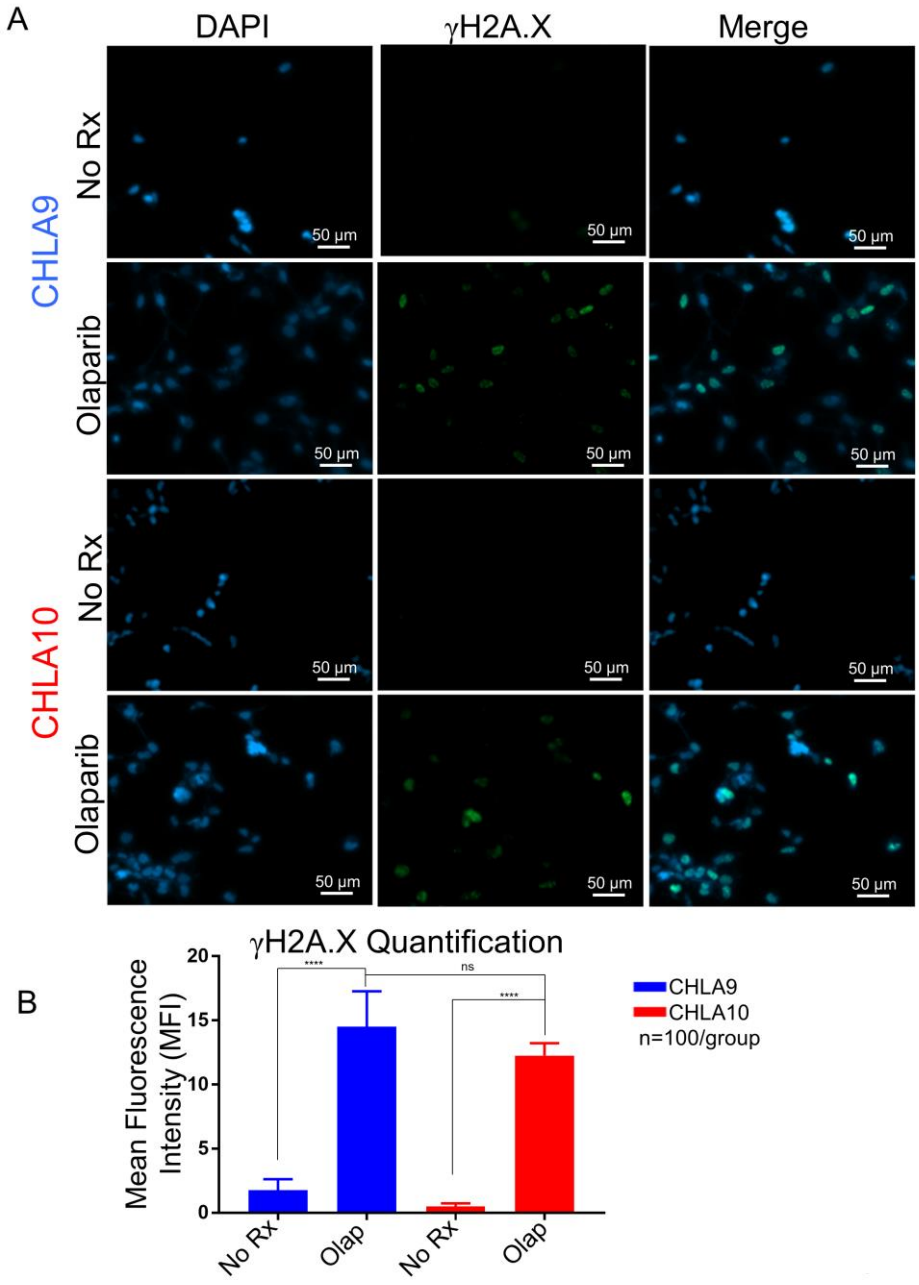

Figure 3.9 Olaparib induces similar levels of DNA damage in CHLA9 and CHLA10

(A) Representative immunofluorescence images showing γH2A.X foci following 72 hour treatment of 5 μM olaparib compared to no treatment control (No Rx). (B) Quantification of immunofluorescence images probed for γH2A.X intensity following 72 hour treatment of 5 μM olaparib compared to no treatment control (No Rx). Error bars are +SEM, asterisks indicate significance between the no treatment control and olaparib treatment for CHLA9 or CHLA10, as determined using the Mann-Whitney *U* test.

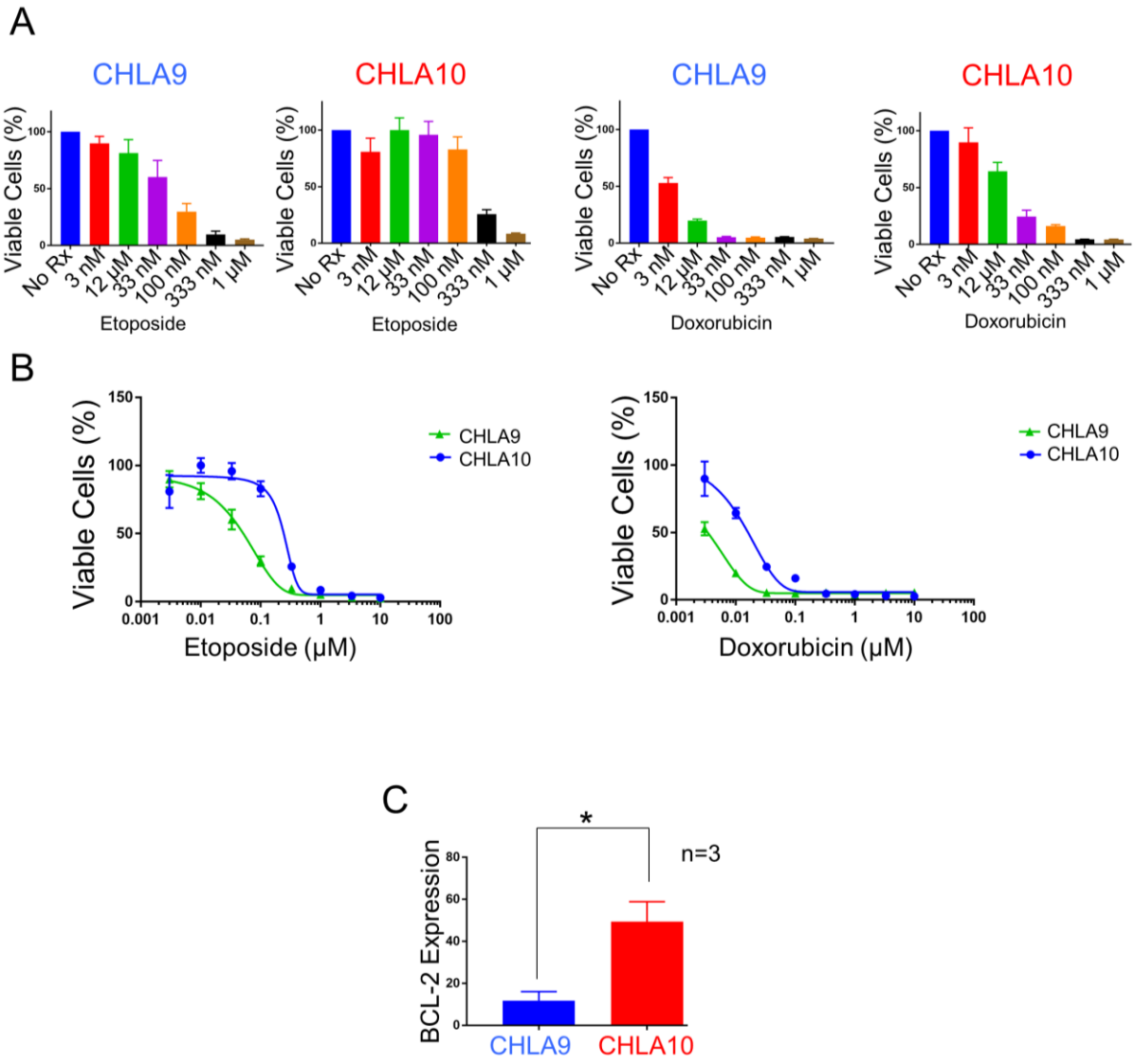

Figure 3.10 A chemotherapy-naive and chemotherapy-resistant cell line pair respond differently to chemotherapeutics

(A) CellTiter Glo of CHLA9 and CHLA10 cells after 72 hour treatment with increasing concentrations of Etoposide and Doxorubicin. Data is graphed as percent viable cells from no treatment control, performed in quadruplicate. Errors bars are +SEM. (B) IC50 curves representing the data collected in (A). (C) Quantification of BCL-2 protein expression represented in Figure 1B, (n=3). Asterisk indicates a significant separation between CHLA9 and CHAL10 BCL-2 protein expression, and significance was determined using the Student's *t* test ($P < 0.05$).

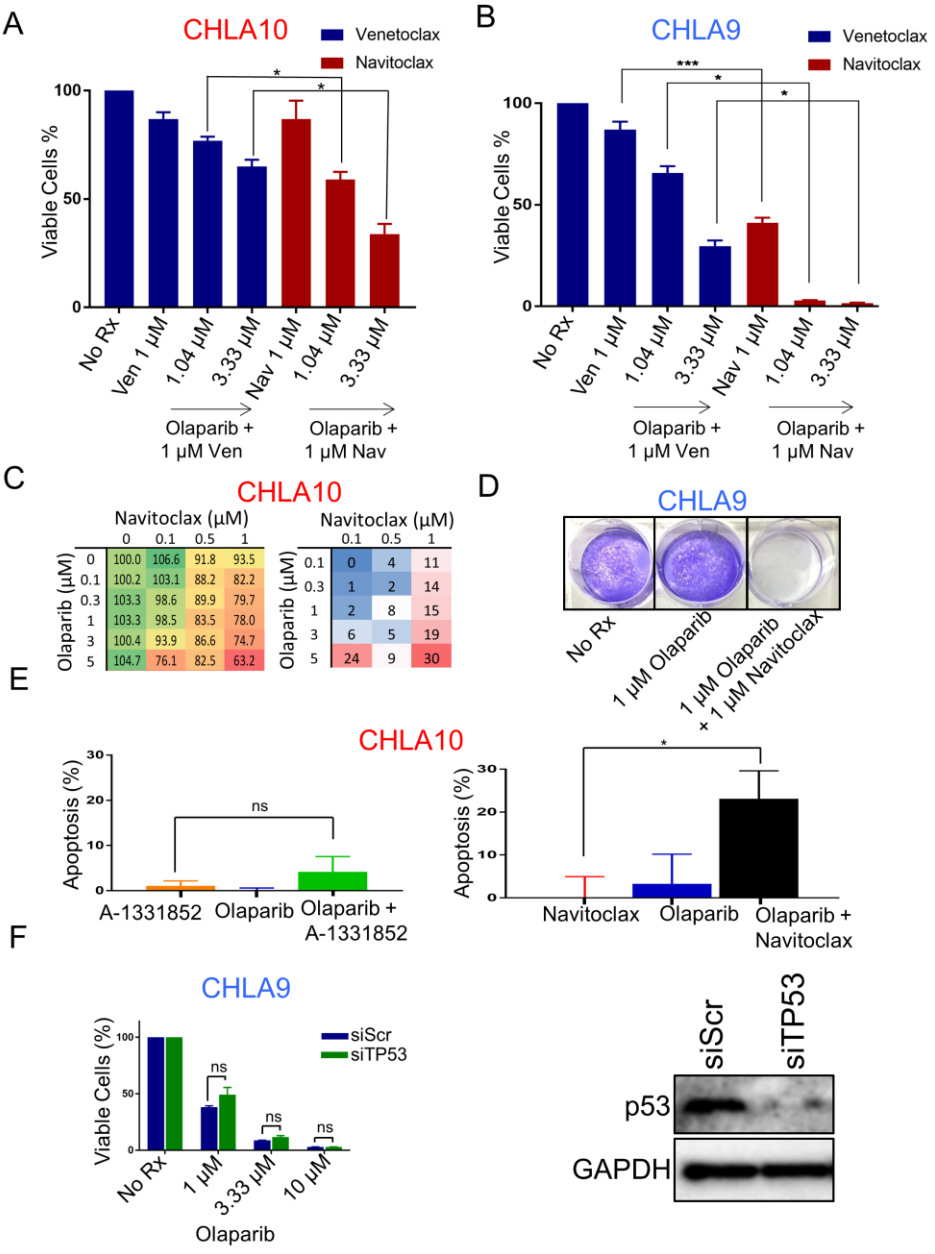

Figure 3.11 Navitoclax sensitizes EWFT to olaparib

(A), (B) CellTiter-Glo of CHLA10 (A) and CHLA9 (B) cells after 72 hour treatment with 1 µM venetoclax or 1 µM navitoclax with increasing concentrations of olaparib. Data is graphed as percent viable cells from no treatment control, performed in quadruplicate. Error bars are +SEM. Asterisks indicate a significant separation between the indicated

Figure 3.11 continued

concentrations of venetoclax + olaparib compared to navitoclax + olaparib. Significance was determined using the Mann-Whitney *U* test. (C) (*left*) CellTiter Glo viability after 24 hour treatment with the indicated concentrations of olaparib and navitoclax. (145) Percent over the bliss score. Positive scores (red) indicate synergy, negative scores (blue) indicate antagonism. All concentrations are presented as µM. (D) Crystal violet staining after 5 day treatment showing sensitivity to the indicated drug treatments (E) FACS analysis of apoptosis in CHLA10 cells after 24 hour treatment with 1 µM of the BCL-X_L inhibitor A-1331852, 5 µM olaparib, 5 µM olaparib + 1 µM A-1331852, 1 µM navitoclax, or 5 µM olaparib + 1 µM navitoclax. Percent of apoptosis induced by drugs is normalized to the no treatment control (No Rx). Error bars are +SEM. Asterisks indicate a significant separation between navitoclax and olaparib + navitoclax. There was no significance between the A-1331852 treatment compared to olaparib + A-1331852. Significance was determined using the Student's *t* Test ($P<0.05$). (F) (*left*) CellTiter Glo analysis after 72 hour treatment with the indicated olaparib concentrations in CHLA9 cells expressing siScramble or siTP53. Error bars are +SEM and there is no significance. (145) Western blot analysis confirming siRNA knockdown of p53 protein in CHLA9 cells.

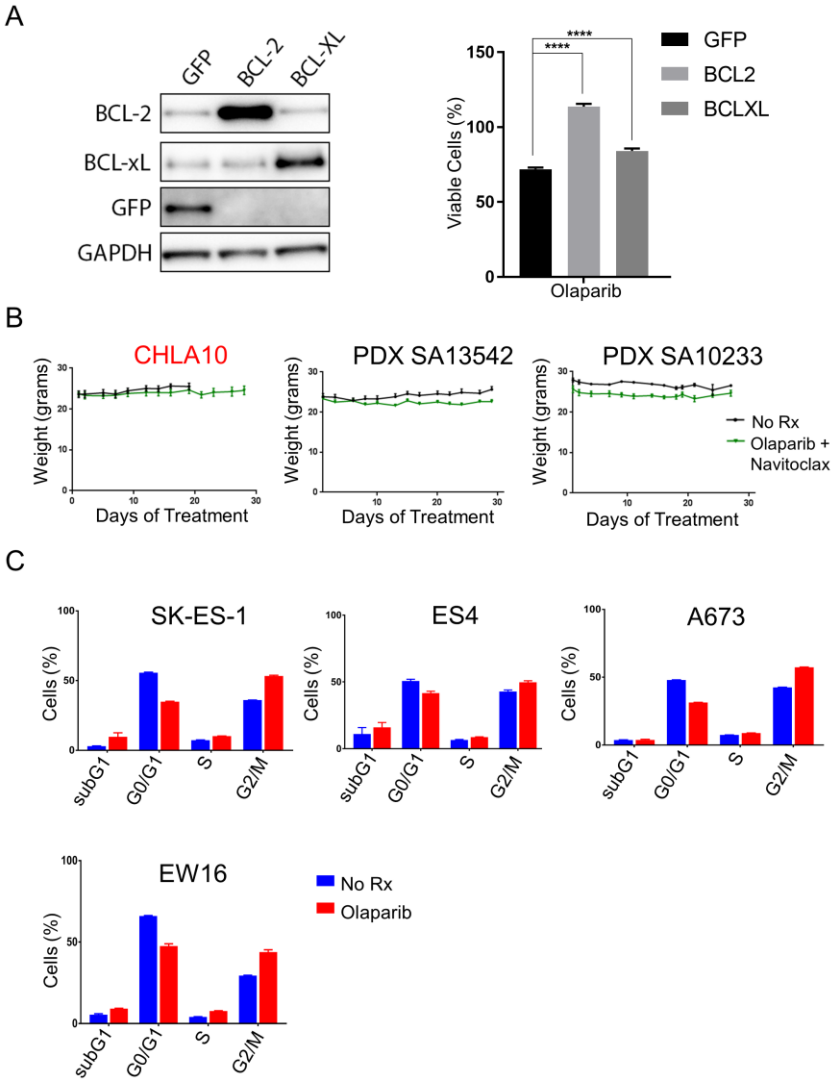

Figure 3.12 Olaparib sensitivity is modulated by BCL2 family expression

(A) (*left)* Western blot analysis of BCL-2 and BCL-X_L, confirming over expression in CHLA9 cells. (145) CellTiter Glo assay after 24 hour treatment with 5 µM olaparib in CHLA9 cells over expressing GFP, BCL-2, or BCL-X_L. Asterisks indicate a significant separation between the GFP control, and BCL-2 cells treated with olaparib or BCL- X_L cells treated with olaparib. Student's *t* test was performed. (B) Average measurement of mouse weight (grams) per condition (n=5 mice or greater per condition) over the course of each *in vivo* experiment. Please note, this data was obtained from the efficacy experiments shown in Fig. 1F and Fig. 4A, respectively. (C) Cell cycle analysis after 24 hour treatment with 5 µM olaparib in the indicated cell lines, compared to no drug treatment controls cells (No Rx).

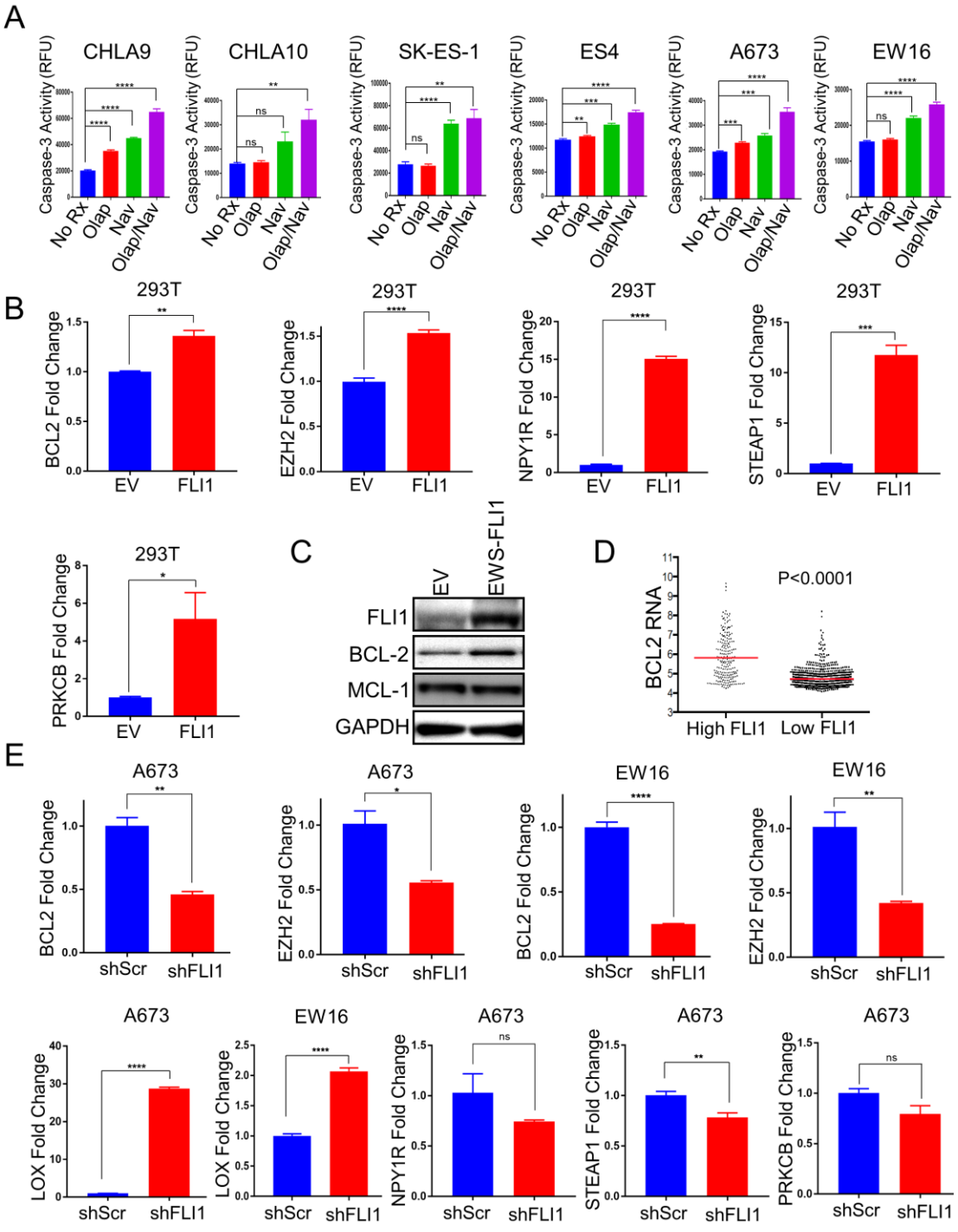

Figure 3.13 EWS-FLI1 increases BCL-2 expression in EWFT

(A) Cleaved Caspase-3 activity after 24 hour treatment with the indicated drugs: 5 µM olaparib, 1 µM navitoclax, or 5 µM olaparib + 1 µM navitoclax, compared to no treatment

Figure 3.13 continued

control (No Rx). Activity is presented as Relative Fluorescent Units (RFU). Experiments were performed in quadruplicate and error bars are plotted as +SEM. Asterisks indicate a significant separation between the no treatment control and each individual treatment. Significance was determined using the Student's *t* Test. (B) RNA expression of the indicated genes in pl4-EWS-FLI1 or pl4-Empty Vector expressing 293T cell lines. Asterisks indicate a significant separation between the empty vector control and the EWS-FLI1 expressing cells and was determined using the Student's *t* Test. (C) Western blot comparison as detected by the indicated antibodies in pl4-EWS-FLI1 and pl4-Empty Vector 293T cell lines. (D) BCL-2 RNA expression from the (CCLE) in high (n=208) and low (n=829) FLI1 expressing tumors. Individual cell lines are represented by a single dot. A Mann-Whitney non-parametric test was performed for significance. (E) RNA expression of the indicated genes after shRNA knockdown of EWS-FLI1 or control (scramble sequence) in A673 and EW16 cell lines. Asterisks indicate a significant separation between the shScramble control and the EWS-FLI1 knockdown cells, significance was determined using the Student's *t* Test.

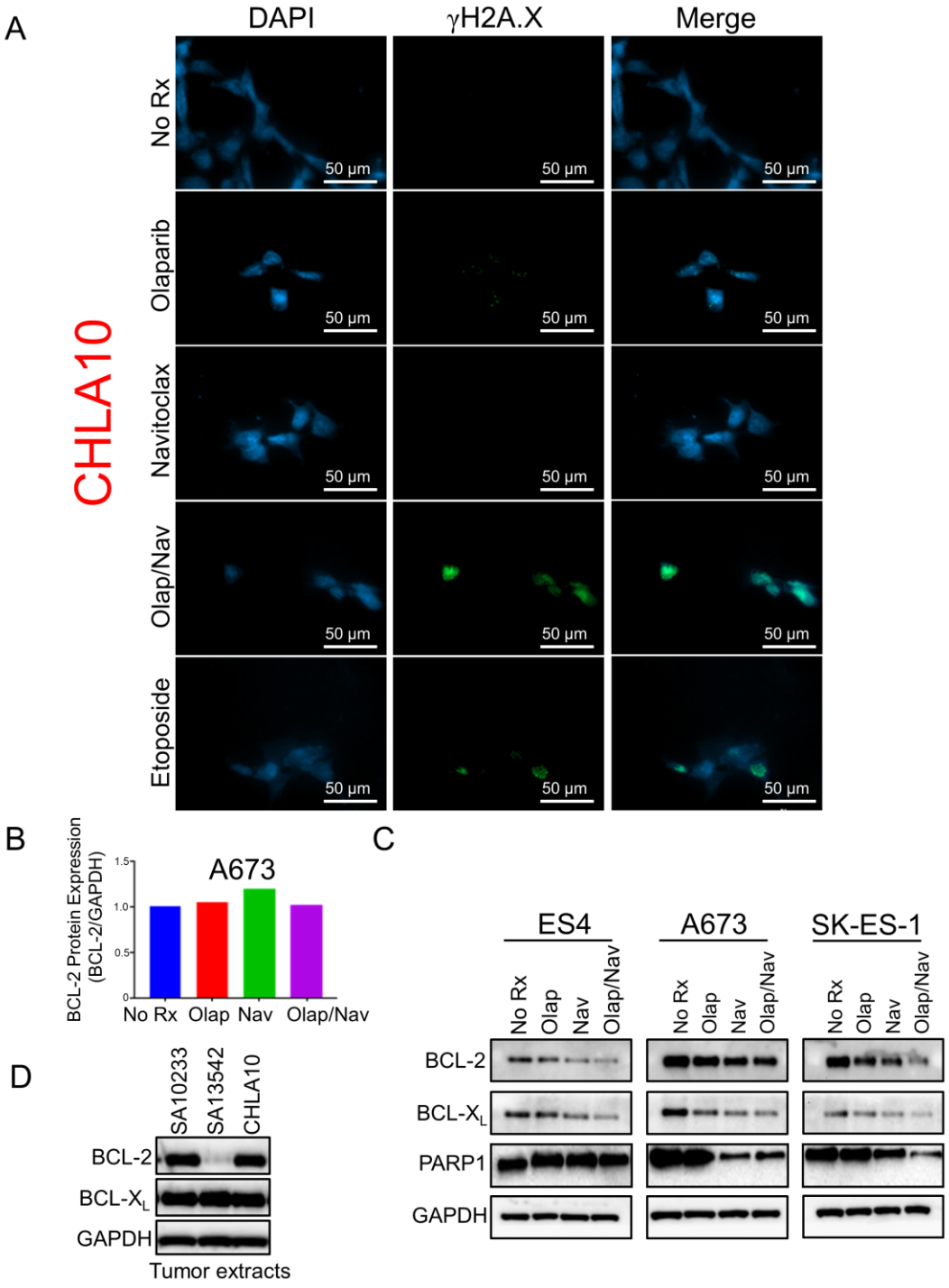

Figure 3.14 DNA damage is increased with the combination of olaparib and navitoclax

(A) Representative immunofluorescence images showing γH2A.X foci following 24 hour treatment 5 μM olaparib, 1 μM navitoclax, 5 μM olaparib + 1 μM navitoclax,1 μM

Figure 3.14 continued

etoposide (serving as a positive control), or no treatment control (No Rx). (B) Densitometry quantification of BCL-2 levels from the whole cell lysates in Fig. 5C normalized to GAPDH. (C) Western blot analysis with the indicated antibodies after 24 hour treatment of 5 µM olaparib, 1 µM navitoclax, 5 µM olaparib + 1 µM navitoclax or no treatment control (No Rx). (D) Tumor lysates from control PDX and cell line xenograft models were analyzed by Western blot with the indicated antibodies.

Chapter 4 – Pharmaceutical Means of Targeting the Fusion Oncogene EWS-FLI1 in the Ewing Family of Tumors

Introduction

Pediatric cancers often have a low mutation burden which suggests epigenetic mechanisms may play major roles in driving tumorigenesis (146). It is well known that EWS-FLI1 induces a myriad of epigenetic changes, including global increases in H3K27ac a marker for enhanced gene activation, which was the most highly regulated histone mark following exogenous EWS-FLI1 expression in mesenchymal stem cells (the potential cell of origin for EWFT), including within enhancer regions bound by FLI1 (24, 26, 39, 67). This would suggest EWS-FLI1 driven changes in H3K27ac are responsible for the activation of FLI1 target genes. In the same study it was found that H3K27 methylation (H3K27me) did not associate with EWS-FLI1 binding, and it is evident that altering H3K27me has an inactivating effect on H3K27ac marked gene targets (147, 148).

We have uncovered an effective therapeutic strategy to target the EWS-FLI1 program by exploiting a hypersensitivity to the inhibition of H3K27 demethylases using a high-throughput pharmacological screen (13). We demonstrate that H3K27 demethylase inhibition is synergistic with RNAP II inhibition, effectively blocking EWS-FLI1 gene target activation and resulting in strong anti-EWFT activity.

Results

Drug screen reveals hypersensitivity of EWFT cell lines to GSK-J4

Utilizing the Genomics of Drug Sensitivity in Cancer (GDSC) platform (13) in a high-throughput drug screening, it was revealed that EWFT are acutely sensitive to GSK-J4 an H3K27 demethylase inhibitor (Fig. 4.1A). Of the ~900 solid tumor cell lines tested, 21 were EWFT. Of those EWFT cell lines tested, 12/21 were among the top 25% most sensitive and 17/21 were among the top 50% most sensitive cell lines. GSK-J4 targets the histone 3 Lysine 27 demethylases: Ubiquitously transcribed tetratricopeptide repeat, X chromosome (UTX), and Jumonji D3 (JMJD3) described in Figure 4.1B. Upon further investigation, we found no correlation between GSK-J4 sensitivity and expression of its targets *KDM6A* (UTX)) and *KDM6B* (JMJD3), nor was there any correlation with the enhancer of zeste homolog 2 (*EZH2*) (80, 81, 149-151) or other members of the polycomb2 repressor complex (PRC2) (data not shown). Interestingly we found an inverse correlation between overall survival and the expression of *KDM6B (152, 153)*, linking higher expression to lower overall survival (Fig. 4.1C), and emphasizing its relationship with EWFT severity.

GSK-J4 inhibits EWFT growth *in vitro* by downregulating EWS-FLI1 targets

To fully characterize the sensitivity of EWFT to GSK-J4 we assessed its activity in a panel of EWFT cell lines. GSK-J4 treatment reduced cell viability in a dose dependent manner (Fig. 4.2A) in 72-hour cell viability assays. We found chemical interrogation with GSK-J4 had a robust effect on EWFT cell lines including a near complete loss of cell

viability in 5-day clonogenic assays (Fig. 4.2B). To ensure on-target specificity of GSK-J4 we utilized western blotting to analyze global histone modifications in cell lines treated with GSK-J4 and found, as expected, a subsequent increase in global levels of H3K27 tri-methylation after treatment with GSK-J4 (Fig. 4.2C). H3K27 methylation and acetylation are closely linked in balancing gene expression, and a loss of H2K27 methylation allows for acetylation at the same regions (92, 147, 148, 154-156). For example, in H3K27M mutant diffuse intrinsic pontine glioma (DIPG), which has a reduced H3K27me3 levels, there are marked increases in H3K27ac (157, 158). We found the addition of GSK-J4 led to global increases in H3K27me3 coupled with a subsequent decrease in H3K27ac (Fig. 4.2C), while other key histone modifications were unaffected (data not shown). This suggests GSK-J4 is able to shift global Histone 3 Lysine 27 epigenetic regulatory marks from a highly active to an inactive state and is verified by a decrease in the expression of bona fide EWS-FLI1 target EZH2 (Fig 4.2C) (80, 81).

Using annexin V/propidium iodide staining we assessed the ability of GSK-J4 to induce apoptosis in cells using shRNA to knockdown EWS-FLI1. We found EWS-FLI1 reduction significantly diminished the ability of GSK-J4 to induce cell death (Fig. 4.2D), demonstrating that EWS-FLI1 expression is responsible for sensitizing cells to the pharmaceutical inhibition of UTX/JMJD3.

The EWS-FLI1 translocation is a strong driver of H3K27ac modifications which results in gene upregulation (24, 76), therefore we investigated the global expression levels of several well characterized EWS-FLI1 target genes: cyclin d1 (*CCND1*) (39), *EZH2*, and neuropeptide Y receptor Y1 (*NPY1R*) (24, 26, 97, 159). Western blot analysis indicates a

strong downregulation of the protein levels for these three genes following GSK-J4 treatment (Fig. 4.3A). Transcript levels were also markedly decreased after the same GSK-J4 treatment conditions (Fig. 4.3B). Using this data, we hypothesize that the H3K27ac marks which can be reduced by GSK-J4 chemical interrogation might overlap with those of EWS-FLI1 target gene enhancers, suggesting an epigenetic means of indirect EWS-FLI1 inhibition.

GSK-J4 is effective and tolerable in multiple PDX models of EWFT

To assess the activity of GSK-J4 *in vivo* we utilized several PDX models derived from relapsed EWFT patients (160). GSK-J4 given once a day (50mg/kg/qd) by intraperitoneal injection demonstrated marked anti-tumor activity and was sufficient to control tumor growth in all four PDX models (Fig. 4.4A). Body weight measurements indicated no overt signs of toxicity in the mice (weight loss >15% or behavioral changes), as demonstrated in Figure 4.4B. This highlights the single agent efficacy of GSK-J4 as a therapy tailored for EWFT and advocates H3K27 demethylase inhibition as a potential candidate to test in combination therapy.

CDK7 inhibition sensitizes EWFT to GSK-J4

Despite the *in* vivo efficacy of GSK-J4 as a single agent in refractory PDX models (Fig. 4.4) we want to enhance the dose response and prevent the possibility of acquired drug resistance by using GSK-J4 as a combination therapy. We have recently demonstrated that targeting cyclin dependent kinases (CDK) can inhibit transcription in

cancer (161), and often sensitizes to additional therapies (162-164). It has been well documented that the inhibition of transcription is a highly effective treatment in several cancer types, and that the EWFTs are sensitive to the very selective CDK7 inhibitor THZ1 (165, 166), which blocks RNA polymerase II (RNAP II) phosphorylation at serine 5. We rationalize that the use of THZ1 to prevent RNAP II activation would prove a viable drug target, working synergistically with GSK-J4 to inhibit EWS-FLI1 driven transcription. CDK7 specific inhibitors are well characterized and have shown preferential suppression of super-enhancer marked genes (167), which would suggest specificity towards EWS-FLI1 driven transcripts.

To assess this hypothesis, we utilized THZ1 in combination with GSK-J4 to calculate Bliss Independence dose-response models (91). We found strong synergy among multiple EWFT cell lines as well as four of our *ex vivo* derived PDX lines (Fig. 4.5A) and notably, the combination was effective at concentrations that demonstrated little single agent activity. The observed synergy at concentrations with limited or no single agent efficacy suggests concentrations of THZ1/GSK-J4 may be used in combination at lower concentrations than those required by single agent treatment for similar efficacy. Western blot analysis further supports this notion as indicated by high expression of cleaved PARP1 in the combination, paired with marked reduction in global H3K27ac (Fig. 4.5B).

CDK7 inhibition combines with GSK-J4 to cooperatively downregulate EWS-FLI1 targets

To better characterize the mechanisms of sensitivity and specificity towards EWS-FLI1 gene target regulation, we performed chromatin immunoprecipitation against H3K27ac in the A673 cell line and designed primers flanking the FLI1 binding site of several EWS-FLI1 target gene enhancers. Consistent with the histone modifications in Figures 4.2C and 4.5B, we found GSK-J4 treatment induced a significant downregulation of H3K27 acetylation at putative FLI1 bound enhancers elements (Fig. 4.6A). We found that the well characterized FLI1 target genes *NPY1R*, *EZH2* (26, 69), and *NKX2.2* (168) had significantly less H3K27ac histone marks at their putative enhancer sites upon treatment with GSK-J4 and THZ1 compared to unmodified EWFT no treatment controls, which correlates with the global protein changes described in Figures 4.2C and 4.5B . These results correlate with RNA transcript levels following the same drug treatments. This data further supports our hypothesis that disrupting UTX/JMJD3 activity functions as an indirect inhibitor of EWS-FLI1 through the reversal of H3K27 acetylation at EWS-FLI1 driven genes.

THZ1 and GSK-J4 combine to induce anti-EWFT activity *in vivo*

We next sought to evaluate the combination of GSK-J4 and THZ1 in our SA10233 PDX model of EWFT. Daily treatment with GSK-J4 (50mg/kg/qd) and THZ1 (10mg/kg/qd) was sufficient to reduce tumor growth in a controlled manner compared to the vehicle and single agent groups (Fig. 4.6B and 4.6C). In the combination cohort, some toxicity was detected with decreases in weight recorded during the final two data collection timepoints.

Discussion

The Ewing Family of Tumors is defined by EWS/ETS translocations which drive tumorigenesis (20, 123). The most abundant translocation being EWS-FLI1 which initiates transcriptional reprograming, resulting in a loss of tumor suppressors and the activation of oncogenes (24, 76, 169). Despite the promising therapeutic opportunity that a single driver event presents, successful targeting of the EWS-FLI1 transcription factor remains elusive.

Recent studies have shown that EWS-FLI1 drastically alters the epigenome and emphasis has been placed on targeting histone modifications as an effective anticancer therapy. Several targeting strategies are currently being investigated which seek to reverse specific epigenetic dysregulations caused by EWS-FLI (80, 169-173). Parrish and colleagues (174) recently demonstrated that the pan-Jumonji-domain histone demethylase inhibitor JIB-04 can dysregulate the EWS-FLI1 oncogenic program. However, pan Jumonji histone demethylase inhibition results in the upregulation of H3K4me3 (through the inhibition of Lysine Demethylase 5A) which is associated with increased transcription and can lead to the expression of not only tumor suppressors but oncogenes, possibly diminishing its effectiveness. Similarly, the Lysine-specific histone demethylase 1 (LSD1/KDM1A) is also responsible for demethylating H3K4, and EWS-FLI1 utilizes LSD1 overexpression to silence tumor suppressors. The use of LSD1 inhibitor HCI2509 is currently being investigated as a potential therapy for EWFT (175).

Another approach to target the EWFT epigenome has focused on increasing H3K27ac using histone deacetylase (HDAC) inhibitors. This can lead to growth arrest and promote differentiation in EWFT, and has a rescuing effect on tumor suppressors which are downregulated by EWS-FLI1 (169, 173). While these strategies prove the efficacy in reversing epigenetic changes caused by EWS-FLI1, they focus on rescuing tumor suppressor expression and fail to address H3K27ac mediated activation of oncogenes, which are the histone mark most highly regulated by EWS-FLI1 (76).

Targeting the histone demethylases UTX/JMJD3 causes the accumulation of H3K27me3 and results in gene repression. This strategy differs from other EWFT epigenetic therapies currently under investigation, which seek to inhibit HDAC or increase H3K4me3 levels to promote the re-expression of tumor suppressors. Our approach differs by silencing EWFT oncogenes directly and does not rely on tumor suppressor function. In fact, HDAC and KDM5A/LSD1 inhibitors have the drawback of promoting oncogene expression in addition to tumor suppressors, putting the cells at a disadvantage. H3K27me3 accumulation does not rescue tumor suppressor expression, however it serves to function as surrogate tumor suppressors by preventing oncogene expression, diminishing the need for tumor suppressor reactivation. Despite the effectiveness of GSK-J4, there remains both a lack of reliable biomarkers to predict its clinical activity and the potential for EWFT to become resistant. We hope that by utilizing the CDK7 inhibitor THZ1 in combination, we can mitigate the development of GSK-J4 resistance.

In summary, we have uncovered an effective therapeutic strategy to epigenetically target the EWS-FLI1 program resulting in reduced FLI1 target gene expression (Fig. 4.7).

By inhibiting UTX/JMJD3 in combination with CDK7 inhibition we are able to both drive H3K27 modifications towards hypermethylation, subsequently reducing H3K27ac activation of EWS-FLI1 targets, and block RNAP II mediated transcription of those same genes. Our studies highlight an effective and promising new epigenetic therapy for the treatment of EWFT, however further work is required to support the mechanistic relationship and to elucidate the clinical efficacy of these drugs in combination.

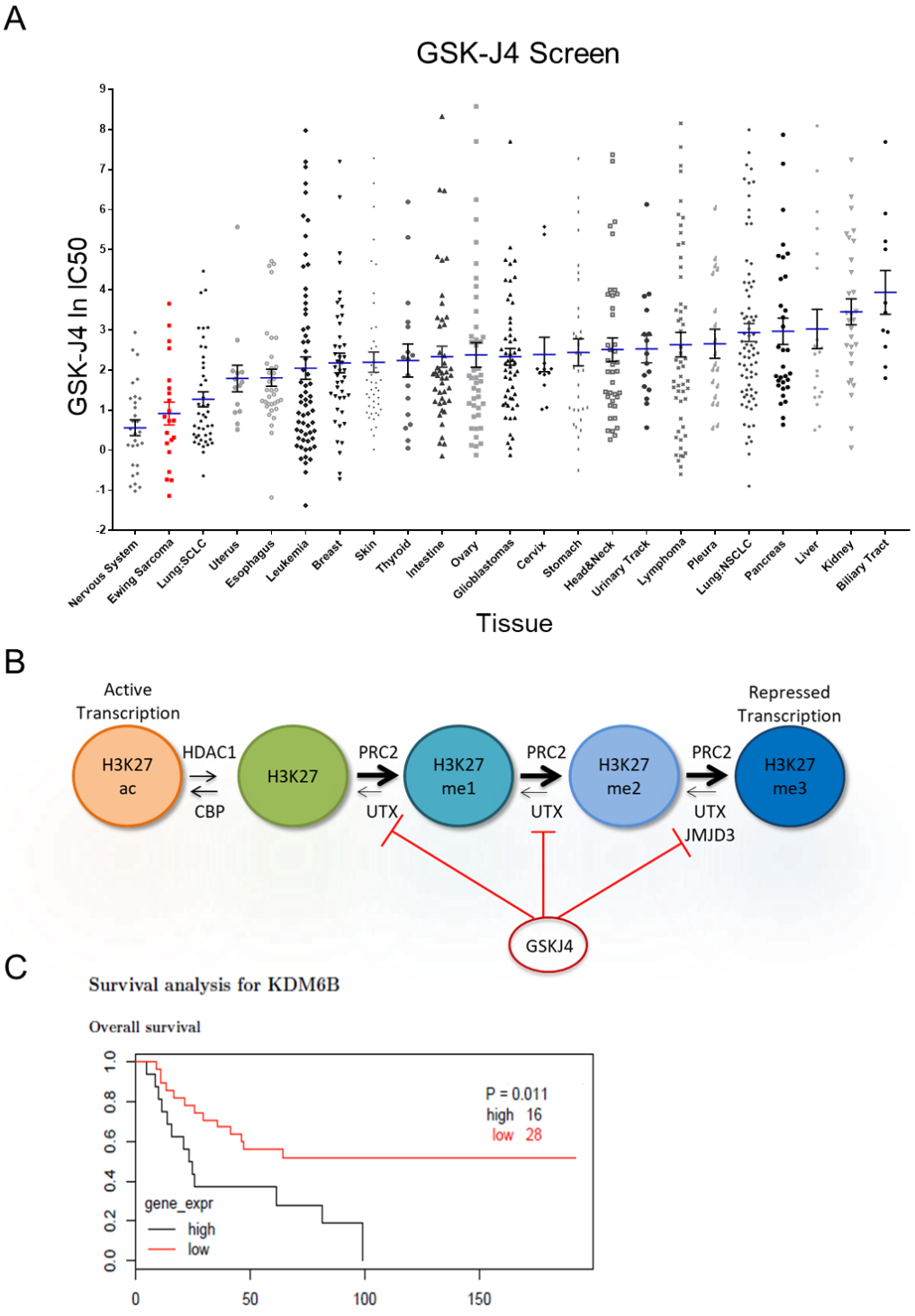

Figure 4.1 Drug Screen reveals sensitivity of EWFT to GSK-J4

Figure 4.1 Continued

(A) High throughput screen of GSK-J4 measuring viability with resazurin, in collaboration with the GDSC. (B) Graphical representation of GSK-J mechanism, directly targeting the histone demethylases JMJD3 and UTX, which are responsible for removing methyl groups in opposition to the PRC2 complex. Drug treatment results in global increases in H3K27 methylation. (C) Survival Analysis of EWFT patients with KDM6B high and low expression from the Gene Expression Omnibus GSE17679. Statistical analysis was performed using the log-rank test.

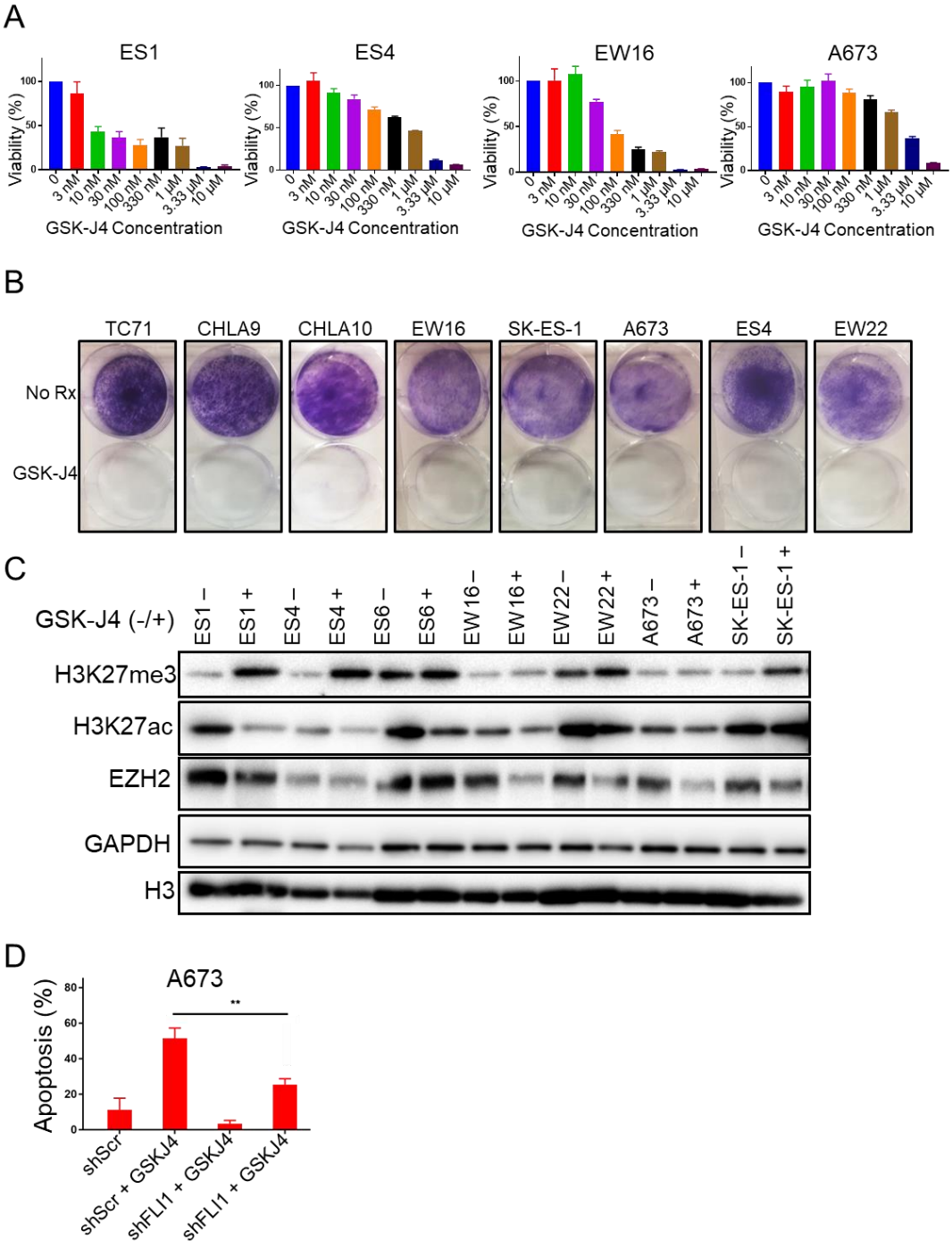

Figure 4.2 GSK-J4 reduces cell viability and alters H3K27 marks in EWFT

(A) 72-hour dose response viability assay with increasing concentrations of GSK-J4,

Figure 4.2 Continued

measured using CellTiter-Glo. Conditions were measured in quadruplicate. Error bars are +SEM. (B) Crystal violet staining after 5-7 day treatment with no treatment (no rx) or 2 µM GSK-J4. (C) Western blot analysis of the indicated antibodies, histone modifications represent global levels after 72-hour treatment no treatment (-) or 2 µM GSK-J4. (D) FACS analysis of apoptosis after 72-hour treatment with 2 µM GSK-J4 in cell lines expression an sh-scrambled sequence, or sh-EWS-FLI1 knockdown. The percentage of induced apoptosis is normalized to the no-treatment controls, error bars are +SEM.

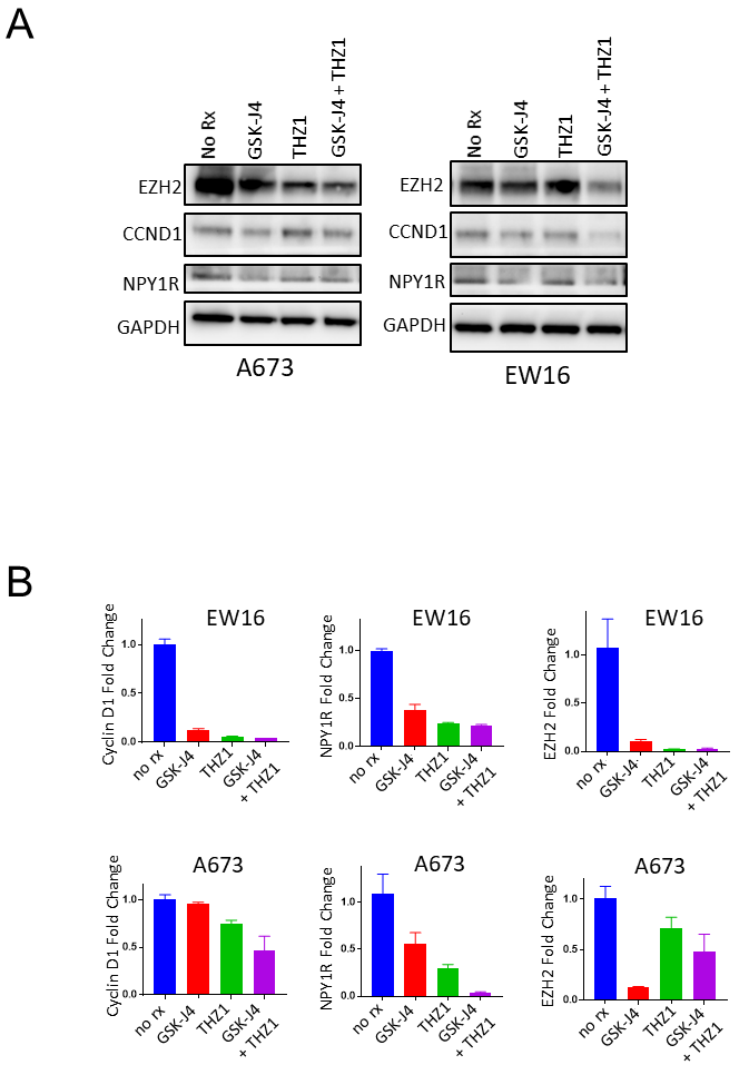

Figure 4.3 EWS-FLI1 driven genes are reduced following GSK-J4/THZ1 treatment

(A) Western blot analysis of the indicated antibodies of FLI1 target genes after 48-hour treatment with no-treatment control (no rx), 1 µM GSK-J4, 6-hour treatment with 10 nm THZ1, or 48-hour 1 µM GSK-J4/6-hour 10 nm THZ1. (B) RNA expression of the indicated genes following 48-hour treatment with no-treatment control (no rx), 1 µM GSK-J4, 6-hour treatment with 10 nm THZ1, or 48-hour 1 µM GSK-J4/6-hour 10 nm THZ1. Error bars are +SEM.

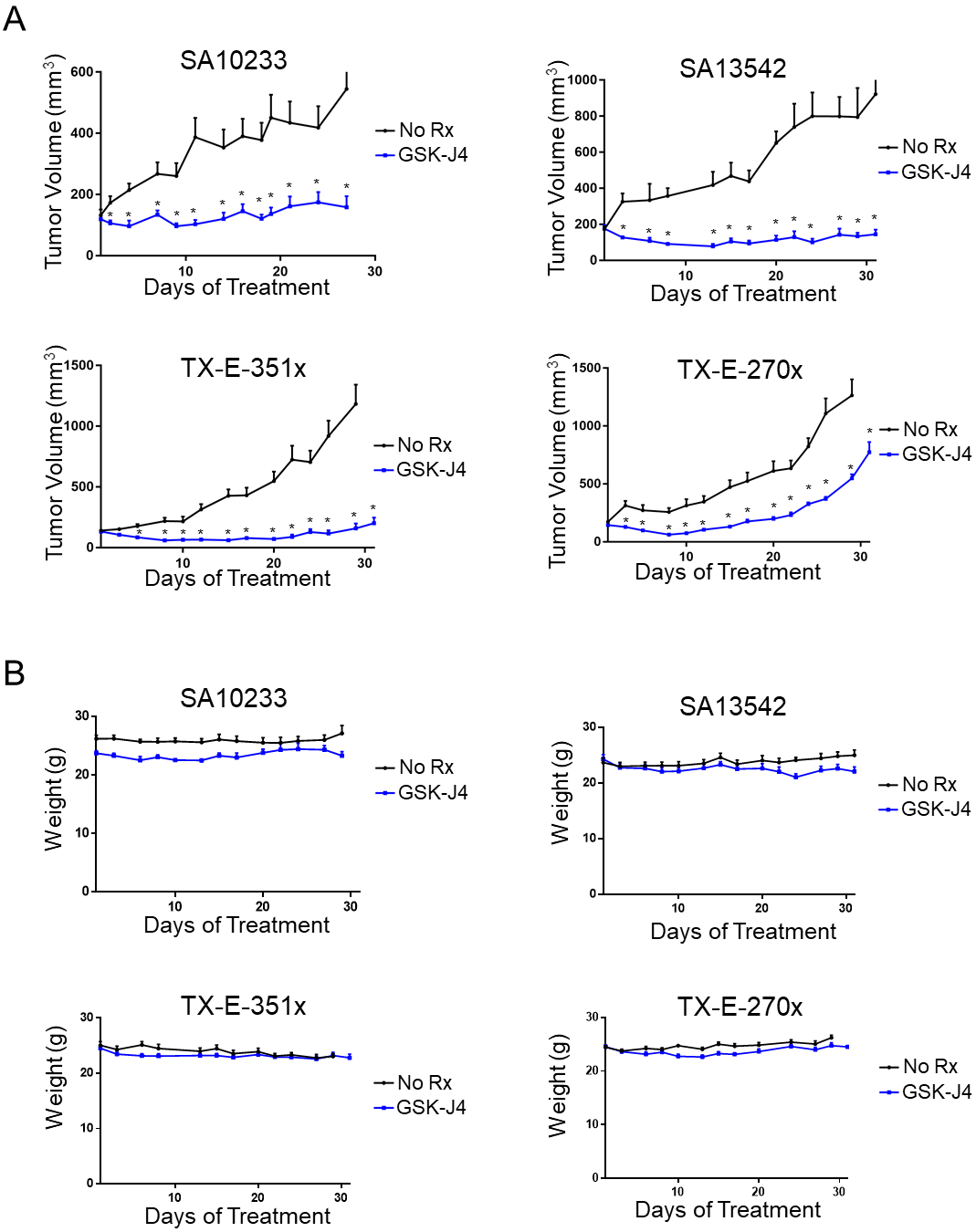

Figure. 4.4 Histone demethylase inhibition slows tumor growth

(A) Patient-derived xenografts treated daily for the indicated timepoint with vehicle

Figure 4.4 Continued

(DMSO) or GSK-J4 (50mg/kg). Asterisks indicated a significant separation between treatment cohorts using the Student *t* test ($P < 0.05$). Error bars are +SEM (B) Average measurements of mouse weight (grams) per PDX over the course of each *in vivo* PDX from figure 4.4A. Error bars are +SEM.

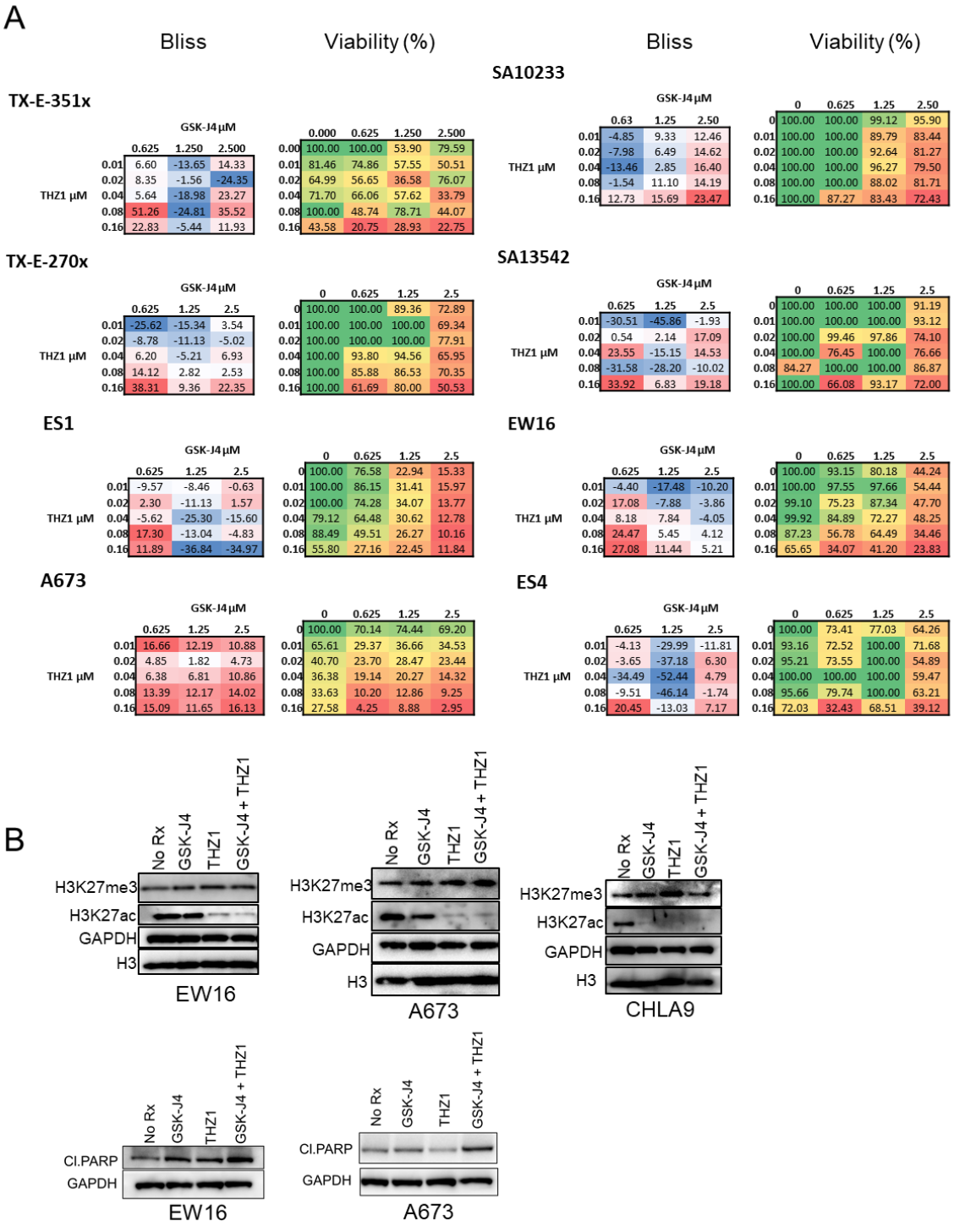

Figure 4.5 GSK-J4 and THZ1 synergistically inhibit EWFT cells and *ex vivo* PDX models

(A) CellTiter Glo Viability of EWFT cell lines and *ex vivo* PDX lines, after 48-hour

Figure 4.5 Continued

treatment with the indicated concentrations of GSK-J4 and THZ1. Data presented as percent viability and as previously described, depicting percent over the bliss score (91). Positive scores (red) indicate synergy, negative scores (blue) indicate antagonism. All concentrations are presented as μM. (B) Western blot analysis of the indicated antibodies, indicating apoptosis with Cleaved PARP or global changes in histone modifications after 48-hour treatment with no-treatment control (no rx), 1 μM GSK-J4, 6-hour treatment with 10 nm THZ1, or 48-hour 1 μM GSK-J4/6-hour 10 nm THZ1.

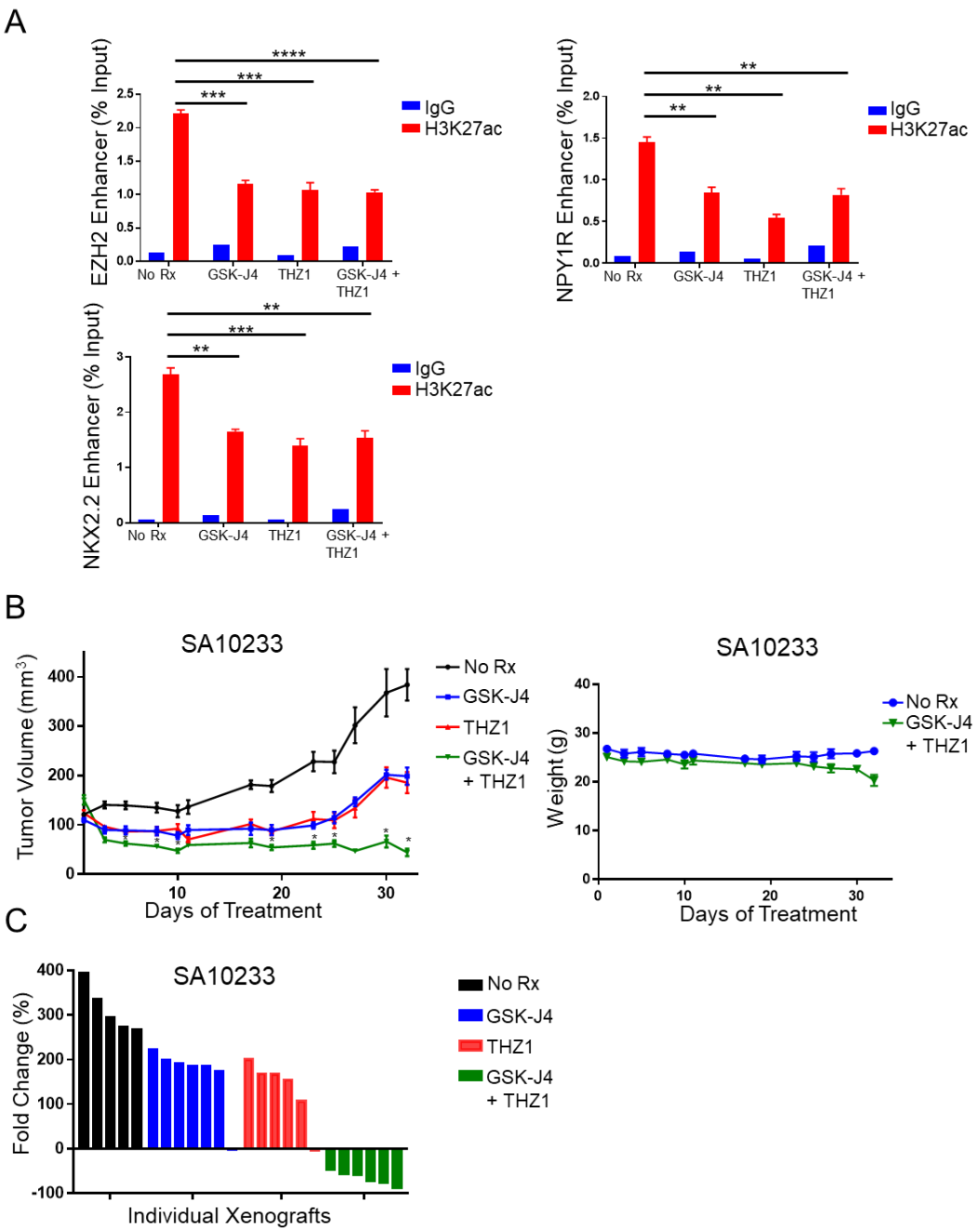

Figure 4.6 The combination of GSK-J4 and THZ1 inhibits EWFT driven gene activation and reduces tumor growth

(A) ChIP on the putative enhancer regions of the indicated genes at their FLI1 binding

Figure 4.6 Continued

sites. Cells were fixed and collected after 48-hour treatment with no-treatment control (no rx), 2 µM GSK-J4, 6-hour treatment with 10 nm THZ1, or 48-hour 2 µM GSK-J4/6-hour 10 nm THZ1 and run using the RT-qPCR conditions described in the materials and methods section. H3K27ac was calculated as a percentage of input, and statistics was performed using the Student's *t* test. Error bars are +SEM. (B) (*left*) Patient-derived xenograft SA10233 treated daily for the indicated timepoint with vehicle (DMSO), GSK-J4 (50mg/kg), THZ1 (10mg/kg), or the combination of GSK-J4 (50mg/kg) + THZ1 (10mg/kg). Asterisks indicated a significant separation between treatment cohorts using the Student *t* test ($P < 0.05$). Error bars are +SEM (145) Average measurements of mouse weight (grams) over the course of the *in vivo* experiment from figure 4.6A (*left*). (C) Fold change in tumor volume. Please note the data is from figure 4.6A (*left*) comparing day 1 to day 32.

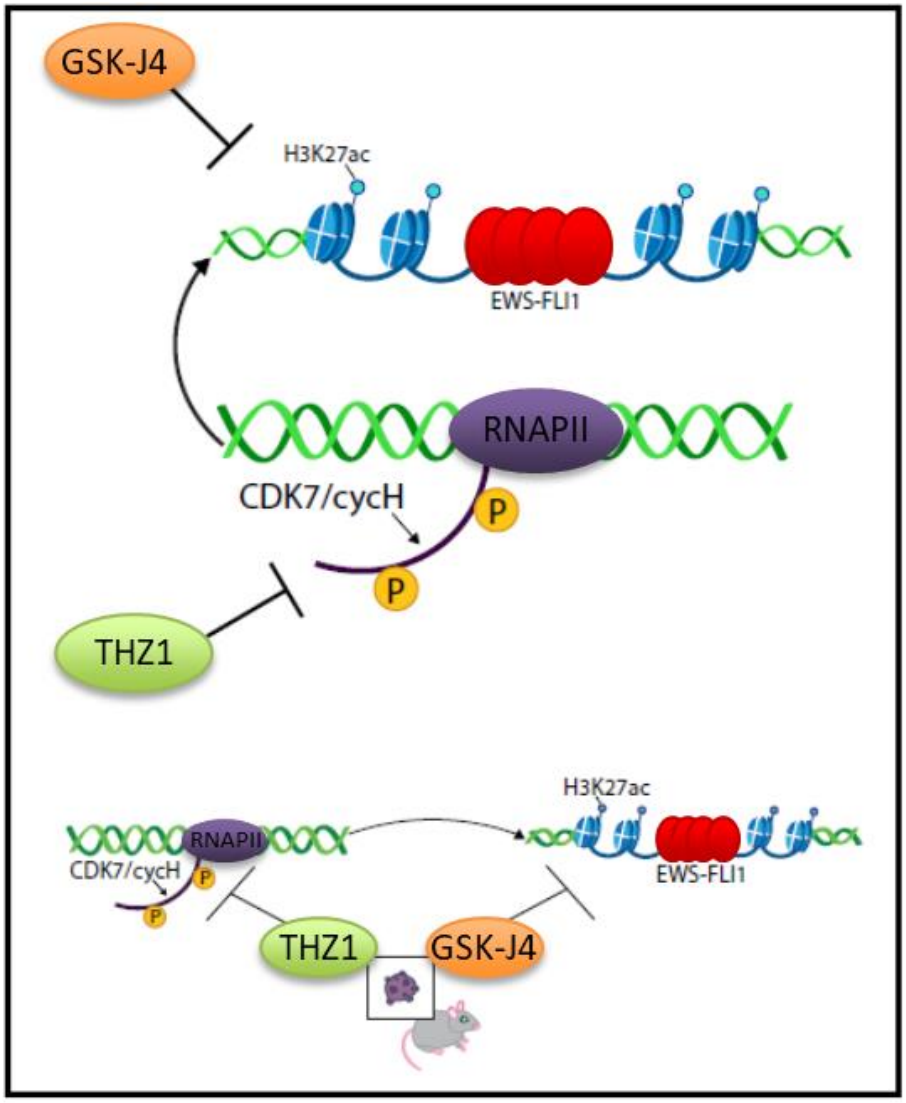

Figure 4.7 Conceptualized mechanism of co-targeting EWS-FLI1

Cartoon representation of the mechanistic role GSK-J4 plays to inhibit H3K27ac at EWS-FLI1 driven transcripts, while cooperatively being downregulated by THZ1 mediated inhibition of RNAPII activation. (TOP) GSK-J4 reduces EWS-FLI1 driven H3K27ac at the enhancer regions of EWS-FLI1 bound target genes, resulting in decreased gene activation. (MIDDLE) THZ1 inhibits CDK7 activity, which results in a loss of RNAPII phosphorylation at serine 5 and the reduction of oncogenic transcripts. (BOTTOM) THZ1 cooperatively blocks EWS-FLI1 driven transcripts, sensitizing EWFT cells to GSK-J4 and inhibiting oncogenesis.

Chapter 5 – General Discussion

Although the occurrence of EWFT is less common than other forms of cancer, this statistic belies its highly aggressive and deadly nature. Despite recent advances that have increased EFS of patients with localized disease, the rate of death in patients who relapse or present with metastasis remains unacceptably high (20, 176). EWFT is unique in that it has one of the lowest somatic mutation rates among all cancer types which places the burden of oncogenesis mainly on the FET/ETS fusions which are hallmarks of the disease. Specifically the t(11;22)(q24;q12) chromosomal translocation which results in the formation of the EWS-FLI1 oncoprotein is found in 85% of EWFT cases (31). Due to EWFT's reliance on FET/ETS translocations, this has been the greatest subject of study for disease therapy, however this aberrant transcription factor also presents an improbable drug target. Within the EWFT family there are only a small number of inactivating mutations in tumor suppressors such as p53 or RB, and other inactivating mutations only occur in a small subset of the disease such as STAG2 (82). This further suggests that the main effector of oncogenesis is mediated by the transcriptional and epigenetic changes that occur as a result of FET/ETS fusions. The future of EWFT treatment rests in our understanding and exploitation of the transcriptional machinery directed by fusions such as EWS-FLI1, and how they incur epigenetic dysregulation. There has been extensive

research describing the vast transcription profile of EWS-FLI1 and its many gene targets that are dysregulated, however the function and role they play in promoting EWFT tumorigenesis remains unknown (73, 76, 133).

In cancers such as EWFT where no viable targeted therapies are clinically available we have to rely on the use of multiple cytotoxic chemotherapeutic agents as the standard of care such as VDC-IE in EWFT (32-34). Despite our best efforts to develop and utilize targeted therapies, drug resistance continues to be a challenge. A perfect example of this is EWFT's reliance on PARP to assist in the repair of DNA damage due to defects in HR proteins such as BRCA1. In normal cells, EWSR1 is able to regulate the formation of R-loops: DNA-RNA hybrids which stall replication forks. However, in EWFT cells the EWS-FLI1 oncoprotein loses this function, leading to a higher incidence of R-loop formation, which have the ability to sequester and inactivate BRCA1, sensitizing the cells to cytotoxic and DNA damaging agents such as olaparib (56). However patients failed to respond to single agent PARPi therapy due to an underappreciated resistance to PARP inhibition as a result of chemotherapy . The work presented herein represents the development of combination targeted therapies through the inhibition of EWS-FLI1 machinery and downstream targets.

However, the efficacy of the discussed targeted therapies should be assessed in additional FET/ETS translocations which cause EWFT. EWSR1 and FUS proteins (representing 100% of the known FET/ETS fusions which cause EWFT) are involved in resolving R-loop formation to prevent stalled replication machinery and subsequent DNA damage, and this function is lost upon FET/ETS fusions (56, 177). This would suggest

that the reduced BRCA1 activity found in the EWS-FLI1 fusion is likely to be found in the entirety of EWFT, as well as their sensitivity to PARP inhibition (94). In addition, members of the ETS family of transcription factors all bind GGAA motifs, suggesting they share similar gene targets, and when translocated to a FET protein would result in similar profiles of gene dysregulation as demonstrated between EWS-FLI1 and EWS-ERG. This would suggest that the targeted therapies we previously discussed would have efficacy in non-EWS-FLI1 translocated EWFT due to analogous genomic and epigenetic dysregulation and susceptibilities (27, 43, 55, 57). This warrants future investigation into the efficacy of these therapies in the remaining translocations found in EWFT.

We focus on exploiting EWFT reliance on many of the FLI1 target genes and the use of combination therapies to prevent acquired resistance, leading to the effective inhibition of EWFT. To this end Chapter 3 reports on a drug combination capable of overcoming acquired chemotherapy resistance mediated by EWS-FLI1 gene dysregulation. We report the lack of efficacy towards the PARP inhibitor olaparib was likely mediated by an upregulation of the anti-apoptotic protein BCL-2, as seen in our pre/post chemotherapy paired EWFT cell lines CHLA9 and CHLA10. We were able to demonstrate that our CHLA10 EWFT derived cell line displayed increased BCL-2 expression as a means of avoiding apoptosis and developing chemotherapy resistance, rendering it insensitive to PARP inhibitor driven toxicity. Although we did not investigate whether FLI1 binds the *BCL2* enhancer or promoter regions to directly upregulate its expression, we did find a correlation between expressing the EWS-FLI1 translocation in naïve HEK293T cells and an increase in BCL-2 levels. We were able to demonstrate that the pro-survival proteins

BCL-2 and BCL-X_L were both capable of resisting olaparib mediated cell death. Given the transcriptome reprogramming that EWS-FLI1 is capable of, the reliance on the anti-apoptotic proteins BCL-2 and BCL-X_L mediated by EWS-FLI1 is likely a common method of acquired chemotherapy resistance in EWFT. To date, the majority of EWFT therapies have focused on DNA-damaging agents in combination with PARP inhibitors to enhance their effect (97, 98, 102, 132). Our use of a duel BCL-2/BCL-X_L inhibitor to sensitize EWFT cells to PARP inhibition represents a novel strategy which differs greatly from those currently being investigated.

Chapter 4 represents a continued investigation of plausible EWS-FLI1 targeted therapies, with a focus on epigenetically blocking the EWFT transcription machinery. These studies originated from a HTS drug screen which revealed EWFT were among the most sensitive cancer type to the histone demethylase inhibitor GSK-J4. We observed similar levels of sensitivity upon chemical interrogation of an EWFT panel of cell lines with GSK-J4, and strong efficacy in several PDX models. This sensitivity was determined to result from the shutting down of global gene activation induced by the EWS-FLI1 translocation and was achieved by preventing H3K27 acetylation through an increase in H3K27 methylation. We verified this mechanism using targeted ChIP and quantified H3K27ac levels at FLI1 bound enhancers of several well-known EWS-FLI1 upregulated genes. Among these genes are: *NKX2.2*, which is required for oncogenic transformation and used as a biomarker for EWFT; *NPY1R* which produces a G Protein coupled receptor whose function is currently not entirely understood but is often used as a predictor of EWFT metastasis; and lastly *EZH2* which has methyltransferase activity and is responsible

for altering the active state of chromatin resulting in gene silencing (24, 26, 81). Although the specific roles that most EWS-FLI1 target genes play in oncogenesis has yet to be identified, we feel these genes are representative of the epigenetic dysregulation caused by EWS-FLI1 and serve as a basis for the mechanism of GSK-J4 sensitivity. This work represents a novel approach, demonstrating GSK-J4 is capable of indirect specificity to the EWS-FLI1 epigenome with powerful anti-tumor activity.

To avoid possible acquired resistance to GSK-J4 as a monotherapy and enhance its anti-tumor potential, we utilized current literature citing CDK inhibitors as a promising new therapeutic opportunity in EWFT (165). By employing a CDK7 inhibitor responsible for the phosphorylation of RNAPII during initiation, we sought to co-target EWS-FLI1 mediated gene transcription. Our findings demonstrate robust anti-tumor activity against EWFT both *in vitro* and in PDX mouse models. Further investigation into CDK7 and CDK9/12 inhibitors available in clinic is warranted to identify additional small molecule inhibitors that synergize with GSK-J4 or the next generation of histone demethylase inhibitors.

Both THZ1 and GSK-J4 vary significantly in the pharmacodynamic rate at which they act, THZ1 activity peaks at 4-6 hours, while GSK-J4 requires several days to affect global H3K27me3 levels. Therefore, changes in dose scheduling may be required to exert the greatest synergistic response. Another potential pitfall to this combination is the effect these drugs have on global gene expression levels, which manifested in the form of toxicity in our mouse models. Several of the mice enrolled in the combination cohort of THZ1 and GSK-J4 lost substantial weight and displayed signs of distress and discomfort which was

followed by mortality in some instances. Upon autopsy it was revealed that these fatalities occurred in mice with excessive Constipation or Obstipation. These side effects could be mitigated pharmaceutically or by altering/lowering the dosing regimen and may have been a result of the DMSO used as a solvent in both THZ1 and GSK-J4. Despite the side effects, both drugs demonstrated the ability to control and reduce tumor growth *in vivo* supporting the efficacy of our two step approach to block EWS-FLI1 gene transcription.

Previous studies to epigenetically target EWS-FLI1 have focused on HDAC inhibitors, in order to maintain the activity of tumor suppressors or promote differentiation (147, 173, 178). Our novel approach is the first of its kind to demonstrate the epigenetic targeting of EWS-FLI1 through the inhibition of histone methyltransferases. When paired with highly synergistic CDK7 inhibitors, this represents a new and exciting area of future research.

Literature Cited

1. Chabner BA, Roberts Jr TG. Chemotherapy and the war on cancer. Nature Reviews Cancer. 2005;5:65.
2. DeVita VT, Chu E. A History of Cancer Chemotherapy. Cancer Research. 2008;68(21):8643.
3. Joo WD, Visintin I, Mor G. Targeted cancer therapy--are the days of systemic chemotherapy numbered? Maturitas. 2013;76(4):308-14.
4. Hanahan D, Weinberg RA. The hallmarks of cancer. Cell. 2000;100(1):57-70.
5. Kan Z, Jaiswal BS, Stinson J, Janakiraman V, Bhatt D, Stern HM, et al. Diverse somatic mutation patterns and pathway alterations in human cancers. Nature. 2010;466(7308):869-73.
6. Vaseva AV, Moll UM. The mitochondrial p53 pathway. Biochim Biophys Acta. 2009;1787(5):414-20.
7. Veloria J, Shin M, Devkota AK, Payne SM, Cho EJ, Dalby KN. Developing Colorimetric and Luminescence-Based High-Throughput Screening Platforms for Monitoring the GTPase Activity of Ferrous Iron Transport Protein B (FeoB). SLAS discovery : advancing life sciences R & D. 2019:2472555219844572.
8. Teicher BA, Polley E, Kunkel M, Evans D, Silvers T, Delosh R, et al. Sarcoma Cell Line Screen of Oncology Drugs and Investigational Agents Identifies Patterns Associated with Gene and microRNA Expression. Mol Cancer Ther. 2015;14(11):2452-62.
9. Worthington P, Drake KM, Li Z, Napper AD, Pochan DJ, Langhans SA. Implementation of a High-Throughput Pilot Screen in Peptide Hydrogel-Based Three-Dimensional Cell Cultures. SLAS discovery : advancing life sciences R & D. 2019:2472555219844570.
10. Simó-Riudalbas L, Esteller M. Cancer genomics identifies disrupted epigenetic genes. Human Genetics. 2014;133(6):713-25.
11. Garraway LA, Lander ES. Lessons from the cancer genome. Cell. 2013;153(1):17-37.
12. Wilks C, Cline MS, Weiler E, Diehkans M, Craft B, Martin C, et al. The Cancer Genomics Hub (CGHub): overcoming cancer through the power of torrential data. Database : the journal of biological databases and curation. 2014;2014:bau093.
13. Yang W, Soares J, Greninger P, Edelman EJ, Lightfoot H, Forbes S, et al. Genomics of Drug Sensitivity in Cancer (GDSC): a resource for therapeutic biomarker discovery in cancer cells. Nucleic acids research. 2013;41(Database issue):D955-61.
14. Simo-Riudalbas L, Esteller M. Cancer genomics identifies disrupted epigenetic genes. Hum Genet. 2014;133(6):713-25.
15. Weinstein IB, Joe A. Oncogene addiction. Cancer Res. 2008;68(9):3077-80; discussion 80.

16. Jones RL, Judson IR. The development and application of imatinib. Expert opinion on drug safety. 2005;4(2):183-91.
17. Salesse S, Verfaillie CM. BCR/ABL: from molecular mechanisms of leukemia induction to treatment of chronic myelogenous leukemia. Oncogene. 2002;21:8547.
18. Fausel C. Targeted chronic myeloid leukemia therapy: Seeking a cure. American Journal of Health-System Pharmacy. 2007;64(24_Supplement_15):S9-S15.
19. Esiashvili N, Goodman M, Marcus RB, Jr. Changes in incidence and survival of Ewing sarcoma patients over the past 3 decades: Surveillance Epidemiology and End Results data. Journal of pediatric hematology/oncology. 2008;30(6):425-30.
20. Balamuth NJ, Womer RB. Ewing's sarcoma. Lancet Oncol. 2010;11(2):184-92.
21. Ewing J. Classics in oncology. Diffuse endothelioma of bone. James Ewing. Proceedings of the New York Pathological Society, 1921. CA: a cancer journal for clinicians. 1972;22(2):95-8.
22. Surdez D, Benetkiewicz M, Perrin V, Han ZY, Pierron G, Ballet S, et al. Targeting the EWSR1-FLI1 oncogene-induced protein kinase PKC-beta abolishes ewing sarcoma growth. Cancer Res. 2012;72(17):4494-503.
23. Renard C, Ranchere-Vince D. [Ewing/PNET sarcoma family of tumors: towards a new paradigm?]. Annales de pathologie. 2015;35(1):86-97.
24. Boulay G, Volorio A, Iyer S, Broye LC, Stamenkovic I, Riggi N, et al. Epigenome editing of microsatellite repeats defines tumor-specific enhancer functions and dependencies. Genes & development. 2018;32(15-16):1008-19.
25. Johnson KM, Mahler NR, Saund RS, Theisen ER, Taslim C, Callender NW, et al. Role for the EWS domain of EWS/FLI in binding GGAA-microsatellites required for Ewing sarcoma anchorage independent growth. Proceedings of the National Academy of Sciences of the United States of America. 2017;114(37):9870-5.
26. Riggi N, Knoechel B, Gillespie SM, Rheinbay E, Boulay G, Suva ML, et al. EWS-FLI1 utilizes divergent chromatin remodeling mechanisms to directly activate or repress enhancer elements in Ewing sarcoma. Cancer Cell. 2014;26(5):668-81.
27. Im YH, Kim HT, Lee C, Poulin D, Welford S, Sorensen PH, et al. EWS-FLI1, EWS-ERG, and EWS-ETV1 oncoproteins of Ewing tumor family all suppress transcription of transforming growth factor beta type II receptor gene. Cancer Res. 2000;60(6):1536-40.
28. Sankar S, Bell R, Stephens B, Zhuo R, Sharma S, Bearss DJ, et al. Mechanism and relevance of EWS/FLI-mediated transcriptional repression in Ewing sarcoma. Oncogene. 2013;32(42):5089-100.
29. Beck R, Monument MJ, Watkins WS, Smith R, Boucher KM, Schiffman JD, et al. EWS/FLI-responsive GGAA microsatellites exhibit polymorphic differences between European and African populations. Cancer genetics. 2012;205(6):304-12.
30. Uchiumi F, Miyazaki S, Tanuma S. The possible functions of duplicated ets (GGAA) motifs located near transcription start sites of various human genes. Cellular and molecular life sciences : CMLS. 2011;68(12):2039-51.
31. Grünewald TGP, Cidre-Aranaz F, Surdez D, Tomazou EM, de Álava E, Kovar H, et al. Ewing sarcoma. Nature Reviews Disease Primers. 2018;4(1):5.

32. May WA, Grigoryan RS, Keshelava N, Cabral DJ, Christensen LL, Jenabi J, et al. Characterization and drug resistance patterns of Ewing's sarcoma family tumor cell lines. PLoS One. 2013;8(12):e80060.
33. Pretz JL, Barysauskas CM, George S, Hornick JL, Raut CP, Chen Y-LE, et al. Localized Adult Ewing Sarcoma: Favorable Outcomes with Alternating Vincristine, Doxorubicin, Cyclophosphamide, and Ifosfamide, Etoposide (VDC/IE)-Based Multimodality Therapy. The oncologist. 2017;22(10):1265-70.
34. Wagner MJ, Gopalakrishnan V, Ravi V, Livingston JA, Conley AP, Araujo D, et al. Vincristine, Ifosfamide, and Doxorubicin for Initial Treatment of Ewing Sarcoma in Adults. The oncologist. 2017;22(10):1271-7.
35. Charville GW, Wang W-L, Ingram DR, Roy A, Thomas D, Patel RM, et al. EWSR1 fusion proteins mediate PAX7 expression in Ewing sarcoma. Modern Pathology. 2017;30:1312.
36. Filion C, Motoi T, Olshen AB, Lae M, Emnett RJ, Gutmann DH, et al. The EWSR1/NR4A3 fusion protein of extraskeletal myxoid chondrosarcoma activates the PPARG nuclear receptor gene. J Pathol. 2009;217(1):83-93.
37. Frege T, Uversky VN. Intrinsically disordered proteins in the nucleus of human cells. Biochemistry and biophysics reports. 2015;1:33-51.
38. Ng KP, Potikyan G, Savene RO, Denny CT, Uversky VN, Lee KA. Multiple aromatic side chains within a disordered structure are critical for transcription and transforming activity of EWS family oncoproteins. Proc Natl Acad Sci U S A. 2007;104(2):479-84.
39. Boulay G, Sandoval GJ, Riggi N, Iyer S, Buisson R, Naigles B, et al. Cancer-Specific Retargeting of BAF Complexes by a Prion-like Domain. Cell. 2017;171(1):163-78.e19.
40. Patel A, Lee HO, Jawerth L, Maharana S, Jahnel M, Hein MY, et al. A Liquid-to-Solid Phase Transition of the ALS Protein FUS Accelerated by Disease Mutation. Cell. 2015;162(5):1066-77.
41. Theisen ER, Miller KR, Showpnil IA, Taslim C, Pishas KI, Lessnick SL. Transcriptomic analysis functionally maps the intrinsically disordered domain of EWS/FLI and reveals novel transcriptional dependencies for oncogenesis. Genes & cancer. 2019;10(1-2):21-38.
42. Nunn MF, Seeburg PH, Moscovici C, Duesberg PH. Tripartite structure of the avian erythroblastosis virus E26 transforming gene. Nature. 1983;306(5941):391-5.
43. Fry EA, Mallakin A, Inoue K. Translocations involving ETS family proteins in human cancer. Integrative cancer science and therapeutics. 2018;5(4):10.15761/ICST.1000281.
44. Oikawa T, Yamada T. Molecular biology of the Ets family of transcription factors. Gene. 2003;303:11-34.
45. Sizemore GM, Pitarresi JR, Balakrishnan S, Ostrowski MC. The ETS family of oncogenic transcription factors in solid tumours. Nature reviews Cancer. 2017;17(6):337-51.

46. Hart A, Melet F, Grossfeld P, Chien K, Jones C, Tunnacliffe A, et al. Fli-1 is required for murine vascular and megakaryocytic development and is hemizygously deleted in patients with thrombocytopenia. Immunity. 2000;13(2):167-77.
47. Spyropoulos DD, Pharr PN, Lavenburg KR, Jackers P, Papas TS, Ogawa M, et al. Hemorrhage, impaired hematopoiesis, and lethality in mouse embryos carrying a targeted disruption of the Fli1 transcription factor. Mol Cell Biol. 2000;20(15):5643-52.
48. Delattre O, Zucman J, Plougastel B, Desmaze C, Melot T, Peter M, et al. Gene fusion with an ETS DNA-binding domain caused by chromosome translocation in human tumours. Nature. 1992;359(6391):162-5.
49. Sharrocks AD. The ETS-domain transcription factor family. Nature reviews Molecular cell biology. 2001;2(11):827-37.
50. Pflueger D, Rickman DS, Sboner A, Perner S, LaFargue CJ, Svensson MA, et al. N-myc downstream regulated gene 1 (NDRG1) is fused to ERG in prostate cancer. Neoplasia (New York, NY). 2009;11(8):804-11.
51. Nakano K, Takahashi S. Translocation-Related Sarcomas. International journal of molecular sciences. 2018;19(12).
52. Le Deley MC, Delattre O, Schaefer KL, Burchill SA, Koehler G, Hogendoorn PC, et al. Impact of EWS-ETS fusion type on disease progression in Ewing's sarcoma/peripheral primitive neuroectodermal tumor: prospective results from the cooperative Euro-E.W.I.N.G. 99 trial. Journal of clinical oncology : official journal of the American Society of Clinical Oncology. 2010;28(12):1982-8.
53. Pishas KI, Drenberg CD, Taslim C, Theisen ER, Johnson KM, Saund RS, et al. Therapeutic Targeting of KDM1A/LSD1 in Ewing Sarcoma with SP-2509 Engages the Endoplasmic Reticulum Stress Response. Mol Cancer Ther. 2018;17(9):1902-16.
54. Maroulakou IG, Bowe DB. Expression and function of Ets transcription factors in mammalian development: a regulatory network. Oncogene. 2000;19(55):6432-42.
55. Ginsberg JP, de Alava E, Ladanyi M, Wexler LH, Kovar H, Paulussen M, et al. EWS-FLI1 and EWS-ERG gene fusions are associated with similar clinical phenotypes in Ewing's sarcoma. Journal of clinical oncology : official journal of the American Society of Clinical Oncology. 1999;17(6):1809-14.
56. Gorthi A, Romero JC, Loranc E, Cao L, Lawrence LA, Goodale E, et al. EWS-FLI1 increases transcription to cause R-loops and block BRCA1 repair in Ewing sarcoma. Nature. 2018;555(7696):387-91.
57. Hu-Lieskovan S, Zhang J, Wu L, Shimada H, Schofield DE, Triche TJ. EWS-FLI1 Fusion Protein Up-regulates Critical Genes in Neural Crest Development and Is Responsible for the Observed Phenotype of Ewing's Family of Tumors. Cancer Research. 2005;65(11):4633.
58. Cidre-Aranaz F, Alonso J. EWS/FLI1 Target Genes and Therapeutic Opportunities in Ewing Sarcoma. Frontiers in oncology. 2015;5:162-.
59. Javaheri T, Kazemi Z, Pencik J, Pham HT, Kauer M, Noorizadeh R, et al. Increased survival and cell cycle progression pathways are required for EWS/FLI1-induced malignant transformation. Cell Death Dis. 2016;7(10):e2419.

60. Kovar H. Downstream EWS/FLI1 - upstream Ewing's sarcoma. Genome medicine. 2010;2(1):8-.
61. May WA, Lessnick SL, Braun BS, Klemsz M, Lewis BC, Lunsford LB, et al. The Ewing's sarcoma EWS/FLI-1 fusion gene encodes a more potent transcriptional activator and is a more powerful transforming gene than FLI-1. Mol Cell Biol. 1993;13(12):7393-8.
62. Grohar PJ, Kim S, Rangel Rivera GO, Sen N, Haddock S, Harlow ML, et al. Functional Genomic Screening Reveals Splicing of the EWS-FLI1 Fusion Transcript as a Vulnerability in Ewing Sarcoma. Cell reports. 2016;14(3):598-610.
63. de Alava E, Kawai A, Healey JH, Fligman I, Meyers PA, Huvos AG, et al. EWS-FLI1 fusion transcript structure is an independent determinant of prognosis in Ewing's sarcoma. Journal of clinical oncology : official journal of the American Society of Clinical Oncology. 1998;16(4):1248-55.
64. Gonzalez I, Vicent S, de Alava E, Lecanda F. EWS/FLI-1 oncoprotein subtypes impose different requirements for transformation and metastatic activity in a murine model. Journal of molecular medicine (Berlin, Germany). 2007;85(9):1015-29.
65. van Doorninck JA, Ji L, Schaub B, Shimada H, Wing MR, Krailo MD, et al. Current treatment protocols have eliminated the prognostic advantage of type 1 fusions in Ewing sarcoma: a report from the Children's Oncology Group. Journal of clinical oncology : official journal of the American Society of Clinical Oncology. 2010;28(12):1989-94.
66. Riggi N, Cironi L, Provero P, Suvà M-L, Kaloulis K, Garcia-Echeverria C, et al. Development of Ewing's Sarcoma from Primary Bone Marrow–Derived Mesenchymal Progenitor Cells. Cancer Research. 2005;65(24):11459.
67. Riggi N, Suva ML, De Vito C, Provero P, Stehle JC, Baumer K, et al. EWS-FLI-1 modulates miRNA145 and SOX2 expression to initiate mesenchymal stem cell reprogramming toward Ewing sarcoma cancer stem cells. Genes Dev. 2010;24(9):916-32.
68. Cavazzana AO, Miser JS, Jefferson J, Triche TJ. Experimental evidence for a neural origin of Ewing's sarcoma of bone. The American journal of pathology. 1987;127(3):507-18.
69. Riggi N, Suva ML, Suva D, Cironi L, Provero P, Tercier S, et al. EWS-FLI-1 expression triggers a Ewing's sarcoma initiation program in primary human mesenchymal stem cells. Cancer Res. 2008;68(7):2176-85.
70. Miyagawa Y, Okita H, Nakaijima H, Horiuchi Y, Sato B, Taguchi T, et al. Inducible expression of chimeric EWS/ETS proteins confers Ewing's family tumor-like phenotypes to human mesenchymal progenitor cells. Molecular and cellular biology. 2008;28(7):2125-37.
71. Amaral AT, Manara MC, Berghuis D, Ordóñez JL, Biscuola M, Lopez-García MA, et al. Characterization of human mesenchymal stem cells from ewing sarcoma patients. Pathogenetic implications. PloS one. 2014;9(2):e85814-e.
72. Rocchi A, Manara MC, Sciandra M, Zambelli D, Nardi F, Nicoletti G, et al. CD99 inhibits neural differentiation of human Ewing sarcoma cells and thereby contributes to oncogenesis. The Journal of Clinical Investigation. 2010;120(3):668-80.

73. Patel M, Simon JM, Iglesia MD, Wu SB, McFadden AW, Lieb JD, et al. Tumor-specific retargeting of an oncogenic transcription factor chimera results in dysregulation of chromatin and transcription. Genome Res. 2012;22(2):259-70.
74. Wang AH, Zare H, Mousavi K, Wang C, Moravec CE, Sirotkin HI, et al. The histone chaperone Spt6 coordinates histone H3K27 demethylation and myogenesis. The EMBO journal. 2013;32(8):1075-86.
75. Erkizan HV, Kong Y, Merchant M, Schlottmann S, Barber-Rotenberg JS, Yuan L, et al. A small molecule blocking oncogenic protein EWS-FLI1 interaction with RNA helicase A inhibits growth of Ewing's sarcoma. Nature medicine. 2009;15(7):750-6.
76. Tomazou EM, Sheffield NC, Schmidl C, Schuster M, Schönegger A, Datlinger P, et al. Epigenome mapping reveals distinct modes of gene regulation and widespread enhancer reprogramming by the oncogenic fusion protein EWS-FLI1. Cell reports. 2015;10(7):1082-95.
77. Dylla L, Moore C, Jedlicka P. MicroRNAs in Ewing Sarcoma. Frontiers in oncology. 2013;3:65-.
78. Blackledge NP, Rose NR, Klose RJ. Targeting Polycomb systems to regulate gene expression: modifications to a complex story. Nature Reviews Molecular Cell Biology. 2015;16:643.
79. Chen S, Ma J, Wu F, Xiong L-J, Ma H, Xu W, et al. The histone H3 Lys 27 demethylase JMJD3 regulates gene expression by impacting transcriptional elongation. Genes & development. 2012;26(12):1364-75.
80. Cho YJ, Kim SH, Kim EK, Han JW, Shin K-H, Hu H, et al. Prognostic implications of polycomb proteins ezh2, suz12, and eed1 and histone modification by H3K27me3 in sarcoma. BMC cancer. 2018;18(1):158-.
81. Richter GH, Plehm S, Fasan A, Rossler S, Unland R, Bennani-Baiti IM, et al. EZH2 is a mediator of EWS/FLI1 driven tumor growth and metastasis blocking endothelial and neuro-ectodermal differentiation. Proc Natl Acad Sci U S A. 2009;106(13):5324-9.
82. Brohl AS, Solomon DA, Chang W, Wang J, Song Y, Sindiri S, et al. The genomic landscape of the Ewing Sarcoma family of tumors reveals recurrent STAG2 mutation. PLoS genetics. 2014;10(7):e1004475.
83. Choy E, Butrynski JE, Harmon DC, Morgan JA, George S, Wagner AJ, et al. Phase II study of olaparib in patients with refractory Ewing sarcoma following failure of standard chemotherapy. BMC Cancer. 2014;14:813.
84. Gayon J. From Mendel to epigenetics: History of genetics. Comptes rendus biologies. 2016;339(7-8):225-30.
85. Werner RJ, Kelly AD, Issa JJ. Epigenetics and Precision Oncology. Cancer journal (Sudbury, Mass). 2017;23(5):262-9.
86. Damhofer H, Ebbing EA, Steins A, Welling L, Tol JA, Krishnadath KK, et al. Establishment of patient-derived xenograft models and cell lines for malignancies of the upper gastrointestinal tract. Journal of translational medicine. 2015;13:115-.

87. Song KA, Niederst MJ, Lochmann TL, Hata AN, Kitai H, Ham J, et al. Epithelial-to-Mesenchymal Transition Antagonizes Response to Targeted Therapies in Lung Cancer by Suppressing BIM. Clin Cancer Res. 2018;24(1):197-208.
88. Hartig SM. Basic image analysis and manipulation in ImageJ. Current protocols in molecular biology. 2013;Chapter 14:Unit14.5.
89. Ham J, Costa C, Sano R, Lochmann TL, Sennott EM, Patel NU, et al. Exploitation of the Apoptosis-Primed State of MYCN-Amplified Neuroblastoma to Develop a Potent and Specific Targeted Therapy Combination. Cancer Cell. 2016;29(2):159-72.
90. Barretina J, Caponigro G, Stransky N, Venkatesan K, Margolin AA, Kim S, et al. The Cancer Cell Line Encyclopedia enables predictive modelling of anticancer drug sensitivity. Nature. 2012;483(7391):603-7.
91. Wong M, Tan N, Zha J, Peale FV, Yue P, Fairbrother WJ, et al. Navitoclax (ABT-263) reduces Bcl-x(L)-mediated chemoresistance in ovarian cancer models. Mol Cancer Ther. 2012;11(4):1026-35.
92. Tomazou EM, Sheffield NC, Schmidl C, Schuster M, Schonegger A, Datlinger P, et al. Epigenome mapping reveals distinct modes of gene regulation and widespread enhancer reprogramming by the oncogenic fusion protein EWS-FLI1. Cell reports. 2015;10(7):1082-95.
93. Sheffield NC, Pierron G, Klughammer J, Datlinger P, Schonegger A, Schuster M, et al. DNA methylation heterogeneity defines a disease spectrum in Ewing sarcoma. Nat Med. 2017;23(3):386-95.
94. Johnson N, Johnson SF, Yao W, Li YC, Choi YE, Bernhardy AJ, et al. Stabilization of mutant BRCA1 protein confers PARP inhibitor and platinum resistance. Proc Natl Acad Sci U S A. 2013;110(42):17041-6.
95. Brohl AS, Patidar R, Turner CE, Wen X, Song YK, Wei JS, et al. Frequent inactivating germline mutations in DNA repair genes in patients with Ewing sarcoma. Genet Med. 2017;19(8):955-8.
96. Dale Rein I, Solberg Landsverk K, Micci F, Patzke S, Stokke T. Replication-induced DNA damage after PARP inhibition causes G2 delay, and cell line-dependent apoptosis, necrosis and multinucleation. Cell Cycle. 2015;14(20):3248-60.
97. Grohar PJ, Segars LE, Yeung C, Pommier Y, D'Incalci M, Mendoza A, et al. Dual targeting of EWS-FLI1 activity and the associated DNA damage response with trabectedin and SN38 synergistically inhibits Ewing sarcoma cell growth. Clinical cancer research : an official journal of the American Association for Cancer Research. 2014;20(5):1190-203.
98. Lee HJ, Yoon C, Schmidt B, Park DJ, Zhang AY, Erkizan HV, et al. Combining PARP-1 inhibition and radiation in Ewing sarcoma results in lethal DNA damage. Mol Cancer Ther. 2013;12(11):2591-600.
99. Stewart E, Goshorn R, Bradley C, Griffiths LM, Benavente C, Twarog NR, et al. Targeting the DNA repair pathway in Ewing sarcoma. Cell Rep. 2014;9(3):829-41.
100. Brenner JC, Feng FY, Han S, Patel S, Goyal SV, Bou-Maroun LM, et al. PARP-1 inhibition as a targeted strategy to treat Ewing's sarcoma. Cancer research. 2012;72(7):1608-13.

101. Garnett MJ, Edelman EJ, Heidorn SJ, Greenman CD, Dastur A, Lau KW, et al. Systematic identification of genomic markers of drug sensitivity in cancer cells. Nature. 2012;483(7391):570-5.
102. Engert F, Schneider C, Weibeta LM, Probst M, Fulda S. PARP Inhibitors Sensitize Ewing Sarcoma Cells to Temozolomide-Induced Apoptosis via the Mitochondrial Pathway. Mol Cancer Ther. 2015;14(12):2818-30.
103. Faber AC, Corcoran RB, Ebi H, Sequist LV, Waltman BA, Chung E, et al. BIM expression in treatment-naive cancers predicts responsiveness to kinase inhibitors. Cancer Discov. 2011;1(4):352-65.
104. Hata AN, Yeo A, Faber AC, Lifshits E, Chen Z, Cheng KA, et al. Failure to induce apoptosis via BCL-2 family proteins underlies lack of efficacy of combined MEK and PI3K inhibitors for KRAS-mutant lung cancers. Cancer Res. 2014;74(11):3146-56.
105. Montero J, Sarosiek KA, DeAngelo JD, Maertens O, Ryan J, Ercan D, et al. Drug-induced death signaling strategy rapidly predicts cancer response to chemotherapy. Cell. 2015;160(5):977-89.
106. Costa C, Molina MA, Drozdowskyj A, Gimenez-Capitan A, Bertran-Alamillo J, Karachaliou N, et al. The impact of EGFR T790M mutations and BIM mRNA expression on outcome in patients with EGFR-mutant NSCLC treated with erlotinib or chemotherapy in the randomized phase III EURTAC trial. Clin Cancer Res. 2014;20(7):2001-10.
107. Ng KP, Hillmer AM, Chuah CT, Juan WC, Ko TK, Teo AS, et al. A common BIM deletion polymorphism mediates intrinsic resistance and inferior responses to tyrosine kinase inhibitors in cancer. Nat Med. 2012;18(4):521-8.
108. Xie M, Park D, You S, Li R, Owonikoko TK, Wang Y, et al. Bcl2 inhibits recruitment of Mre11 complex to DNA double-strand breaks in response to high-linear energy transfer radiation. Nucleic acids research. 2015;43(2):960-72.
109. Batra S, Reynolds CP, Maurer BJ. Fenretinide cytotoxicity for Ewing's sarcoma and primitive neuroectodermal tumor cell lines is decreased by hypoxia and synergistically enhanced by ceramide modulators. Cancer Res. 2004;64(15):5415-24.
110. Vanden Heuvel JP, Maddox E, Maalouf SW, Reproducibility Project: Cancer B, Iorns E, Tsui R, et al. Replication Study: Systematic identification of genomic markers of drug sensitivity in cancer cells. Elife. 2018;7.
111. Vo TT, Ryan J, Carrasco R, Neuberg D, Rossi DJ, Stone RM, et al. Relative mitochondrial priming of myeloblasts and normal HSCs determines chemotherapeutic success in AML. Cell. 2012;151(2):344-55.
112. Montero J, Letai A. Dynamic BH3 profiling-poking cancer cells with a stick. Mol Cell Oncol. 2016;3(3):e1040144.
113. Ni Chonghaile T, Sarosiek KA, Vo TT, Ryan JA, Tammareddi A, Moore Vdel G, et al. Pretreatment mitochondrial priming correlates with clinical response to cytotoxic chemotherapy. Science. 2011;334(6059):1129-33.
114. Souers AJ, Leverson JD, Boghaert ER, Ackler SL, Catron ND, Chen J, et al. ABT-199, a potent and selective BCL-2 inhibitor, achieves antitumor activity while sparing platelets. Nat Med. 2013;19(2):202-8.

115. Bose P, Gandhi V, Konopleva M. Pathways and mechanisms of venetoclax resistance. Leuk Lymphoma. 2017;58(9):1-17.
116. Vogler M, Dinsdale D, Dyer MJ, Cohen GM. ABT-199 selectively inhibits BCL2 but not BCL2L1 and efficiently induces apoptosis of chronic lymphocytic leukaemic cells but not platelets. Br J Haematol. 2013;163(1):139-42.
117. Wiese C, Pierce AJ, Gauny SS, Jasin M, Kronenberg A. Gene conversion is strongly induced in human cells by double-strand breaks and is modulated by the expression of BCL-x(L). Cancer Res. 2002;62(5):1279-83.
118. Tse C, Shoemaker AR, Adickes J, Anderson MG, Chen J, Jin S, et al. ABT-263: a potent and orally bioavailable Bcl-2 family inhibitor. Cancer Res. 2008;68(9):3421-8.
119. Gandhi L, Camidge DR, Ribeiro de Oliveira M, Bonomi P, Gandara D, Khaira D, et al. Phase I study of Navitoclax (ABT-263), a novel Bcl-2 family inhibitor, in patients with small-cell lung cancer and other solid tumors. Journal of clinical oncology : official journal of the American Society of Clinical Oncology. 2011;29(7):909-16.
120. Leverson JD, Phillips DC, Mitten MJ, Boghaert ER, Diaz D, Tahir SK, et al. Exploiting selective BCL-2 family inhibitors to dissect cell survival dependencies and define improved strategies for cancer therapy. Sci Transl Med. 2015;7(279):279ra40.
121. Lin X, Morgan-Lappe S, Huang X, Li L, Zakula DM, Vernetti LA, et al. 'Seed' analysis of off-target siRNAs reveals an essential role of Mcl-1 in resistance to the small-molecule Bcl-2/Bcl-XL inhibitor ABT-737. Oncogene. 2007;26(27):3972-9.
122. Hemann MT, Lowe SW. The p53-Bcl-2 connection. Cell Death Differ. 2006;13(8):1256-9.
123. Takigami I, Ohno T, Kitade Y, Hara A, Nagano A, Kawai G, et al. Synthetic siRNA targeting the breakpoint of EWS/Fli-1 inhibits growth of Ewing sarcoma xenografts in a mouse model. Int J Cancer. 2011;128(1):216-26.
124. Kaefer A, Yang J, Noertersheuser P, Mensing S, Humerickhouse R, Awni W, et al. Mechanism-based pharmacokinetic/pharmacodynamic meta-analysis of navitoclax (ABT-263) induced thrombocytopenia. Cancer Chemother Pharmacol. 2014;74(3):593-602.
125. Grunewald TG, Diebold I, Esposito I, Plehm S, Hauer K, Thiel U, et al. STEAP1 is associated with the invasive and oxidative stress phenotype of Ewing tumors. Mol Cancer Res. 2012;10(1):52-65.
126. Cidre-Aranaz F, Alonso J. EWS/FLI1 Target Genes and Therapeutic Opportunities in Ewing Sarcoma. Front Oncol. 2015;5:162.
127. Kamesaki S, Kamesaki H, Jorgensen TJ, Tanizawa A, Pommier Y, Cossman J. bcl-2 protein inhibits etoposide-induced apoptosis through its effects on events subsequent to topoisomerase II-induced DNA strand breaks and their repair. Cancer Res. 1993;53(18):4251-6.
128. Faber AC, Farago AF, Costa C, Dastur A, Gomez-Caraballo M, Robbins R, et al. Assessment of ABT-263 activity across a cancer cell line collection leads to a potent combination therapy for small-cell lung cancer. Proc Natl Acad Sci U S A. 2015;112(11):E1288-96.

129. Del Gaizo Moore V, Schlis KD, Sallan SE, Armstrong SA, Letai A. BCL-2 dependence and ABT-737 sensitivity in acute lymphoblastic leukemia. Blood. 2008;111(4):2300-9.
130. Harada H, Grant S. Targeting the regulatory machinery of BIM for cancer therapy. Crit Rev Eukaryot Gene Expr. 2012;22(2):117-29.
131. Faber AC, Ebi H, Costa C, Engelman JA. Apoptosis in targeted therapy responses: the role of BIM. Adv Pharmacol. 2012;65:519-42.
132. Ordonez JL, Amaral AT, Carcaboso AM, Herrero-Martin D, del Carmen Garcia-Macias M, Sevillano V, et al. The PARP inhibitor olaparib enhances the sensitivity of Ewing sarcoma to trabectedin. Oncotarget. 2015;6(22):18875-90.
133. Soldatenkov VA, Albor A, Patel BK, Dreszer R, Dritschilo A, Notario V. Regulation of the human poly(ADP-ribose) polymerase promoter by the ETS transcription factor. Oncogene. 1999;18(27):3954-62.
134. Byers LA, Wang J, Nilsson MB, Fujimoto J, Saintigny P, Yordy J, et al. Proteomic profiling identifies dysregulated pathways in small cell lung cancer and novel therapeutic targets including PARP1. Cancer Discov. 2012;2(9):798-811.
135. Hopkins TA, Shi Y, Rodriguez LE, Solomon LR, Donawho CK, DiGiammarino EL, et al. Mechanistic Dissection of PARP1 Trapping and the Impact on In Vivo Tolerability and Efficacy of PARP Inhibitors. Mol Cancer Res. 2015;13(11):1465-77.
136. Murai J, Huang SY, Das BB, Renaud A, Zhang Y, Doroshow JH, et al. Trapping of PARP1 and PARP2 by Clinical PARP Inhibitors. Cancer Res. 2012;72(21):5588-99.
137. Gill SJ, Travers J, Pshenichnaya I, Kogera FA, Barthorpe S, Mironenko T, et al. Combinations of PARP Inhibitors with Temozolomide Drive PARP1 Trapping and Apoptosis in Ewing's Sarcoma. PLoS One. 2015;10(10):e0140988.
138. Tang SW, Bilke S, Cao L, Murai J, Sousa FG, Yamade M, et al. SLFN11 Is a Transcriptional Target of EWS-FLI1 and a Determinant of Drug Response in Ewing Sarcoma. Clin Cancer Res. 2015;21(18):4184-93.
139. Zoppoli G, Regairaz M, Leo E, Reinhold WC, Varma S, Ballestrero A, et al. Putative DNA/RNA helicase Schlafen-11 (SLFN11) sensitizes cancer cells to DNA-damaging agents. Proc Natl Acad Sci U S A. 2012;109(37):15030-5.
140. LoRusso PM, Li J, Burger A, Heilbrun LK, Sausville EA, Boerner SA, et al. Phase I Safety, Pharmacokinetic, and Pharmacodynamic Study of the Poly(ADP-ribose) Polymerase (PARP) Inhibitor Veliparib (ABT-888) in Combination with Irinotecan in Patients with Advanced Solid Tumors. Clin Cancer Res. 2016;22(13):3227-37.
141. Hayward RL, Macpherson JS, Cummings J, Monia BP, Smyth JF, Jodrell DI. Antisense Bcl-xl down-regulation switches the response to topoisomerase I inhibition from senescence to apoptosis in colorectal cancer cells, enhancing global cytotoxicity. Clin Cancer Res. 2003;9(7):2856-65.
142. Hata AN, Engelman JA, Faber AC. The BCL2 Family: Key Mediators of the Apoptotic Response to Targeted Anticancer Therapeutics. Cancer Discov. 2015;5(5):475-87.
143. Reed JC. Bcl-2 family proteins: regulators of chemoresistance in cancer. Toxicol Lett. 1995;82-83:155-8.

144. Mendoza-Naranjo A, El-Naggar A, Wai DH, Mistry P, Lazic N, Ayala FR, et al. ERBB4 confers metastatic capacity in Ewing sarcoma. EMBO Mol Med. 2013;5(7):1087-102.
145. Wright ML, Dozmorov MG, Wolen AR, Jackson-Cook C, Starkweather AR, Lyon DE, et al. Establishing an analytic pipeline for genome-wide DNA methylation. Clin Epigenetics. 2016;8:45.
146. Alexandrov LB, Nik-Zainal S, Wedge DC, Aparicio SA, Behjati S, Biankin AV, et al. Signatures of mutational processes in human cancer. Nature. 2013;500(7463):415-21.
147. Pasini D, Malatesta M, Jung HR, Walfridsson J, Willer A, Olsson L, et al. Characterization of an antagonistic switch between histone H3 lysine 27 methylation and acetylation in the transcriptional regulation of Polycomb group target genes. Nucleic acids research. 2010;38(15):4958-69.
148. Xu B, On DM, Ma A, Parton T, Konze KD, Pattenden SG, et al. Selective inhibition of EZH2 and EZH1 enzymatic activity by a small molecule suppresses MLL-rearranged leukemia. Blood. 2015;125(2):346-57.
149. Knutson SK, Wigle TJ, Warholic NM, Sneeringer CJ, Allain CJ, Klaus CR, et al. A selective inhibitor of EZH2 blocks H3K27 methylation and kills mutant lymphoma cells. Nat Chem Biol. 2012;8(11):890-6.
150. Kang SC, Kim SK, Chai JC, Kim SH, Won K-J, Lee YS, et al. Transcriptomic Profiling and H3K27me3 Distribution Reveal Both Demethylase-Dependent and Independent Regulation of Developmental Gene Transcription in Cell Differentiation. PloS one. 2015;10(8):e0135276-e.
151. Benyoucef A, Palii CG, Wang C, Porter CJ, Chu A, Dai F, et al. UTX inhibition as selective epigenetic therapy against TAL1-driven T-cell acute lymphoblastic leukemia. Genes Dev. 2016;30(5):508-21.
152. Edgar R, Domrachev M, Lash AE. Gene Expression Omnibus: NCBI gene expression and hybridization array data repository. Nucleic acids research. 2002;30(1):207-10.
153. Savola S, Klami A, Myllykangas S, Manara C, Scotlandi K, Picci P, et al. High Expression of Complement Component 5 (C5) at Tumor Site Associates with Superior Survival in Ewing's Sarcoma Family of Tumour Patients. ISRN oncology. 2011;2011:168712.
154. Aranda S, Mas G, Di Croce L. Regulation of gene transcription by Polycomb proteins. Science Advances. 2015;1(11):e1500737.
155. LaMere SA, Thompson RC, Meng X, Komori HK, Mark A, Salomon DR. H3K27 Methylation Dynamics during CD4 T Cell Activation: Regulation of JAK/STAT and IL12RB2 Expression by JMJD3. Journal of immunology (Baltimore, Md : 1950). 2017;199(9):3158-75.
156. Wong RWJ, Ishida T, Sanda T. Targeting General Transcriptional Machinery as a Therapeutic Strategy for Adult T-Cell Leukemia. Molecules. 2018;23(5).
157. Hashizume R. Epigenetic Targeted Therapy for Diffuse Intrinsic Pontine Glioma. Neurol Med Chir (Tokyo). 2017;57(7):331-42.

158. Long W, Yi Y, Chen S, Cao Q, Zhao W, Liu Q. Potential New Therapies for Pediatric Diffuse Intrinsic Pontine Glioma. Frontiers in pharmacology. 2017;8:495-.
159. Kinsey M, Smith R, Lessnick SL. NR0B1 is required for the oncogenic phenotype mediated by EWS/FLI in Ewing's sarcoma. Mol Cancer Res. 2006;4(11):851-9.
160. Heisey DAR, Lochmann TL, Floros KV, Coon CM, Powell KM, Jacob S, et al. The Ewing family of tumors rely on BCL-2 and BCL-XL to escape PARP inhibitor toxicity. Clin Cancer Res. 2018.
161. Song KA, Hosono Y, Turner C, Jacob S, Lochmann TL, Murakami Y, et al. Increased Synthesis of MCL-1 Protein Underlies Initial Survival of EGFR-Mutant Lung Cancer to EGFR Inhibitors and Provides a Novel Drug Target. Clin Cancer Res. 2018;24(22):5658-72.
162. Alagpulinsa DA, Ayyadevara S, Yaccoby S, Shmookler Reis RJ. A Cyclin-Dependent Kinase Inhibitor, Dinaciclib, Impairs Homologous Recombination and Sensitizes Multiple Myeloma Cells to PARP Inhibition. Molecular cancer therapeutics. 2016;15(2):241-50.
163. Cayrol F, Praditsuktavorn P, Fernando TM, Kwiatkowski N, Marullo R, Calvo-Vidal MN, et al. THZ1 targeting CDK7 suppresses STAT transcriptional activity and sensitizes T-cell lymphomas to BCL2 inhibitors. Nature communications. 2017;8:14290-.
164. Liu X, Gao Y, Shen J, Yang W, Choy E, Mankin H, et al. Cyclin-Dependent Kinase 11 (CDK11) Is Required for Ovarian Cancer Cell Growth In Vitro and In Vivo, and Its Inhibition Causes Apoptosis and Sensitizes Cells to Paclitaxel. Molecular cancer therapeutics. 2016;15(7):1691-701.
165. Iniguez AB, Stolte B, Wang EJ, Conway AS, Alexe G, Dharia NV, et al. EWS/FLI Confers Tumor Cell Synthetic Lethality to CDK12 Inhibition in Ewing Sarcoma. Cancer cell. 2018;33(2):202-16.e6.
166. Kwiatkowski N, Zhang T, Rahl PB, Abraham BJ, Reddy J, Ficarro SB, et al. Targeting transcription regulation in cancer with a covalent CDK7 inhibitor. Nature. 2014;511(7511):616-20.
167. Chipumuro E, Marco E, Christensen CL, Kwiatkowski N, Zhang T, Hatheway CM, et al. CDK7 inhibition suppresses super-enhancer-linked oncogenic transcription in MYCN-driven cancer. Cell. 2014;159(5):1126-39.
168. Smith R, Owen LA, Trem DJ, Wong JS, Whangbo JS, Golub TR, et al. Expression profiling of EWS/FLI identifies NKX2.2 as a critical target gene in Ewing's sarcoma. Cancer Cell. 2006;9(5):405-16.
169. Sakimura R, Tanaka K, Nakatani F, Matsunobu T, Li X, Hanada M, et al. Antitumor effects of histone deacetylase inhibitor on Ewing's family tumors. International Journal of Cancer. 2005;116(5):784-92.
170. Di Pompo G, Salerno M, Rotili D, Valente S, Zwergel C, Avnet S, et al. Novel Histone Deacetylase Inhibitors Induce Growth Arrest, Apoptosis, and Differentiation in Sarcoma Cancer Stem Cells. Journal of Medicinal Chemistry. 2015;58(9):4073-9.
171. Hashizume R, Andor N, Ihara Y, Lerner R, Gan H, Chen X, et al. Pharmacologic inhibition of histone demethylation as a therapy for pediatric brainstem glioma. Nat Med. 2014;20(12):1394-6.

172. Lochmann TL, Powell KM, Ham J, Floros KV, Heisey DAR, Kurupi RIJ, et al. Targeted inhibition of histone H3K27 demethylation is effective in high-risk neuroblastoma. Sci Transl Med. 2018;10(441).
173. Souza BK, da Costa Lopez PL, Menegotto PR, Vieira IA, Kersting N, Abujamra AL, et al. Targeting Histone Deacetylase Activity to Arrest Cell Growth and Promote Neural Differentiation in Ewing Sarcoma. Molecular neurobiology. 2018;55(9):7242-58.
174. Parrish JK, McCann TS, Sechler M, Sobral LM, Ren W, Jones KL, et al. The Jumonji-domain histone demethylase inhibitor JIB-04 deregulates oncogenic programs and increases DNA damage in Ewing Sarcoma, resulting in impaired cell proliferation and survival, and reduced tumor growth. Oncotarget. 2018;9(69):33110-23.
175. Sankar S, Theisen ER, Bearss J, Mulvihill T, Hoffman LM, Sorna V, et al. Reversible LSD1 inhibition interferes with global EWS/ETS transcriptional activity and impedes Ewing sarcoma tumor growth. Clinical cancer research : an official journal of the American Association for Cancer Research. 2014;20(17):4584-97.
176. Gaspar N, Hawkins DS, Dirksen U, Lewis IJ, Ferrari S, Le Deley MC, et al. Ewing Sarcoma: Current Management and Future Approaches Through Collaboration. Journal of clinical oncology : official journal of the American Society of Clinical Oncology. 2015;33(27):3036-46.
177. Richard P, Manley JL. R Loops and Links to Human Disease. J Mol Biol. 2017;429(21):3168-80.
178. Sakimura R, Tanaka K, Nakatani F, Matsunobu T, Li X, Hanada M, et al. Antitumor effects of histone deacetylase inhibitor on Ewing's family tumors. Int J Cancer. 2005;116(5):784-92.

VITA

Daniel Andrew Russell Heisey was born in Springfield Virginia on June 19, 1989. At a young age he quickly grasped science's ability to answer life's many questions, and its pursuit eventually him led to Christopher Newport University where he was awarded his Bachelor of Science degree in 2011.

Upon graduation he pursued his longing for science and spent 3 years researching Arboviruses for the FDA at the NIH. It was during this time that he realized his love of research and in 2014 began his Doctoral studies in the Biomedical Sciences Doctoral Program at Virginia Commonwealth University. During his first year of studies he joined the Translational Oncology lab of Dr. Anthony Faber where he remained to complete his degree.

Service and Awards:

- Award for Outstanding Student Publication in Biology and Genetics
  Molecular Biology and Genetics Department, May 10, 2019

- Excellence in Cancer Research Award
  VCU Massey Cancer Center Research Retreat, June 16, 2017

- Ad Hoc Reviewer – Clinical Cancer Research

- Promotion and Tenure Committee Member
  Department of Oral and Craniofacial Molecular Biology
  Virginia Commonwealth University, School of Medicine, 2018

- Beta Beta Beta, National Biological Honor Society
  Christopher Newport University, Newport News, VA

Publications:

1. **Heisey DAR**, Lochmann TL, Floros KV, Coon CM, Powell KM, Jacob S, Calbert ML, Ghotra MS, Stein GT, Maves YK, Smith SC, Benes CH, Leverson JD, Souers AJ, Boikos SA, Faber AC (2018). The Ewing family of tumors rely on BCL-2 and BCL-XL to escape PARP inhibitor toxicity. Clin Cancer Res. 2018 Oct 22; PMID: 30348635

2. Lochmann TL, Powell KM, Ham J, Floros KV, **Heisey DAR**, Kurupi RIJ, Calbert ML, Ghotra MS, Greninger P, Dozmorov M, Gowda M, Souers AJ, Reynolds CP, Benes CH, Faber AC. Targeted inhibition of histone H3K27 demethylation is effective in high-risk neuroblastoma. Sci Transl Med. 2018 May 16; 10(441). PMID: 29769286

3. Song KA, Niederst MJ, Lochmann TL, Hata AN, Kitai H, Ham J, Floros KV, Hicks MA, Hu H, Mulvey HE, Drier Y, **Heisey DAR**, Hughes MT, Patel NU, Lockerman EL, Garcia A, Gillepsie S, Archibald HL, Gomez-Caraballo M, Nulton TJ, Windle BE, Piotrowska Z, Sahingur SE, Taylor SM, Dozmorov M, Sequist LV, Bernstein B, Ebi H, Engelman JA, Faber AC. Epithelial-to-Mesenchymal Transition Antagonizes Response to Targeted Therapies in Lung Cancer by Suppressing BIM. Clin Cancer Res. 2018 Jan 1; 24(1):197-208. PMID: 29051323

4. Añez, G., Volkova, E., Jiang, Z., **Heisey, D. A. R.,** Chancey, C., and Fares, R. C. G. (2017). Collaborative study to establish World Health Organization international reference reagents for dengue virus Types 1 to 4 RNA for use in nucleic acid testing. Transfusion 57, 1977–1987. doi: 10.1111/trf.14130

5. Ham J, Costa C, Sano R, Lochmann TL, Sennott EM, Patel NU, Dastur A, Gomez-Caraballo M, Krytska K, Hata AN, Floros KV, Hughes MT, Jakubik CT, **Heisey DAR**, Ferrell JT, Bristol ML, March RJ, Yates C, Hicks MA, Nakajima W, Gowda M, Windle BE, Dozmorov MG, Garnett MJ, McDermott U, Harada H, Taylor SM, Morgan IM, Benes CH, Engelman JA, Mossé YP, Faber AC. Exploitation of the Apoptosis-Primed State of MYCN-Amplified Neuroblastoma to Develop a Potent and Specific Targeted Therapy Combination. Cancer Cell. 2016 Feb 8; 29(2):159-72. PMID: 26859456

6. Grinev, A., Chancey, C., Volkova, E., Añez, G., **Heisey, D.A.R.**, Winkelman, V., Foster, G. A., Williamson, P., Stramer, S. L., Rios, M. (2016). Genetic Variability of West Nile Virus in U.S. Blood Donors from the 2012 Epidemic Season. PLoS neglected tropical diseases, 10(5), e0004717. doi:10.1371/journal.pntd.0004717 PMID: 27182734

7. Añez, G., **Heisey, D.A.R.**, Chancey, C., Fares, R. C., Espina, L. M., Souza, K. P., Teixeira-Carvalho, A., Krysztof, D. E., Foster, G. A., Stramer, S. L., Rios, M. (2016). Distribution of Dengue Virus Types 1 and 4 in Blood Components from Infected Blood Donors from Puerto Rico. PLoS neglected tropical diseases, 10(2), e0004445. doi:10.1371/journal.pntd.0004445. PMID: 26871560

8. Añez, G., **Heisey, D.A.R.**, Volkova, E., & Rios, M. (2016). Complete Genome Sequences of Dengue Virus Type 1 to 4 Strains Used for the Development of CBER/FDA RNA Reference Reagents and WHO International Standard Candidates for Nucleic Acid Testing. Genome announcements, 4(1), e01583-15. doi:10.1128/genomeA.01583-15. PMID: 26868382

9. Anez G, Jiang Z, **Heisey DA**, Kerby S, Rios M. Collaborative study for the characterization of a chikungunya virus RNA reference reagent for use in nucleic acid testing. Vox sanguinis. 2015;109(4):312-8

10. Añez, G., **Heisey, D.A.R.**, & Rios, M. (2014). Complete Coding Region Sequence of a Chikungunya Virus Strain Used for Formulation of CBER/FDA RNA Reference Reagents for Nucleic Acid Testing. Genome announcements, 2(4), e00587-14. doi:10.1128/genomeA.00587-14. PMID: 25081254

11. Añez, G., **Heisey, D.A.R.**, Espina, L. M., Stramer, S. L., & Rios, M. (2012). Phylogenetic analysis of dengue virus types 1 and 4 circulating in Puerto Rico and Key West, Florida, during 2010 epidemics. The American journal of tropical medicine and hygiene, 87(3), 548-53. PMID: 22826483